PHILOSOPHICAL TRANSACTIONS OF THE ROYAL SOCIETY A MATHEMATICAL, PHYSICAL & ENGINEERING SCIENCES

A Study of the Interactions between Large-Scale Coherent Structures and Fine-Grained Turbulence in a Round Jet

R. Mankbadi and J. T. C. Liu

Phil. Trans. R. Soc. Lond. A 1981 **298**, 541-602
doi: 10.1098/rsta.1981.0001

A STUDY OF THE INTERACTIONS BETWEEN LARGE-SCALE COHERENT STRUCTURES AND FINE-GRAINED TURBULENCE IN A ROUND JET

By R. MANKBADI† and J. T. C. LIU‡

Division of Engineering, Brown University, Providence, Rhode Island 02912, *U.S.A.*

(*Communicated by Sir James Lighthill, F.R.S. – Received* 12 *July* 1979)

CONTENTS

† Present address: Fluid Dynamics Department, General Motors Research Laboratories, Warren, Michigan 48090, U.S.A.

‡ On sabbatical leave 1979/80 at the Department of Mathematics, Imperial College of Science and Technology, London SW7 2BZ, U.K.

Our recent studies of the interactions between large-scale structures and fine-grained turbulence in plane mixing layers have shown that many physical features of the problem may easily be obtained from an approximate energy integral description (Liu & Merkine 1976; Alper & Liu 1978), and this is confirmed by computational models (Gatski & Liu 1980). In this work, therefore, the approximate description is used to study at length the development of large-scale coherent structures in the technologically important problem of the round turbulent jet. The analysis begins from the radially integrated form of the kinetic energy equations of the mean flow, the large-scale structure and the fine-grained turbulence, which are obtained through the use of the usual Reynolds time average and a conditional average with reference to the frequency of the idealized monochromatic component of the large-scale wavelike structure. This forms the basis for obtaining the 'amplitude equations' for the three components of the flow in terms of the mean flow momentum thickness, the large-scale structure kinetic energy and the fine-grained turbulence kinetic energy across the jet. These are obtained via the accompanying shape assumptions which also implicitly address the closure problems. The large-scale structure is also characterized by the Strouhal number $St = fd/U_e$, where f is the frequency, d is the jet diameter and U_e is the jet exit velocity, and by the azimuthal wave number n. The calculations are compared with the well controlled forced-jet observations of Binder & Favre-Marinet (1973), Favre-Marinet (1975), Favre-Marinet & Binder (1979) and Moore (1977). Although the present approximate considerations are not directed at structural details, the comparisons with observations on this aspect are most encouraging. Further theoretical work is presented that addresses the fundamental understanding of the mechanisms leading to the development of large-scale structures in turbulent jets. In general, large-scale structures in the range $0.02 \leqslant St \leqslant 1.60$ are found first to amplify in the streamwise direction and subsequently to decay. As St is increased, the streamwise location of the peak signal moves upstream, and the streamwise lifespan shortens. Consequently, high-frequency components of the large-scale structure dominate upstream while low-frequency components prevail further downstream. The Strouhal number that gives rise to maximum amplification is about 0.70 for weak initial levels of the large-scale structure and decreases to about 0.35 for very strong initial levels. As the initial energy level of the large-scale structure increases, its maximum relative amplification decreases until a level is reached beyond which the large-scale structure decays immediately downstream. This is explained in terms of the modification of the mean flow by the increasingly high energy levels of the large-scale structure in such a manner that it chokes off its own energy supply from the mean flow. At low Strouhal numbers

the $n = 1$ helical component amplifies initially more than the $n = 0$ axisymmetric component for the same initial energy level. However, the $n = 1$ mode decays subsequently much faster than the $n = 0$ mode for all Strouhal numbers. This is attributable to the azimuthally-related wave-induced turbulent shear stresses in the $n = 1$ mode which give rise to additional mechanisms for energy transfer to the fine-grained turbulence. The possible control of the large-scale structure is fully explored through considering adjustments of the energy levels of the fine-grained turbulence and changes in initial mean velocity profile through changes in the momentum thickness at the nozzle exit. Increasing the initial turbulence levels and smoothing the mean nozzle exit velocity profile places restraints upon the downstream amplification of the large-scale structure. The non-equilibrium development of the large-scale structure is sensitive to its own initial conditions and spectral content, the initial condition of the fine-grained turbulence and the mean flow. Physical and quantitative studies of the large-scale structure in turbulent shear flows thus necessitate that the nature of such an initial environment be established and understood.

1. Introduction

Observations on large-scale coherent structures in turbulent shear flows have now become rather plentiful; indeed, aspects of the problem have provoked stimulating conferences (Davies & Yule 1975; Murthy 1975; Smith & Abbott 1978). If one extends the physical ideas from nonlinear hydrodynamic instability and transition in laminar flows (Stuart 1963, 1965; Lighthill 1963), it is not entirely surprising that such instabilities and transitional structures should also occur in the geometrically similar turbulent shear flows. The mechanisms for the production of large-scale instabilities still remain; however, the competitive limitations on the strength of these instabilities come necessarily from the more efficient 'dissipative' actions of the finer-scale turbulent eddies rather than the dissipative actions of viscosity in laminar shear flows, and 'bursts' of fine-grained turbulence generally occur at the expense of large-scale coherent structures.

This interplay between large-scale coherent structures and fine-grained turbulence has been the subject of our recent work on free shear layers (Liu & Merkine 1976; Liu & Alper 1977; Liu *et al.* 1977; Alper & Liu 1978; Gatski & Liu 1980). There the mechanisms of the interaction are illustrated without the dynamical complications arising from the simultaneous occurrence of several modes of the coherent structure, or of randomized phases of a single mode. These latter phenomena, probably attributable to uncontrolled initial and background disturbances, lead to 'pairing' or agglomeration of the coherent structures (Winant & Browand 1974; Roshko 1976). Such agglomerations are also observed in laminar shear layers and are identified as subharmonic formations (Freymuth 1966; Browand 1966; Kelly 1967; Miksad 1972, 1973). It has recently been shown experimentally that the agglomeration process can be enhanced in an orderly fashion or entirely suppressed through proper control (Ho & Huang 1978; Bouchard & Reynolds 1978) so that a single mode persists downstream. It has been shown that in this situation a relatively clean experiment could conceivably be designed, to study the interactions between a single-mode coherent structure and the fine-grained turbulence.

In this paper we shall present studies of the large-scale coherent structure in a developing round turbulent jet. This problem is motivated in part by the jet noise source problem (Bishop *et al.* 1971; Liu 1974) and the need to understand the interactive roles of entrainment on the large-scale and the mixing on the fine scale in the turbulent fuel jet problem (Marble & Broadwell 1977). The basic theoretical framework utilized here follows from the approximate description based on shape assumption ideas, discussed in Liu & Merkine (1976) and Alper & Liu

PHILOSOPHICAL TRANSACTIONS OF THE ROYAL SOCIETY A MATHEMATICAL, PHYSICAL & ENGINEERING SCIENCES

(1978). A recent numerical solution of a similar problem (Gatski & Liu 1980) confirms the usefulness of those approximation ideas and demonstrates the simplicity with which the desired physical information may be obtained.

The existence of large-scale coherent structures in the initial region of a round jet has been well-established by several investigations. To bring out the earlier observations of Bradshaw *et al.* (1964) and Mollo-Christensen (1967) more clearly, Crow & Champagne (1971) repeated, under well controlled conditions, an experiment in which a disturbance of a given frequency is forced into the jet ahead of the nozzle exit and its subsequent downstream behaviour is observed. Crow & Champagne (1971) pointed out that if there is no inherent coherent structure in the unforced case, then the result of forcing will be damped. On the other hand, if there is a natural tendency toward order, the periodic forcing may raise the inherent structure above the background turbulence. By using several methods of flow visualization and by measuring the fluctuating velocity along the jet centreline, Crow & Champagne (1971) were able to detect a travelling wave system the amplitude of which reached a maximum and then decayed gradually downstream. By measuring the pressure fluctuations inside the jet and displaying their spatial signature, Chan (1974*a*, *b*) also demonstrated the instability-wavelike behaviour of the large-scale structure. Through flow visualization, Moore (1977) also showed that a turbulent round jet has a definite coherent structure that starts as an instability wave on the shear layer. Binder & Favre-Marinet (1973), Favre-Marinet (1975) and Favre-Marinet & Binder (1979) have imposed disturbances of very high relative magnitude in a turbulent round jet. By means of a butterfly valve mounted ahead of the nozzle, a periodic fluctuation of a relatively large amplitude was imposed on the mean efflux velocity. Through phase-averaging, the coherent structure was educed and its amplitude was found to rise to a maximum and then to decay farther downstream. In an experiment on a natural jet by Lau & Fisher (1975), spikes appeared regularly in the hot-wire signals. By locking to these spikes and taking the phase average of the signal, Lau & Fisher found that the shape of the resulting trace became sinusoidal. This, in effect, shows the existence of coherent structures in natural jets also. Such experimental evidence supports Roshko's (1976) conclusion that there is little doubt that coherent structures play a central role in the development of many turbulent shear flows such as mixing layers, boundary layers, and the early regions of jets and wakes. On the basis of earlier observations, Liepmann (1952) had pointed out the importance of large-scale structures some time ago.

2. Discussion of the formulation

The problem considered here is that of a jet at room temperature emitted at low speeds into still air by a nozzle of a given radius. The Reynolds number is large enough for the flow to be turbulent at the nozzle exit. The fluctuating flow components at the nozzle exit are considered here to be made up of two constituents: random fine-grained turbulence and a wavelike single-frequency large-scale coherent structure. The development of the latter is governed by its interaction with the mean flow and the fine-grained turbulence.

The problem can be viewed as a simplified model of the situation in natural or forced jets. In a natural jet the fluctuating flow components at the nozzle exit consist of fine-grained turbulence and a large-scale structure of multi-frequency components. Each frequency component of the large-scale structure interacts with the mean flow, the fine-grained turbulence and the other frequency components of the large-scale structure. The energy levels of the large-scale structure components are, in general, much lower than those of the mean flow or the fine-grained turbu-

lence. Therefore, if one considers a single-frequency component of the large-scale structure, the energy that this fundamental component exchanges with other large-scale structure frequency components may be neglected with respect to the energy that it exchanges with the mean flow or the fine-grained turbulence. Thus, the work described here models the situation in a natural jet by considering several frequency components one at a time, while neglecting the interactions among these frequency components. The *simultaneous* presence of several large-scale structure frequency components is neglected with regard to the energy exchanges.

For a forced jet, a disturbance of a single frequency is imposed upon the jet. Its development along the jet is governed by its interaction with the mean-flow, the fine-grained turbulence and the large-scale structure that is naturally present at the nozzle exit plane. However, the energy level of this forced wave is usually much higher than that of the natural large-scale structure. Hence, the energy that this forced wave exchanges with the natural large-scale structure may be neglected with respect to the energy it exchanges with the mean flow or the fine-grained turbulence. Thus, we model the forced jet here by considering a single azimuth-frequency wave identical to the forced one. The development of this forced wave is given by its interaction with the mean flow and the fine-grained turbulence, and the interaction with the natural large-scale structure is neglected.

Further, by considering the frequency of the forced wave as fixed, we exclude the vortex pairing (Winant & Browand 1974) possibly produced by the forcing of large-scale structures of different phase velocities (Liu & Alper 1977). Thus, this situation corresponds to a 'clean' experiment and we focus attention here on the interaction between the large-scale structure and the fine-grained turbulence to isolate and understand the mechanisms involved in the interaction process in a round jet.

To account for the wave's observed rotation around the jet centreline, we consider both the axisymmetric and the asymmetric azimuthal components of the large-scale structure (which observations have shown to be the two dominant components). Since the energies of these azimuthal components are, in general, much smaller than those of the mean flow or the fine-grained turbulence, the interaction between these azimuthal components can be neglected. Thus by considering these two azimuthal components one at a time, we account for the wave's rotation around the centreline, but their *simultaneous* presence is neglected with regard to the energy exchanges. Furthermore, the azimuthal wavenumber is considered to be constant along the jet. Hence switching from one azimuthal mode to another along the jet is precluded from consideration. The appearance of harmonics of the fundamental wave, observed by Crow & Champagne (1971), may also be neglected with regard to the energy exchanges. First, the energy of these harmonics is much smaller than that of the fundamental. Secondly, since these harmonics were found to be comparable to the fundamental harmonic only in the final stages of the wave's decay, their effect, if any, will be restricted to these final stages, and thus the development of the wave ahead of these final stages may be studied without taking them into consideration.

With the above simplifications, the conditional average (which is here the phase average) is taken in addition to the usual time average to sort the flow quantity into three components: steady mean flow, large-scale coherent structure and fine-grained turbulence. Observations (see, for instance, Mollo-Christensen 1967) show that the large-scale structure in a turbulent jet can be successfully modelled by a wave-train that oscillates in time and space, with its amplitude increasing or decaying along the jet. The development of this large-scale structure and its interaction with the fine-grained turbulence in a two-dimensional free shear layer have been studied by Lui & Merkine (1976) in the temporal case and by Alper & Liu (1978) in the spatial case.

PHILOSOPHICAL TRANSACTIONS OF THE ROYAL SOCIETY A MATHEMATICAL, PHYSICAL & ENGINEERING SCIENCES

In the work described here, it is emphasised that the interaction between the large-scale structure and the fine-grained turbulence is based on the detailed physical mechanisms of the wave-induced stresses. These wave-induced stresses, defined as the difference between the conditional and the time average of the instantaneous fine-grained turbulent stresses, play an essential role in the energy exchange between the large-scale structure and the fine-grained turbulence. By time-averaging the product of these stresses with the appropriate wave-rates of strain, one can explain the local kinetic energy transfer mechanism. In earlier work eddy viscosity was used to model these wave-induced stresses (Liu 1971, 1974; Merkine & Liu 1975; Morris 1974; Chan 1975). However, such an eddy viscosity model implies a one-way energy transfer mechanism from the large-scale structure to the fine-grained turbulence. Although this assumption may be true in the large, the local energy exchange can in fact go either way, from the large-scale structure to the fine-grained turbulence or vice versa. Thus, an eddy viscosity model ignores the detailed physical picture of the energy transfer mechanism although it has been useful in assessing its overall process. Favre-Marinet (1975) concluded from his experiments that an eddy viscosity model for the wave-induced stresses is incorrect locally. In work described here, therefore, we follow Liu & Merkine (1976) and Alper & Liu (1978) and obtain these wave-induced stresses, in detail, through an approximate consideration of their transport equations.

3. Conservation equations

The procedure of applying both conditional- and time-averaging techniques to describe the interactions between the mean flow, a monochromatic large-scale coherent structure and the fine-grained turbulence has been thoroughly discussed in the literature (Hussain & Reynolds 1970; Reynolds & Hussain 1972; Kendall 1970; Binder & Favre-Marinet 1973; Favre-Marinet 1975; Liu & Merkine 1976; Alper & Liu 1978; Gatski & Liu 1980). The usual time average is defined as

$$\bar{q}(x) = T^{-1}\int_0^T q(x,t)\,\mathrm{d}t,$$

where T is greater than the period τ of the large-scale structure at least. The conditional average, which is here the phase average, is defined as

$$\langle q(x,t)\rangle = \lim_{N\to\infty} N^{-1}\sum_{n=0}^{N} q(x,t+n\tau).$$

The conditional average is denoted by $\langle\ \rangle$ and the usual time average is denoted by $\bar{(\ )}$.

The relevant conservation equations for the round jet can be obtained from basic principles; one begins from, say, Appendix 2 of Batchelor (1967) and systematically applies the three-component splitting procedure and the two appropriate types of averaging (Hussain & Reynolds 1970). Here, we shall state the integrated forms of the kinetic energy equations for a round turbulent jet that is axisymmetric in the mean.

The coordinates and geometrical arrangements are shown in figure 1; x, r and ϕ are the streamwise, radial and azimuthal displacements, respectively, and u, v and w are the respective velocity components. Mean quantities will be denoted by capital letters; the large-scale structure is identified by a tilde ($\tilde{}$) and the fine-grained turbulence by a prime ($'$). The mean flow integral kinetic energy flux equation is

$$\frac{1}{2}\frac{\mathrm{d}}{\mathrm{d}x}\int_0^\infty U^3 r\,\mathrm{d}r = -\int_0^\infty (-\overline{u'v'}-\overline{\tilde{u}\tilde{v}})\frac{\partial U}{\partial r}\,r\,\mathrm{d}r, \tag{3.1}$$

PHILOSOPHICAL TRANSACTIONS OF THE ROYAL SOCIETY A MATHEMATICAL, PHYSICAL & ENGINEERING SCIENCES

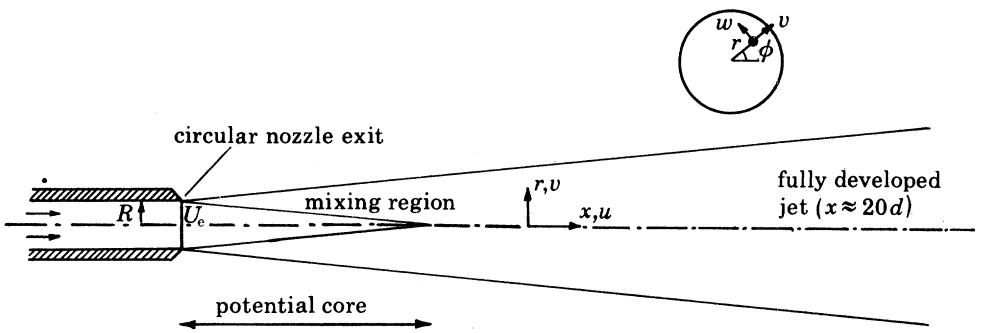

FIGURE 1. Diagram of the initial region of a round jet.

where all velocities are normalized by the jet exit velocity U_e and lengths are normalized by the nozzle radius R (subsequently, the pressure p will be normalized by ρU_e^2, where ρ is the fluid density). The large-scale structure integral kinetic energy flux equation is

$$\frac{\mathrm{d}}{\mathrm{d}x}\int_0^\infty U\bar{Q}r\,\mathrm{d}r = \int_0^\infty -\overline{\tilde{u}\tilde{v}}\frac{\partial U}{\partial r}\,r\,\mathrm{d}r - \int_0^\infty -\overline{\tilde{r}_{ij}\tilde{e}_{ij}}\,r\,\mathrm{d}r, \tag{3.2}$$

where the kinetic energy is $\bar{Q} = \frac{1}{2}\overline{\tilde{u}_i\tilde{u}_i}$, the wave-induced stresses are $\tilde{r}_{ij} = \langle u_i' u_j'\rangle - \overline{u_i' u_j'}$ and the components of the coherent-structure rate of strain tensor are

$$\tilde{e}_{xx} = \frac{\partial\tilde{u}}{\partial x}, \quad \tilde{e}_{xr} = \frac{1}{2}\left(\frac{\partial\tilde{v}}{\partial x}+\frac{\partial\tilde{u}}{\partial r}\right), \quad \tilde{e}_{x\phi} = \frac{1}{2}\left(\frac{\partial\tilde{u}}{r\partial\phi}+\frac{\partial\tilde{w}}{\partial x}\right),$$

$$\tilde{e}_{rr} = \frac{\partial\tilde{v}}{\partial r}, \quad \tilde{e}_{r\phi} = \frac{1}{2}\left[\frac{r\partial(\tilde{w}/r)}{\partial r}+\frac{\partial\tilde{v}}{r\partial\phi}\right], \quad \tilde{e}_{\phi\phi} = \frac{\partial\tilde{w}}{r\partial\phi}+\frac{\tilde{v}}{r}.$$

If the coherent structure is axisymmetric then $\tilde{e}_{x\phi}$ and $\tilde{e}_{r\phi}$ are absent. The fine-grained turbulence integral kinetic energy flux equation is

$$\frac{\mathrm{d}}{\mathrm{d}x}\int_0^\infty U\bar{q}r\,\mathrm{d}r = \int_0^\infty -\overline{u'v'}\frac{\partial U}{\partial r}\,r\,\mathrm{d}r + \int_0^\infty -\overline{\tilde{r}_{ij}\tilde{e}_{ij}}\,r\,\mathrm{d}r - \int_0^\infty \bar{\epsilon}r\,\mathrm{d}r, \tag{3.3}$$

where the turbulent kinetic energy is $\bar{q} = \frac{1}{2}(\overline{u_i' u_i'})$ and the dimensionless rate of viscous dissipation of the fine-grained turbulence is $\bar{\epsilon}$. (The rates of viscous dissipation of the mean flow and coherent structure have been neglected.)

4. SHAPE ASSUMPTIONS

As in previous work (Liu & Merkine 1976; Alper & Liu 1978), the integral energy equations provide the fundamental basis for deriving the 'amplitude' equations for the study of nonlinear interactions among the three cascading scales of motion after shape assumptions are made. The parameters that characterize the mean jet flow are the local momentum thickness and the jet centreline velocity; these are related through the conservation of total jet momentum flux, thus leaving, say, the momentum thickness as the sole parameter. The large-scale structure and the fine-grained turbulence are characterized by their respective energy content across a slice of the jet. Essentially, the closure problems are entirely encompassed in the shape assumptions that follow.

(*a*) *The mean flow*

Using Freymuth's (1966) experimental results, Michalke (1971) proposed the following two profiles that were used subsequently by Favre-Marinet (1975) and Morris (1977) to describe the adjustment from a top-hat profile, at the nozzle exit, to a fully developed jet profile downstream. Near the nozzle exit, where the local momentum thickness $\theta < 0.08$, the mean flow velocity is given by profile I:

$$U/U_c = \begin{cases} 1, & 0 \leqslant r < 1-\frac{1}{2}\delta, \\ \frac{1}{2}\{1+\tanh[(1-r)/2\theta]\}, & 1-\frac{1}{2}\delta < r, \end{cases} \tag{4.1a}$$

where U_c is the mean velocity at the jet centreline, δ is the shear layer thickness (chosen such that $\tanh(\delta/4\theta) \approx 1$, in order to minimize the discontinuity of the profile at $r = 1-\frac{1}{2}\delta$) and θ is the local momentum thickness. In the region toward the end of the potential core, where $\theta \geqslant 0.08$, the mean flow velocity profile is given by profile II:

$$U/U_c = \tfrac{1}{2}\{1+\tanh[(r^{-1}-r)/4\theta]\}. \tag{4.1b}$$

The first profile is equivalent to the hyperbolic tangent profile of a plane free shear layer (Liepmann & Laufer 1947). Such a similarity is not surprising since, close to the jet exit, the axisymmetric shear layer is approximately two-dimensional. The transition from one profile to the other is smooth and the two profiles are almost identical at the switching location $\theta = 0.08$. Near $r = 1$, $(r^{-1}-r)/4\theta \approx (1-r)/2\theta$, profile II could thus have been directly used to represent the mean velocity profile near $r = 1$ for small θ. However, it could not adequately describe the top-hat nature of the profile near the jet nozzle exit. Profile I is thus used for $\theta < 0.08$ (which is attained when $x < d$) in the computation for $x < d$ only, while profile II is used for the rest of the jet. The latter is a good approximation of the jet transition region and not of the fully developed jet. Our interest is primarily in the study of large-scale structures, the decay of which takes place, essentially before the fully developed region. Our concern here, therefore, does not include profiles further downstream.

The mean flow shape given by (4.1) represents a family of profiles governed by the two parameters U_c and θ. These two parameters are related through the integral momentum equation

$$\int_0^\infty U^2 r\,\mathrm{d}r = \text{const.}$$

Thus, only one parameter, θ, is left to be determined by the energy exchange among the three flow components. The mean flow shape is coupled, through θ, with the large-scale structure as well as with the fine-grained turbulence. Thus we obtain $U_c = 1$ for profile I; for profile II, U_c is a slowly decreasing function of θ, in accordance with the general experimental observations (see for example, Maestrello & McDaid (1971)). However, the actual distribution of U_c along the jet cannot be known until θ along the jet is obtained from the nonlinear analysis. Because the mean flow shape depends explicitly on θ and only implicitly on x, the radial integrals involved in the integral energy equations can be obtained for a given θ instead of a given x. Therefore, in the shape assumptions that follow, functional dependence on x will, for convenience, be replaced by functional dependence on θ.

(*b*) *The fine-grained turbulence correlations*

With regard to the fine-grained turbulent stresses, Mellor & Herring (1973) point out that it is appropriate to compute the turbulent kinetic energy, since it is the primary property that dis-

tinguishes a turbulent from a laminar flow; the turbulent stresses can be related to the turbulent energy through a relation representing the departure from isotropy:

$$\overline{u_i' u_j'} = (\alpha_{ij} + \tfrac{1}{3}\delta_{ij})\,\bar{q}, \tag{4.2}$$

where the constants α_{ij} are such that $\alpha_{ii} = 0$, with repeated indices denoting the summation convention; δ_{ij} is the Kronecker delta.

Guided by the measurements of Bradshaw *et al.* (1964), Candel, Guedel & Julienne (1975), Davies *et al.* (1963), Ko & Davies (1971), Laurence (1956) and Sami *et al.* (1967), we model the turbulent stresses in the jet as

$$\overline{u_i' u_j'} = a_{ij}\,E(x)\,G(\theta)\exp(-\eta^2), \tag{4.3}$$

where $\eta^2 = (r-1)^2/\theta^2 c_1$ and a_{ij} and c_1 are constants. Within the potential core, $\overline{u_i' u_j'}$ has the same value as it does at the inner edge of the shear layer. The constants a_{ij}, relative to a_{11}, are, from the above experiments,

$$\begin{bmatrix} a_{11} \\ a_{22} \\ a_{33} \\ a_{12} \\ a_{13} \\ a_{23} \end{bmatrix} = \begin{bmatrix} 1.00 \\ 0.50 \\ 0.50 \\ 0.33 \\ 0.00 \\ 0.00 \end{bmatrix}, \tag{4.4}$$

and c_1 is taken to be 20 to give the best match with experiments up to $x/d \approx 10$. The coefficient $G(\theta)$ is a normalization function which gives $E(x)$ as the fine-grained turbulence energy over a disk across the jet. Thus

$$E(x) = \int_0^\infty \bar{q} r\,\mathrm{d}r. \tag{4.5}$$

Consequently, it follows from (4.3) and (4.5) that $G(\theta)$ is defined as

$$G(\theta) = 1 \Big/ \int_0^\infty \exp(-\eta^2)\, r\,\mathrm{d}r. \tag{4.6}$$

Equation (4.3) is thus the same as (4.2) provided that the local energy, $\bar{q}$, is related to the integrated energy, E, through the exponential shape of (4.3).

The shape assumption (4.3) is similar to that of Liu & Merkine (1976) and Alper & Liu (1978) for the plane mixing layer. However, $E(x)$ is taken here to be the integrated energy across the jet, while in the plane mixing layer problem it was taken as an energy density, the total energy per unit shear layer thickness. The normalization function here, $G(\theta)$, corresponds to the normalization constant $\sqrt{\pi}$ in the plane mixing layer problem. The vertical distribution here, however, is given in terms of the momentum thickness θ instead of the shear layer thickness.

The magnitude and local shape of $\overline{u_i' u_j'}$ are thus functions of E and θ respectively. Since both E and θ are determined from the nonlinear analysis, both the magnitude and the local shape of $\overline{u_i' u_j'}$ are coupled to the mean flow and the large-scale structure.

Mellor & Herring (1973) pointed out that almost all investigators base their models of viscous dissipation on its relation to the isotropic small-scale turbulence, and take it to be

$$\bar{\epsilon} = a_2\,\bar{q}^{\frac{3}{2}}/\delta, \tag{4.7}$$

where $a_2 \approx 1.5$. This is the same model as that used by Alper & Liu (1978), following Bradshaw *et al.* (1967). The shear layer thickness is related to the momentum thickness by $\delta = a_3\theta$, where $a_3 \approx 4.4$ for the mean velocity profile (4.1).

(c) *The large-scale coherent structure*

By following previous works (for example, Alper & Liu 1978), the radial distribution of the large-scale structure and the wave-induced stresses will be given by the local linear theory, but the finite amplitude function $A(x)$ is to be simultaneously solved with $E(x)$ and $\theta(x)$. The shape assumption for the large-scale structure, which essentially evolved from studies of such structures in laminar transitional flows (Ko *et al.* 1970; Ko 1971; Liu & Gururaj 1974; Liu & Lees 1970; Stuart 1958), then takes the form

$$\begin{bmatrix}\tilde{u}_i\\ \tilde{p}\\ \tilde{r}_{ij}\end{bmatrix} = A(x)\exp\mathrm{i}\left(\int_0^x \alpha_{\mathrm{r}}(\xi)\,\mathrm{d}\xi - \omega t + n\phi\right)\begin{bmatrix}\hat{u}_i(r;\theta,St,n)\\ \hat{p}(r;\theta,St,n)\\ E(x)\,\hat{r}_{ij}(r;\theta,St,n)\end{bmatrix} + \begin{bmatrix}\text{c.c.}\\ \text{c.c.}\\ \text{c.c.}\end{bmatrix}, \tag{4.8}$$

where c.c. denotes a complex conjugate, α_{r} is the streamwise wave number, n is the azimuthal wave number, ω is the frequency and $A(x)$ is the complex amplitude function. We recall that all physical length scales have been made dimensionless by the jet radius R and all velocities by the jet exit velocity U_{e}. The radial shape functions are denoted by $(\hat{\ })$, and their implicit dependence upon x results from the dependence of the local linear theory upon the momentum thickness $\theta(x)$. The radial shape functions are dependent also on n and ω, the latter through the Strouhal number $St = fd/U_{\mathrm{e}}$, where $f = \omega/2\pi$ is the frequency in hertz. Several observations, such as those of Crow & Champagne (1971), Binder & Favre-Marinet (1973), Favre-Marinet (1975) and Moore (1977), lend strong support to the travelling-wave representation of the large-scale structure. That $\tilde{r}_{ij} \propto E$ in (4.8) will be apparent from the discussion of the transport equation for $\tilde{r}_{ij}$ that is to follow.

The radial shape functions $\hat{u}_i$, $\hat{p}$ and $\hat{r}_{ij}$ form a coupled linear local parallel flow problem, and in obtaining their governing equations from the original nonlinear conservation equations E is taken as constant and A is taken locally as being exponential in x, $\exp(-\mathrm{i}\int_0^x \alpha_{\mathrm{i}}(\xi)\,\mathrm{d}\xi)$, where α_{i} is the imaginary part of the complex wave number α. We thus have the continuity and momentum equations

$$\mathrm{i}\alpha\hat{u} + \frac{1}{r}(r\hat{v})' + \frac{\mathrm{i}n}{r}\hat{w} = 0, \tag{4.9}$$

$$\mathrm{i}\alpha(U-c)\begin{bmatrix}\hat{u}\\ \hat{v}\\ \hat{w}\end{bmatrix} + \begin{bmatrix}\hat{v}\\ 0\\ 0\end{bmatrix}U' = -\begin{bmatrix}\mathrm{i}\alpha\\ D\\ \mathrm{i}n/r\end{bmatrix}\hat{p} + \mathrm{i}\alpha\begin{bmatrix}\hat{r}_{xx}\\ \hat{r}_{xr}\\ \hat{r}_{x\phi}\end{bmatrix} + \frac{1}{r}D\left(r\begin{bmatrix}\hat{r}_{xr}\\ \hat{r}_{rr}\\ \hat{r}_{r\phi}\end{bmatrix}\right) + \frac{\mathrm{i}n}{r}\begin{bmatrix}\hat{r}_{x\phi}\\ \hat{r}_{r\phi}\\ \hat{r}_{\phi\phi}\end{bmatrix}, \tag{4.10}$$

where c is the complex phase velocity, and both D and $(\ )'$ in (4.9) and (4.10) denote differentiation with respect to r. In (4.10), momentum diffused by the wave-induced stresses replaces that diffused by viscous stresses. The system (4.9) and (4.10) is coupled to the governing equations for $\hat{r}_{ij}$, which are

$$\mathrm{i}\alpha(U-c)\begin{bmatrix}\hat{r}_{xx}\\ \hat{r}_{rr}\\ \hat{r}_{\phi\phi}\\ \hat{r}_{xr}\\ \hat{r}_{x\phi}\\ \hat{r}_{r\phi}\end{bmatrix} + \begin{bmatrix}2\hat{r}_{xr}\\ 0\\ 0\\ \hat{r}_{rr}\\ \hat{r}_{r\phi}\\ 0\end{bmatrix}U' + \frac{1}{T}\begin{bmatrix}\hat{r}_{xx}-\frac{1}{3}\hat{r}_{kk}\\ \hat{r}_{rr}-\frac{1}{3}\hat{r}_{kk}\\ \hat{r}_{\phi\phi}-\frac{1}{3}\hat{r}_{kk}\\ \hat{r}_{xr}\\ \hat{r}_{x\phi}\\ \hat{r}_{r\phi}\end{bmatrix} + \tfrac{1}{2}a_{12}U'\begin{bmatrix}\hat{r}_{kk}\\ \hat{r}_{kk}\\ \hat{r}_{kk}\\ 0\\ 0\\ 0\end{bmatrix}$$

advection by the mean flow — production — pressure–velocity correlation — dissipation

$$= -\hat{v}\begin{bmatrix} R'_{xx} \\ R'_{rr} \\ R'_{\phi\phi} + 2R_{\phi\phi}/r \\ R'_{xr} \\ 0 \\ 0 \end{bmatrix} - \frac{\hat{w}}{r}\begin{bmatrix} 0 \\ 0 \\ 0 \\ 0 \\ R_{xr} \\ -2R_{\phi\phi} + R_{rr} \end{bmatrix} - \begin{bmatrix} 2(R_{xx}\,\mathrm{i}\alpha + R_{xr}D)\,\hat{u} \\ 2(R_{xr}\,\mathrm{i}\alpha + R_{rr}D)\,\hat{v} \\ 2R_{\phi\phi}\,\mathrm{i}n\hat{w}/r \\ (R_{xx}\,\mathrm{i}\alpha + R_{xr}D)\,\hat{v} + (R_{xr}\,\mathrm{i}\alpha + R_{rr}D)\,\hat{u} \\ (R_{xx}\,\mathrm{i}\alpha + R_{xr}D)\,\hat{w} + R_{\phi\phi}\,\mathrm{i}n\hat{u}/r \\ (R_{xr}\,\mathrm{i}\alpha + R_{rr}D)\,\hat{w} + R_{\phi\phi}\,\mathrm{i}n\hat{v}/r) \end{bmatrix}, \quad (4.11)$$

advection of mean stresses by wave

work done by the mean stresses against wave rates of strain

where $T^{-1} = -1.445\partial U/\partial r > 0$ is the time scale for return to isotropy and $\hat{r}_{kk} = \hat{r}_{xx} + \hat{r}_{rr} + \hat{r}_{\phi\phi}$. These equations are supplemented by the appropriate boundary conditions (see Reynolds (1972) for a discussion of the conditions across a turbulent-non-turbulent interface appropriate for (4.10) and (4.11)).

As (4.9) and (4.10) were obtained from their respective original conservation equations, (4.11) was obtained from the nonlinear transport equation derived for $\tilde{r}_{ij}$. The sources on the right side of (4.11) reveal that, to lowest order, $\tilde{r}_{ij}$ must be proportional to the product of a large-scale structure quantity and a mean turbulent stress, such that as formed by the work done by the mean stresses against the rates of strain of the large-scale structure. In this situation, the $\tilde{r}_{ij}$ are indeed proportional to $A(x)\,E(x)$ as postulated in (4.8).

In obtaining (4.11), closure assumptions for the modulated turbulence quantities are used and these are patterned after those for the mean quantities (Liu & Merkine 1976; Alper & Liu 1978). These included the modulated pressure–velocity correlations

$$-\left(\left\langle u'_j \frac{\partial p'}{\partial x_i}\right\rangle - \overline{u'_j \frac{\partial p'}{\partial x_i}} + \left\langle u'_i \frac{\partial p'}{\partial x_j}\right\rangle - \overline{u'_i \frac{\partial p'}{\partial x_j}}\right) = \frac{1}{T}\left(\tilde{r}_{ij} - \tfrac{1}{3}\tilde{r}_{kk}\,\delta_{ij}\right),$$

which is patterned after Rotta's (1962) closure model for the corresponding mean quantities. The modulated viscous dissipation rate is taken to be

$$\tilde{\epsilon} = \tfrac{3}{4}a_{12}\frac{\partial U}{\partial r}\,\tilde{r}_{kk}$$

by following Alper & Liu (1978). In the $\tilde{\epsilon}$-relation, the local equilibrium value of $\bar{q}$ is taken to approximate $\bar{q}^{\frac{1}{2}}$. The sensitivity of such assumptions in the overall nonlinear interaction problem for A, E and θ is checked numerically by inserting an approximation for $\bar{q}$ that takes no account of the large-scale structure. It is found that the overall interaction problem is not sensitive to such closure assumptions, for the determination of the stress shape functions $\hat{r}_{ij}$. This is to be expected, since $\hat{r}_{ij}$ enters the problem in the integral for the energy transfer process, which smooths the local variations or errors in the computations for $\hat{r}_{ij}$.

Since we are considering an axisymmetric jet with no swirl, the mean stresses $\overline{u'w'}$ and $\overline{v'w'}$ are absent. Thus they play no role in (4.11), for $\hat{r}_{ij}$, in terms of the shape functions $R_{x\phi}$ and $R_{r\phi}$ advected radially and azimuthally by the large-scale structure. For the axisymmetric mode of the large-scale structure, $n = 0$ and $\hat{w} = 0$; (4.11) then shows that both $\hat{r}_{r\phi}$ and $\hat{r}_{x\phi}$ vanish identically. In this case, except for the curvature effects through $\hat{v}/r$, the system of equations for $\hat{r}_{xx}$, $\hat{r}_{rr}$, $\hat{r}_{\phi\phi}$ and $\hat{r}_{xr}$, is entirely analogous to that for the plane shear layer problem (Liu & Merkine 1976; Alper & Liu 1978). For asymmetrical modes of the large-scale structure $\hat{w}$ and n do not vanish and $\hat{r}_{x\phi}$ and $\hat{r}_{r\phi}$ are both present, as are additional contributions to the sources for $\hat{r}_{\phi\phi}$ and $\hat{r}_{xr}$ owing, to

PHILOSOPHICAL TRANSACTIONS OF THE ROYAL SOCIETY A MATHEMATICAL, PHYSICAL & ENGINEERING SCIENCES

the asymmetry. Thus for $n \neq 0$, additional mechanisms for energy transfer between the large-scale structure and fine-grained turbulence are anticipated.

By using the arguments of Liu & Merkine (1976) about the large-scale structure in inflexional mean flows arising as a result of dynamical instabilities, (4.10) and (4.11) can be considerably simplified: the diffusive effects of the wave-induced stresses can be omitted as far as the shape characteristics of the large-scale structure are concerned, the latter being given, to a good approximation, by an 'inviscid' consideration. This then uncouples (4.10) from (4.11). After $\hat{u}$, $\hat{v}$ and $\hat{w}$ have been obtained from the simplified (4.10), they serve as advecting velocities in (4.11) in the solution for $\hat{r}_{ij}$. The distribution of energy transfer between the large-scale structure and fine-grained turbulence across the jet is then obtained from $\overline{\tilde{r}_{ij}\,\tilde{e}_{ij}} = A(x)\,E(x)\,\hat{r}_{ij}\,\hat{e}_{ij}$. The eigenfunctions $\hat{u}_i, \hat{p}$ are normalized in such a manner that $|A(x)|^2$ becomes the kinetic energy content of the large-scale structure across the jet:

$$|A(x)|^2 = \int_0^\infty \bar{Q} r \, \mathrm{d}r.$$

The 'inviscid' forms of (4.10) and (4.9), with the usual boundary conditions appropriate for the *inviscid* problem, together form an eigenvalue problem. The mean flow shapes appropriate for the jet, (4.1*a*) and (4.1*b*), are not similar, and therefore (4.9) and (4.10) cannot be cast into a general form independent of $\theta(x)$. Thus, for a given azimuthal wave number n and Strouhal number St, (4.9) and (4.10) are solved for a given local momentum thickness θ. Similar considerations apply to $\hat{r}_{ij}$. To follow a given mode (St, n) downstream, the shape functions $\hat{u}, \hat{v}, \hat{w}, \hat{p}$ and $\hat{r}_{ij}$ are obtained in terms of a series of values of θ. The detailed distribution of θ as a function of x must necessarily come from the *nonlinear* problem involving a simultaneous solution for $\theta(x)$, $E(x)$, and $A(x)$ via (3.1)–(3.3), as in Liu & Merkine (1976) and Alper & Liu (1978).

The method of solution for the inviscid problem (4.9) and (4.10). is well-known (see, for instance, Batchelor & Gill 1962; Lees & Gold 1964; Betchov & Criminale 1967; Michalke 1971). In the numerical problem, Michalke's (1971) formalism is used for amplified solutions. For damped solutions, a method similar to that discussed by Lin (1955) and Mack (1965) is followed. We note that for $n = 0$: $\hat{u} \neq 0$; $\hat{p} \neq 0$ and $\hat{v} = 0$ on the jet centreline, while for $n = 1$: $\hat{u} = \hat{p} = 0$ and $\hat{v} \neq 0$. If $\tilde{p}$ or $\tilde{u}$ occurs along the jet centreline, they must arise only from the axisymmetric mode. If $\tilde{v}$ occurs along the jet centreline, it must have been contributed by the asymmetric modes. The local eigenvalues, including the phase velocities, are obtained as functions of θ. We shall delay discussion of these eigenvalues until $\theta(x)$ has been obtained from the nonlinear interaction problem.

The velocity shape functions $\hat{u}_i$ obtained as described above are then utilized in (4.11) for the algebraic solution for $\hat{r}_{ij}$. It is of interest to discuss some features of $\hat{r}_{ij}$ since they are obtained from fundamental, though approximate, considerations and contribute to the important energy exchange mechanisms between the large-scale coherent and random fine-scaled motions. The exchange mechanisms here are quite different from the plane mixing layer problem (Liu & Merkine 1976; Alper & Liu 1978), not only in the curvature effect but also in the possibility of energy transfer mechanisms for the $n = 1$ mode additional to those of the $n = 0$ mode, as pointed out earlier. Typical radial distributions of $|\hat{r}_{ij}|$ are presented in figure 2 for $St = 0.5$, $\theta = 0.08$, and $n = 0$ and $n = 1$. Since both $\overline{u_i' u_j'}$ and $\tilde{u}_i$ diminish outside the shear layer, the $|\hat{r}_{ij}|$ vanish rapidly away from $r = 1$. For $n = 0$, $|\hat{r}_{xr}|$, $|\hat{r}_{rr}|$ and $|\hat{r}_{\phi\phi}|$ are of the same order, while $|\hat{r}_{xx}| \approx 2|\hat{r}_{xr}|$. Both $|\hat{r}_{x\phi}| = 0$ and $|\hat{r}_{r\phi}| = 0$, as noted earlier. The results are consistent with the assumed ratio of mean turbulent stresses given in (4.4), stresses which are the sources for the $|\hat{r}_{ij}|$. The shape

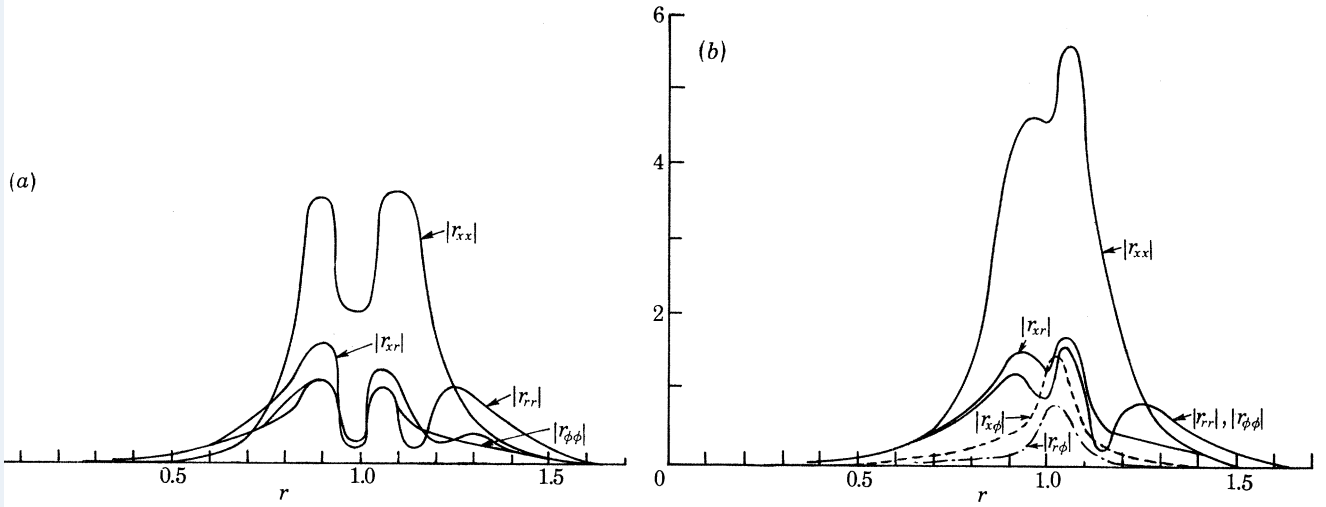

FIGURE 2. Magnitude of the wave-induced stresses, $|r_{xx}|$, $|r_{rr}|$, $|r_{\phi\phi}|$, $|r_{xr}|$, $|r_{x\phi}|$, $|r_{r\phi}|$, across the jet. $St = 0.5$, $\theta = 0.08$. (*a*) $n = 0$, (*b*) $n = 1$.

functions $|\hat{r}_{ij}|$ are similar for $n = 0$ and 1. However, the $|\hat{r}_{ij}|$ for $n = 1$ are slightly larger than the corresponding $|\hat{r}_{ij}|$ for $n = 0$. In addition, $|\hat{r}_{x\phi}|$ and $|\hat{r}_{r\phi}|$, which are zero for $n = 0$, attain non-negligible values for $n = 1$. The difference in the behaviour of $|\hat{r}_{ij}|$ for $n = 0$ and $n = 1$ follows directly from (4.11) through the additional sources for the $n = 1$ mode: the work done by the mean stresses against the azimuthal large-scale rates of strain and the azimuthal advection of mean stresses by the large-scale structure. These sources vanish for $n = 0$. Consequently, the azimuthal motion of the large-scale structure for $n = 1$ produces $\tilde{r}_{x\phi}$ and $\tilde{r}_{r\phi}$, and enhances the rest of the wave-induced stresses.

The local energy transfer between the large-scale structure and the fine-grained turbulence is obtained by multiplying each $\tilde{r}_{ij}$ by the appropriate large-scale rates of strain, as in the integrand of (3.2) or (3.3). To bring out the role of $\tilde{r}_{ij}$, the local energy transfer by each $\tilde{r}_{ij}$ component is shown in figure 3 for $St = 0.5$, $\theta = 0.08$, and $n = 0$ and $n = 1$. Since both the large-scale rates of strain and $\tilde{r}_{ij}$ vanish away from the centre of the shear layer, the energy transfer is localized around $r = 1$. The relative phase between $\tilde{r}_{ij}$ and the rates of strain determines the direction of this transfer. The total energy transfer between the large-scale structure and the fine-grained turbulence is the sum of the local transfers integrated across the jet. Since most of the local energy transfer is positive, the direction of the net total energy transfer is anticipated to be from the large-scale structure to the fine-grained turbulence. However, it is also clear from figure 3 that the local energy transfer can be in both directions; by no means is it restricted to being from the large-scale structure to the fine-grained turbulence. This indicates the intrinsic weaknesses in the eddy viscosity model. Now, $\hat{r}_{xx}$ is the largest among all the wave-induced stresses and the large-scale rates of strain corresponding to $\hat{r}_{xr}$ are the greatest; thus the $\tilde{r}_{xx}$ and $\tilde{r}_{xr}$ components produce the largest energy transfer, as can be seen from figures 3*a–f*. This also indicates that the stresses and rates of strain for the *xx*- and *xr*-components are also nearly in phase. Figure 3 also shows that the local energy transfer is larger for $n = 1$ than for $n = 0$. For this mode the values of $\hat{r}_{ij}$ are larger and additional local energy transfer mechanisms are produced by the azimuthal large-scale rates of strain, namely

$$\overline{\tilde{r}_{x\phi}\left(\frac{1}{r}\frac{\partial\tilde{u}}{\partial\phi}+\frac{\partial\tilde{w}}{\partial x}\right)}, \quad \overline{\tilde{r}_{\phi\phi}\left(\frac{1}{r}\frac{\partial\tilde{w}}{\partial\phi}\right)}, \quad \overline{\tilde{r}_{r\phi}\left(\frac{1}{r}\frac{\partial\tilde{v}}{\partial\phi}+\frac{\partial\tilde{w}}{\partial r}-\frac{\tilde{w}}{r}\right)}.$$

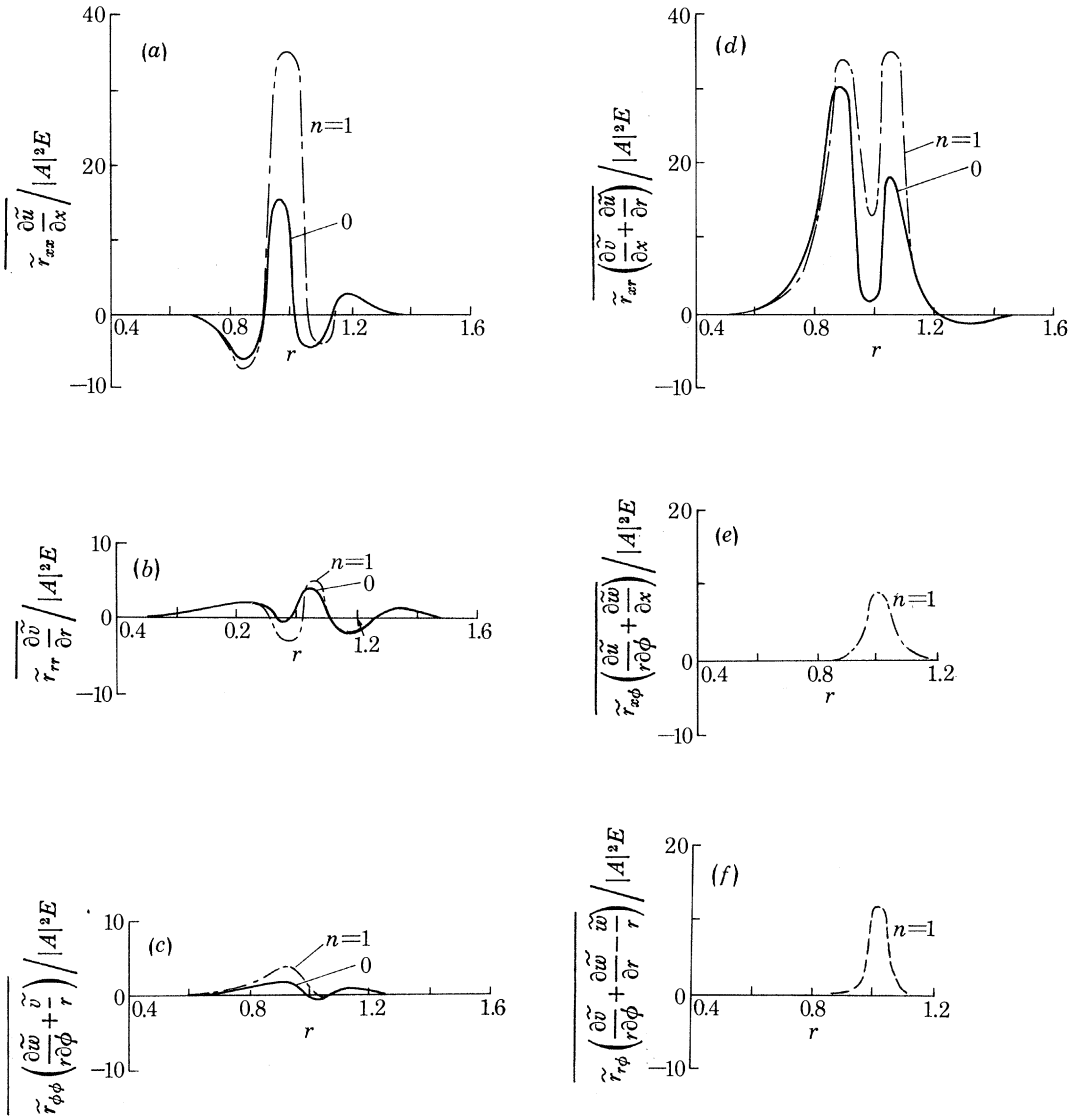

FIGURE 3. Contributions to the energy transfer mechanisms between the large-scale structure and the fine-grained turbulence across the jet; $n = 0$ and $n = 1$, $St = 0.5$, $\theta = 0.08$. (*a*) xx-mechanism, (*b*) rr-mechanism, (*c*) $\phi\phi$-mechanism, (*d*) xr-mechanism, (*e*) $x\phi$-mechanism, (*f*) $r\phi$-mechanism.

Such mechanisms are absent for $n = 0$. Thus, the $n = 1$ mode has additional mechanisms by which local energy can be transferred between the large-scale structure and the fine-grained turbulence and thus the total energy transfer for this mode is larger than that for the $n = 0$ mode.

5. NONLINEAR ANALYSIS

In this section we shall present the nonlinear 'amplitude' equations and discuss the properties of the interaction integrals which are coefficients in such equations.

The following set of three nonlinear ordinary differential equations for θ, $|A|^2$ and E is obtained after the substitution of the shape assumptions of §4 into (3.1)–(3.3):

$$\frac{1}{2}\frac{\mathrm{d}}{\mathrm{d}x} I_1(\theta) = -I'_{\mathrm{R.s.}}(\theta)\, E - \tilde{I}_{\mathrm{R.s.}}(\theta; St, n)\, |A|^2, \tag{5.1}$$

$$\frac{\mathrm{d}}{\mathrm{d}x}[I_2(\theta; St, n)\, |A|^2] = \tilde{I}_{\mathrm{R.s.}}(\theta; St, n)\, |A|^2 - I_{\mathrm{w.t.}}(\theta; St, n)\, |A|^2 E, \tag{5.2}$$

$$\frac{\mathrm{d}}{\mathrm{d}x}[I_3(\theta)\, E] = I'_{\mathrm{R.s.}}(\theta)\, E + I_{\mathrm{w.t.}}(\theta; St, n)\, |A|^2 E - I_\epsilon(\theta)\, E^{\frac{3}{2}}. \tag{5.3}$$

The initial conditions are $\theta(0) = \theta_0$, $|A(0)|^2 = |A|_0^2$ and $E(0) = E_0$.

Because of the shape assumptions discussed in §4, integrals involving only the mean flow velocity profile and mean fine-grained turbulence stresses are functions of the local momentum thickness alone, while integrals involving the large-scale structure depend not only on θ but also on St and n. The mean flow energy advection integral is defined as

$$I_1(\theta) = \int_0^\infty U^3 r\, \mathrm{d}r.$$

Note that (5.1) is actually an equation for $\mathrm{d}\theta/\mathrm{d}x$ with $\mathrm{d}I_1(\theta)/\mathrm{d}\theta < 0$. The large-scale structure energy advection integral is

$$I_2(\theta; St, n) = \int_0^\infty U(|\hat{u}|^2 + |\hat{v}|^2 + |\hat{w}|^2)\, r\, \mathrm{d}r,$$

and the fine-grained turbulence energy advection integral is

$$I_3(\theta) = G(\theta) \int_0^\infty U \exp(-\eta^2)\, r\, \mathrm{d}r.$$

The production integrals of the fine-grained turbulence and large-scale structure are, respectively

$$I'_{\mathrm{R.s.}}(\theta) = (-a_{12})\, G(\theta) \int_0^\infty \exp(-\eta^2)\, \frac{\partial U}{\partial r}\, r\, \mathrm{d}r,$$

$$\tilde{I}_{\mathrm{R.s.}}(\theta; St, n) = -2 \int_0^\infty \mathrm{Re}\,(\hat{u}\hat{v}^*)\, \frac{\partial U}{\partial r}\, r\, \mathrm{d}r,$$

where Re denotes the real part and $(\ )^*$ denotes the complex conjugate of $(\ )$. The large-scale structure–turbulence energy exchange integral is

$$\begin{aligned} I_{\mathrm{w.t.}}(\theta; St, n) = -2 \int_0^\infty \mathrm{Re}\{&\hat{r}^*_{xx}(\mathrm{i}\alpha\hat{u}) + \hat{r}^*_{rr}\hat{v}' + \hat{r}^*_{\phi\phi}(\mathrm{i}n\hat{w}/r + \hat{v}/r) \\ &+ \hat{r}^*_{r\phi}[\mathrm{i}n\hat{v}/r + r(\hat{w}/r)'] + \hat{r}^*_{x\phi}(\mathrm{i}n\hat{u}/r + \mathrm{i}\alpha\hat{w}) + \hat{r}^*_{xr}(\mathrm{i}\alpha\hat{v} + \hat{u}')\}r\, \mathrm{d}r, \end{aligned}$$

where $(\ )^*$ again denotes the complex conjugate and $(\ )'$ denotes differentiation with respect to r. The fine-grained turbulence dissipation integral is

$$I_\epsilon(\theta) = (a_2/a_3\theta)\, G^{\frac{3}{2}}(\theta) \int_0^\infty \exp(-\tfrac{3}{2}\eta^2)\, r\, \mathrm{d}r.$$

The integrals which involve only the mean flow† and mean turbulence stresses, I_1, I_3, $I'_{\mathrm{R.s.}}$ and I_ϵ, are functions of θ alone and are shown in figure 4, as is the normalization function $G(\theta)$. The

† The integrand in each case vanished rapidly outside the jet, the integrals converged and there was no need to use a 'fairing' technique as was used by Crow & Champagne (1971).

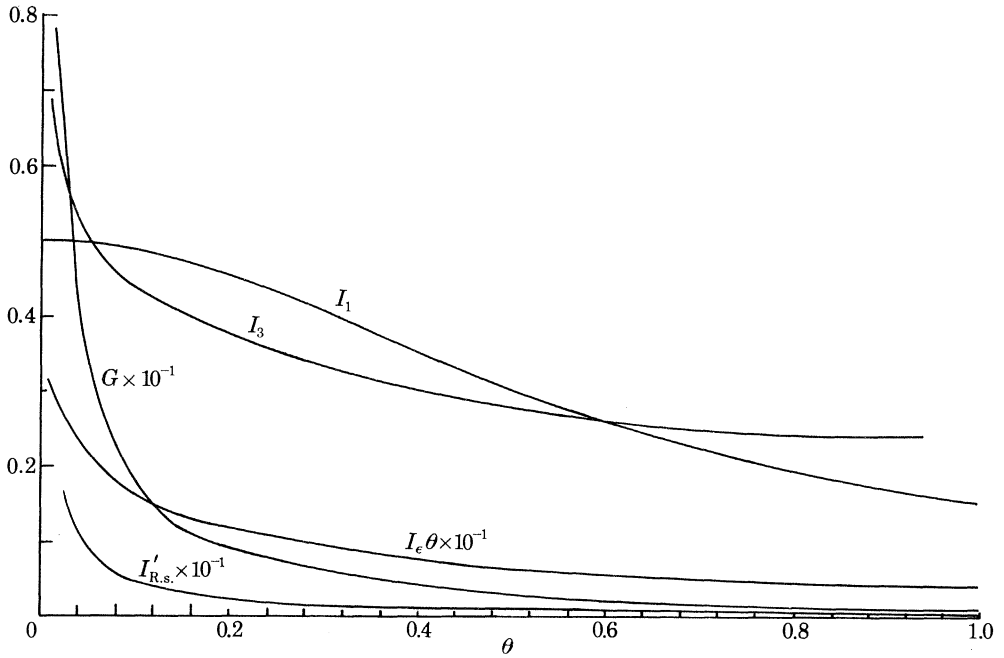

FIGURE 4. Mean flow and fine-grained turbulence energy advection integrals I_1 and I_3, fine-grained turbulence production and dissipation integrals $I'_{R.S}$ and I_ϵ, and normalization function G as functions of the local displacement thickness θ.

slope of $I_1(\theta)$ is always negative and (5.1) indicates that the energy loss from the mean flow produces a growth in the mean flow momentum thickness. Since the mean shear decreases with increasing θ, $I'_{R.S.}(\theta)$ is a decreasing function of θ; it is, however, always positive, indicating that energy is transferred from the mean flow to the fine-grained turbulence. The integral $I_3(\theta)$ decreases along the jet to an asymptotic value of about 0.24. The integral I_ϵ is a rapidly decreasing function of θ, and is therefore normalized by θ^{-1}, for plotting in figure 4. The function $G(\theta)$ is a measure of the jet spreading and for most of the jet (except the initial region) can be approximated by $G(\theta) \sim \theta^{-1}$. All the mean motion integrals I_1, I_3, $I'_{R.S.}$ and I_ϵ tend to become constant for large θ. This indicates the possibility that self-similarity is achievable far downstream within the present framework.

From the shape assumptions for the large-scale structure discussed in § 4, we see that the integrals I_2, $\tilde{I}_{R.S.}$ and $I_{w.t.}$ are functions of θ, St and n. They are shown in figures 5–7 for the $n = 0$ and $n = 1$ modes. As a result of the radial spreading of the jet, I_2 is a gradually increasing function of θ and its distribution has the same trend for both values of n, as shown in figure 5. The rate at which I_2 varies along the jet increases with Strouhal number. Since the mean shear is inversely proportional to θ, the tendency toward instability decreases along the jet. Therefore, the production integral $\tilde{I}_{R.S.}$ is a decreasing function of θ, as shown in figure 6. For small Strouhal numbers, $\tilde{I}_{R.S.}$ asymptotically approaches zero downstream. As the Strouhal number increases, the wave oscillates rapidly and the rate of energy transfer between the large-scale structure and the mean flow increases, on average. Thus the initial value of $\tilde{I}_{R.S.}$ increases, but it goes rapidly to negative values along the jet, corresponding to the damped linear solution. (This feature is also observed in direct numerical computations (Gatski & Liu 1980).) A negative value of $\tilde{I}_{R.S.}$ indicates a reversal in the direction of energy transfer. Thus, in the initial region of the jet, energy is transferred from the mean flow to the large-scale structure. But downstream, for large Strouhal

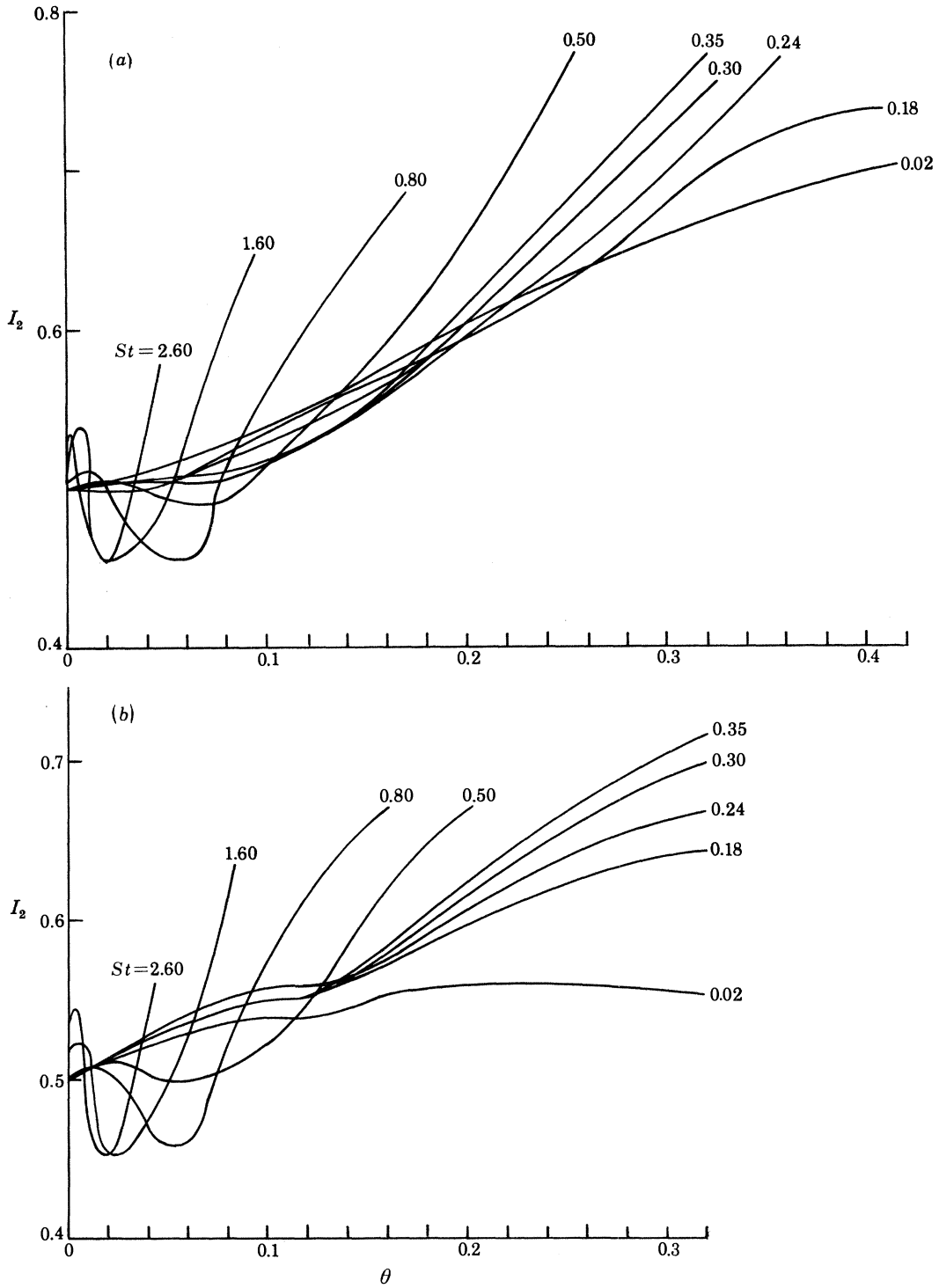

FIGURE 5. Large-scale structure energy advection integral I_2 as a function of the local displacement thickness θ for various Strouhal numbers. (*a*) $n = 0$, (*b*) $n = 1$.

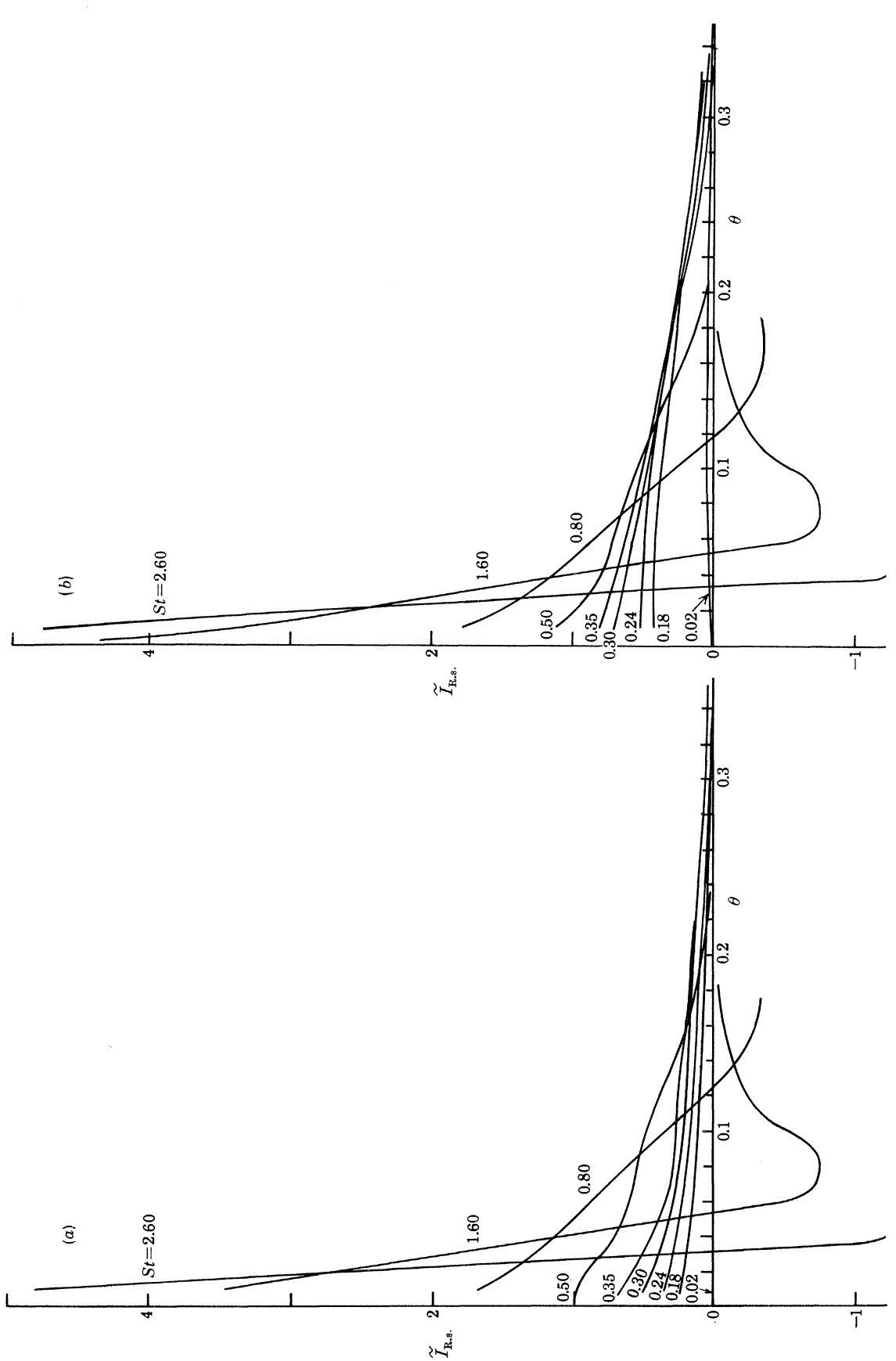

FIGURE 6. Large-scale structure production integral $\tilde{I}_{\text{R.s.}}$ as a function of the local displacement thickness θ for various Strouhal numbers. (*a*) $n = 0$, (*b*) $n = 1$.

PHILOSOPHICAL TRANSACTIONS OF THE ROYAL SOCIETY A MATHEMATICAL, PHYSICAL & ENGINEERING SCIENCES

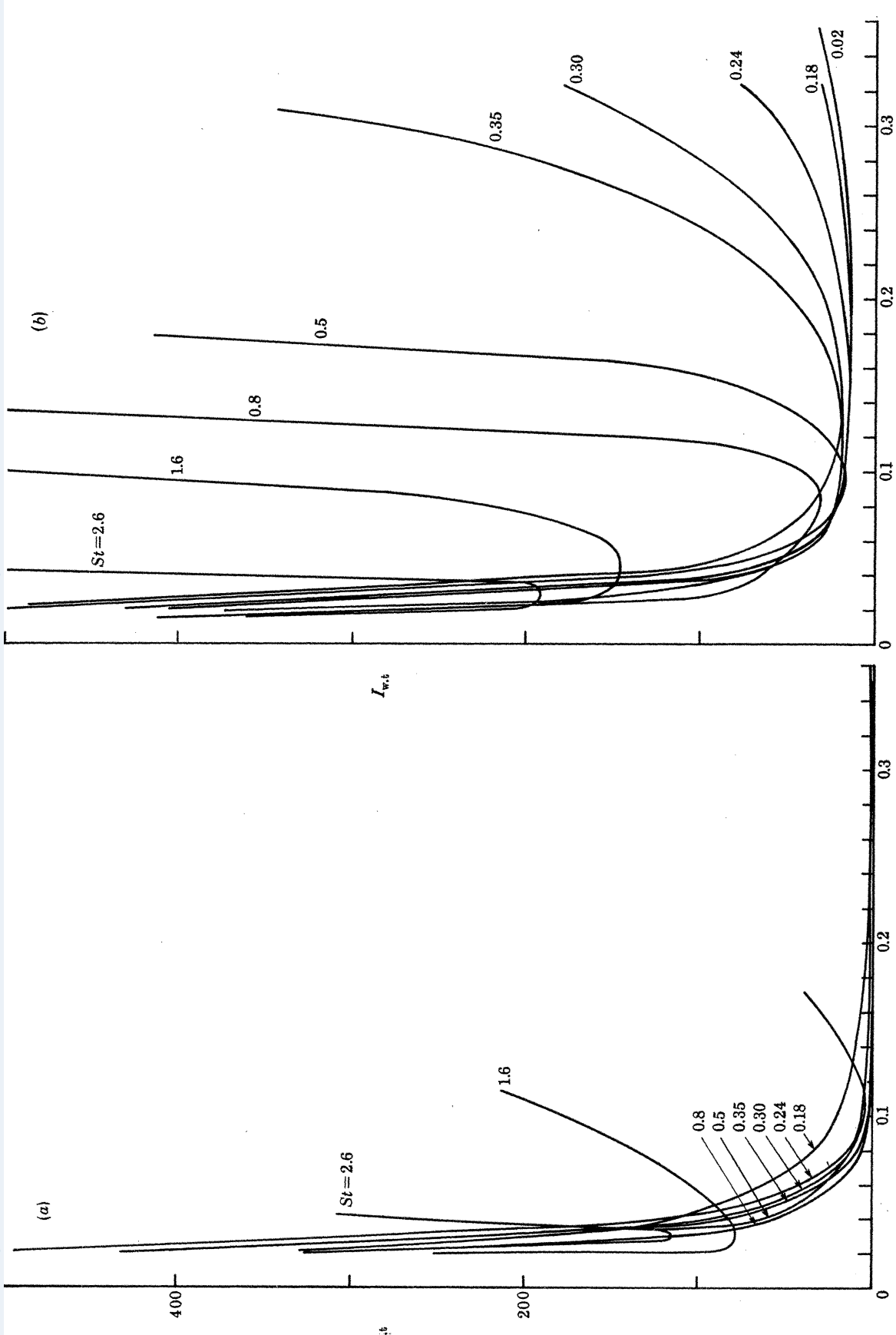

FIGURE 7. Large-scale structure–fine-grained turbulence energy transfer integral $I_{w.t.}$ as a function of the local displacement thickness θ for various Strouhal numbers. (*a*) $n = 0$, (*b*) $n = 1$.

numbers, energy is transferred from the large-scale structure to the mean flow. The axial location at which the wave attains its maximum amplification, according to the inviscid *nonlinear* stability theory, is where $\tilde{I}_{\mathrm{R.s.}} = 0$. Figure 6 shows that this location moves upstream as the Strouhal number increases. Therefore, just as in a local linear theory, inviscid *nonlinear* considerations also show that the axial location at which the wave peaks, moves closer to the nozzle as the Strouhal number increases.

The large-scale energy production has the same trend for $n = 0$ and $n = 1$, as can be seen by comparing figures 6*a* and *b*. However, at small Strouhal numbers, $\tilde{I}_{\mathrm{R.s.}}$ is larger for $n = 1$ than for $n = 0$. Therefore, at small Strouhal numbers the $n = 1$ mode will be initially more amplified than the $n = 0$ mode.

With regard to the large-scale–turbulence energy exchange integral $I_{\mathrm{w.t.}}$, some physical features of the integrand have already been discussed in §4. Now, since the mean shear decreases along the jet, the large-scale rates of strain also decrease along the jet (i.e. with increasing θ), as does $\hat{r}_{ij}$. Consequently, the integral $I_{\mathrm{w.t.}}$ first decreases with θ, behaving as $\theta^{-\frac{3}{2}}$ (see figure 7). However, as a result of the radial spreading of the jet, $I_{\mathrm{w.t.}}$ increases again downstream at a rate that is proportional to the Strouhal number. Thus, for given A and E, the energy exchange between the two fluctuating flow components increases with increasing Strouhal number. The local energy exchange between the large-scale structure and the fine-grained turbulence is larger for the $n = 1$ mode, as already noted in §4. Consequently, $I_{\mathrm{w.t.}}$, the integration of the net local energy transfer, is larger for $n = 1$ than for $n = 0$, as can be seen by comparing figures 7*a* and *b*. Thus, the resistance to the formation of large-scale structure downstream is greater for $n = 1$. Figure 7 also shows that $I_{\mathrm{w.t.}}$ is always positive. Therefore, we see clearly that the overall energy transfer is from the large-structure to the fine-grained turbulence for all Strouhal numbers, and at least for the $n = 0$ and $n = 1$ modes.

The variations in $\tilde{I}_{\mathrm{R.s.}}$, I_2 and $I_{\mathrm{w.t.}}$ along the jet with several different Strouhal numbers are quantitatively similar to the initial behaviour of the corresponding two-dimensional integrals of Alper & Liu (1978). But further downstream, the behaviour of the integrals differs from that in the plane problem because of geometrical effects and also because the present calculation extends beyond the local neutral condition covered in Alper & Liu's (1978) calculations of the shape functions. The geometrical similarity to the two-dimensional mixing layer problem in the first few diameters of the round jet is, of course, consistent with measurements. The calculations of the local large-scale structure shape functions, which allow damped solutions as the shear layer spreads, give rise to the possibility that energy is fed back to the mean flow from the coherent structure. The latter feature, which is a familiar one in hydrodynamic stability, is one which is also obtained from numerical solutions of the plane shear layer problem (Gatski & Liu 1980).

Equations (5.1)–(5.3), together with the three initial conditions, provide a complete set of simultaneous first-order ordinary differential equations for obtaining $|A|^2$, E and θ as functions of x. The coefficients in the differential equations are presented as functions of θ when St and n have been specified. It is, of course, also possible to treat θ as a dependent variable by dividing (5.1) into (5.2) and (5.3), with $x(\theta)$ subsequently found from (5.1). With respect to the initial conditions, experimental observations such as those of Moore (1977) provide an estimate for θ_0 from the initial mean flow shape and an estimate for E_0 from the initial intensity of turbulence. These are found to be $\theta_0 \approx 0.034$ and $E_0 \approx 10^{-3}$. $|A|_0^2$ can vary quite considerably depending on the level of excitation. For forced jets, $|A|_0^2$ can be as large as 10^{-1}, as in the experiment of Binder & Favre-Marinet (1973). For natural jets, or for low levels of forcing, $|A|_0^2$ can be $10^{-6.5}$ or less, as in

Moore's (1977) experiment. Further estimates of initial conditions will be discussed in detail in §6 where comparisons with experiments are made. Such comparisons establish some confidence in our discussion in §§7 and 8, of large-scale structures under conditions for which there are no experimental data, but that are relevant to our understanding of the problem.

6. Comparisons with observations

In this section we shall compare our idealized theoretical problem of a single mode of large-scale structure in a round turbulent jet with the observations of Binder & Favre-Marinet (1973), Favre-Marinet (1975) and Favre-Marinet & Binder (1979). They used hot wires and an education technique (see also, Hussain & Reynolds 1970; Kendall 1970) conditioned to the periodic forcing of the jet. The experiments distinguish the development of the radial and streamwise distributions of the large-scale structure from the fine-grained turbulence for different forcing Strouhal numbers. Such comparisons place quite a severe test upon the present theoretical results, in that the experimental forcing was done at rather large amplitudes. Well controlled turbulent jet experiments were recently done by Moore (1977), following Crow & Champagne (1971). Some reservations about the comparison of our 'conditionally averaged' results with the filtered data of Moore (1977) are discussed in greater detail in §6(*b*).

Prior to the more detailed comparisons, we remark that, in general, the overall features of the present theoretical results are physically consistent with those of observations. Specifically, the turbulent jet spreading rate, and therefore the entrainment rate, are found to be enhanced by the increasing activity of the large-scale structure (Binder & Favre-Marinet 1973; Crow & Champagne 1971). This feature is, of course, understood from studies of nonlinear instabilities of laminar shear flows (Ko *et al.* 1970; Ko 1971; Liu & Gururaj 1974) to result from the increased diffusional activity contributed by the Reynolds stresses of the instability waves. In the turbulent jet problem, however, the large-scale structures contribute to the spreading of the jet in two ways: explicitly, as in unstable laminar flows, and implicitly, through their enhancement of the fine-grained turbulence which in turn causes further spreading of the jet. (The local physical details are, of course, quite different (Roshko 1976). The large-scale structures contribute to massive gulping, as it were, of free-stream undisturbed fluid, while the fine-scale structures contribute to a local nibbling.

It is found theoretically that the relative amplification of the large-scale structure decreases if the initial amplitude $|A|_0^2$ is increased. This is because of the relatively severe energy loss for the more energetic large-scale structure resulting from the choking off of its own energy supply from the mean flow and enhancing its own energy dissipation into turbulence. This is indeed the situation found in Crow & Champagne's (1971) experiments.

For small Strouhal numbers, the helical $n = 1$ mode is found here to be more amplified than the axisymmetric $n = 0$ mode (this would also be the situation for the fully developed mean jet profile (Batchelor & Gill 1965), which is not used in the present computations), and this is consistent with the turbulence intensity measurements of Yamamoto & Arndt (1978) which indicate the existence of the helical-wavelike motion of the jet 'turbulence' of relatively large wavelength and hence of relatively low frequency. The helical mode is also found to decay rapidly because of the additional energy transfer to the fine-grained turbulence. The observations of Chan (1976) support this and also indicate that the axisymmetric mode eventually dominates, as also observed by Michalke & Fuchs (1974). These observations do seem to suggest that the more

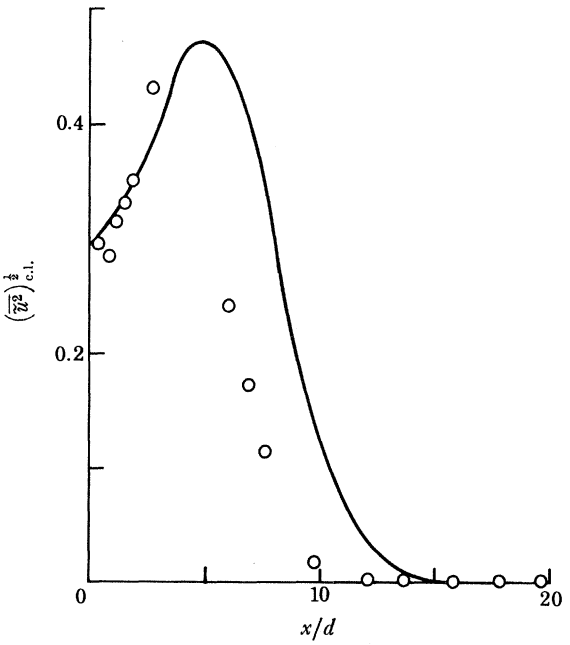

FIGURE 8. Large-scale structure r.m.s. axial velocity component along the jet centreline, $(\overline{\tilde{u}^2})^{\frac{1}{2}}_{\text{c.l.}}$; comparison with Favre-Marinet's (1975) experimental data for $St = 0.18$ (○).

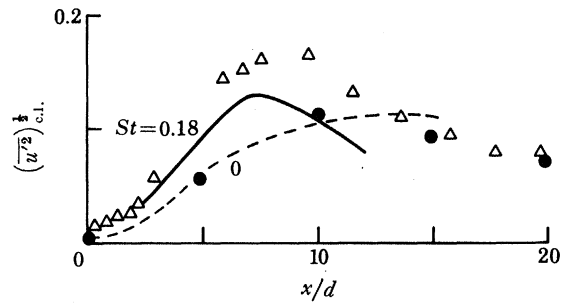

FIGURE 9. Fine-grained turbulence r.m.s. axial velocity component $(\overline{u'^2})^{\frac{1}{2}}_{\text{c.l.}}$ along the jet centreline; comparison with Favre-Marinet's (1975) experimental data for $St = 0.18$ (△) and with the unforced jet, $St = 0$ (●).

energetic fine-grained turbulence has led to the early demise of the helical mode in that region. This situation is quite different from that of coherent structures in a laminar flow, where the efficiency in the extraction of energy from the mean flow alone gives rise to the development of such structures in dynamically unstable flows.

More specific comparisons with observations are made in the following.

(*a*) *Observations of Binder & Favre-Marinet* (1973), *Favre-Marinet* (1975) *and Favre-Marinet & Binder* (1979)

Binder and Favre-Marinet performed well controlled unsteady forcing of a round jet by means of a rotating butterfly valve, upstream of the nozzle exit. The phase-averaging technique, with the frequency of forcing as a reference, is used to educe the large-scale structure from the total fluctuations. Figure 8 compares these observations and the present calculations for the r.m.s. large-scale structure streamwise valocity $(\overline{\tilde{u}^2})^{\frac{1}{2}}$ on the jet axis at $St = 0.18$ and for $n = 0$. The velocities presented here are normalized by the mean jet exit velocity rather than by the local mean velocity on the jet axis, as was done originally by Favre-Marinet (1975). Figure 9 shows

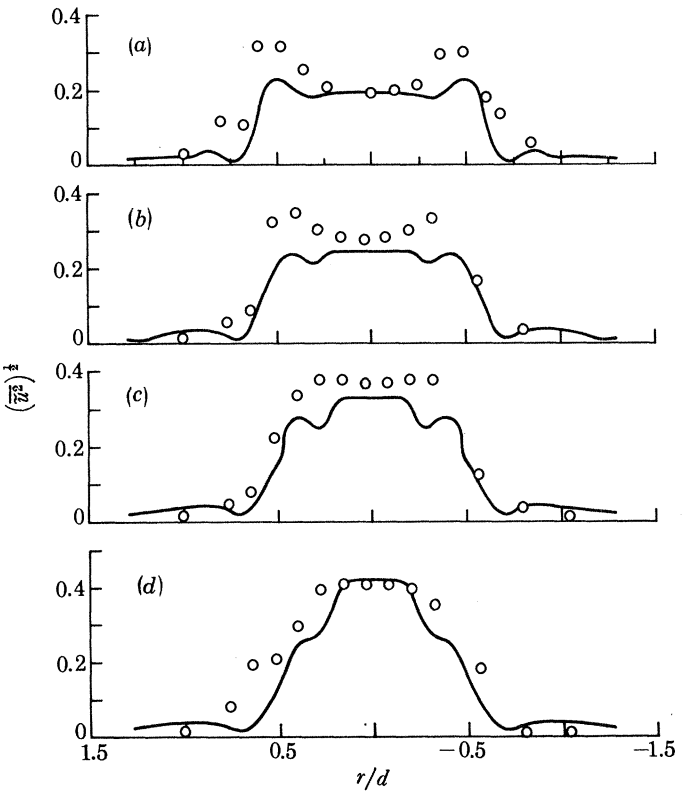

FIGURE 10. Radial distribution of the large-scale structure r.m.s. axial velocity component $(\overline{\tilde{u}^2})^{\frac{1}{2}}$ at several streamwise locations along the jet; comparison with Favre-Marinet's (1975) experimental data for $St = 0.24$ (○). (*a*) $x/d = 0.48$, (*b*) $x/d = 1.28$, (*c*) $x/d = 2.08$, (*d*) $x/d = 2.88$.

the corresponding r.m.s. fine-grained turbulence axial velocity $(\overline{u'^2})^{\frac{1}{2}}$ on the jet axis and for no forcing. Both $(\overline{\tilde{u}^2})^{\frac{1}{2}}$ and $(\overline{u'^2})^{\frac{1}{2}}$ are given, in the experiments at the nozzle exit on the jet axis, and these are used, in conjunction with the shape assumptions (4.8) and (4.3), to obtain the corresponding $|A|_0^2$ and E_0 for the present calculations (for any θ_0) by matching on the axis. However, θ_0 was, unfortunately, not available from the observations. The value $\theta_0 = 0.3$ was used which is reasonable, and also gives the best qualitative match between theory and experiment. The physical picture derived from figures 8 and 9 indicates that the large-scale structure first amplifies, because of extraction of energy from the mean flow, and subsequently decays downstream because of energy transfer† to the fine-grained turbulence. The fine-grained turbulence obtains energy directly from the mean flow and indirectly through the large-scale structure, as may be seen by contrasting the forced and unforced cases. The fine-grained turbulence indeed becomes more energetic, and this added energy could not be extracted from the mean motion were it not for the intermediary action of the large-scale structure. We note here that both the forcing amplitude and the subsequent amplitude of the amplified large-scale structure are rather large, in the range of 30–45 % of the jet exit velocity. This places a severe strain on the present formulation, associated with the shape assumptions, that makes use of the eigenfunctions of a local linear theory. The comparisons, though encouraging, are not directed towards 'predictive' purposes. They lend support in further studies directed towards the understanding of the physical mechanisms in the interaction problem.

† With the possibility that some energy is transferred back to the mean flow.

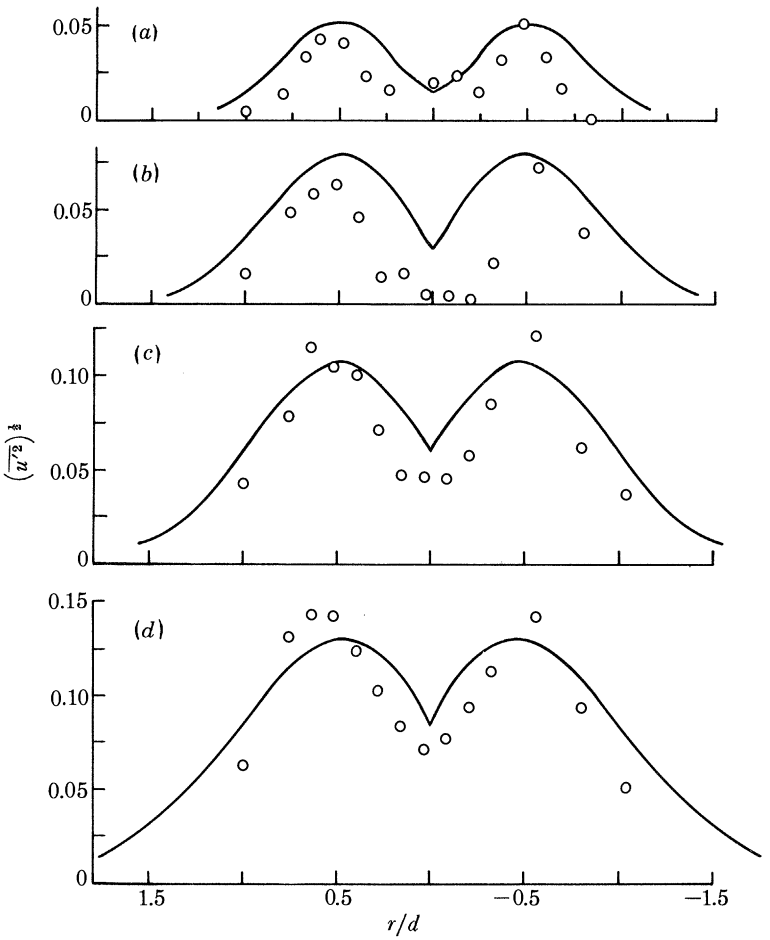

FIGURE 11. Radial distribution of the fine-grained turbulence r.m.s. axial velocity component $(\overline{u'^2})^{\frac{1}{2}}$ at several streamwise locations along the jet; comparison with Favre-Marinet's (1975) experimental data for $St = 0.24$ (○). (*a*) $x/d = 0.48$, (*b*) $x/d = 1.28$, (*c*) $x/d = 2.08$, (*d*) $x/d = 2.88$.

For $St = 0.24$ Favre-Marinet's (1975) experiments provide the structural details of $(\overline{\tilde{u}^2})^{\frac{1}{2}}$ and $(\overline{u'^2})^{\frac{1}{2}}$ as functions of (x, r). Here the initial data are given at $x/d = 0.48$, where d is the nozzle diameter. (We recall that all physical lengths were normalized by the nozzle radius.) The corresponding initial values for the calculation are obtained from the data as $|A|_0^2 = 0.0193$, $E_0 = 0.00345$, and from the mean velocity profile it is found that $\theta_0 = 0.144$ at $x/d = 0.48$. Thus, all the initial conditions may be obtained from the data. The comparison for the streamwise evolution of the radial distribution of $(\overline{\tilde{u}^2})^{\frac{1}{2}}$ is shown in figure 10, again in terms of a normalization by the jet exit velocity rather than by the local mean velocity (Favre-Marinet 1975)†. The calculations were made up to values of θ for which the eigenfunctions of the local inviscid linear theory exhibited damped solutions; the local shape functions calculated for this case are available up to $x/d = 3.62$. The comparisons of the calculated and observed distributions of the large-scale structure are much better than originally anticipated, given the shape assumptions. The linear shape functions are, however, questionable further downstream where much stronger nonlinear effects are accumulated. Calculations and observations for $(\overline{u'^2})^{\frac{1}{2}}$ are compared in figure 11. The

† We thank M. Favre-Marinet for making available to us data in this form.

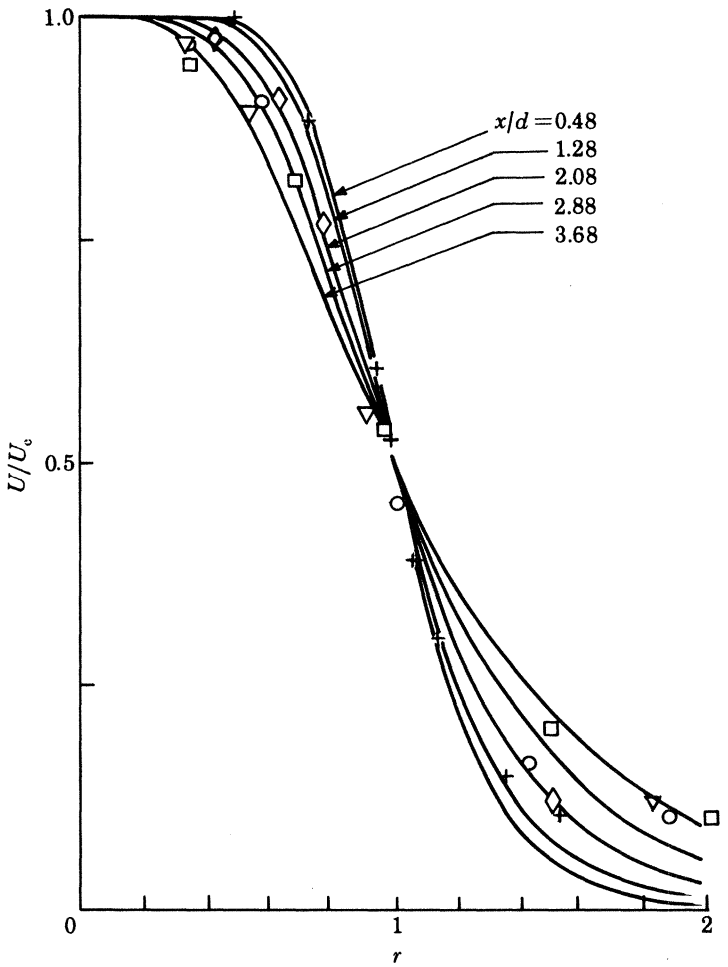

FIGURE 12. Radial distribution of the mean flow velocity U/U_c for several axial locations along the jet; comparison with Favre-Marinet's (1975) experimental data for $St = 0.24$: +, $x/d = 0.48$; ◇, $x/d = 1.28$; ○, $x/d = 2.08$; ▽, $x/d = 2.88$; □, $x/d = 3.68$.

qualitative development is, in general, rather good. The mean velocity profile comparisons in figure 12 also show reasonable agreement in the streamwise development. However, the rate of spread is larger than that in the observations. This discrepancy may be attributed to an overestimation of the large-scale structure which brings about an overestimation of its production $|A|^2\tilde{I}_{\text{R.s.}}$. This would then give rise to the slight increase in the jet spreading rate.

(*b*) *Observations of Moore* (1977)

In Moore's (1977) experiments, an acoustic wave of $|A|_0^2 \approx 10^{-6.5}$ was applied to the jet by using an acoustic horn ahead of the nozzle exit. This form of excitation limits the response to plane-wave excitation of the $n = 0$ mode. Moore's (1977) stroboscopic illumination constituted a 'visual' conditional sampling technique. However, his quantitative data, like those of Crow & Champagne (1971), were filtered rather than conditionally sampled. Moore's measurements were obtained by using a microphone with a nose cone pointed into the flow and a constant-temperature hot-wire anemometer to measure the pressure and velocity, respectively. Both pressure and velocity signals were then *filtered* at the excitation frequency. If phase-averaged, the large-scale structure component at a given frequency could thus be educed, as was done by

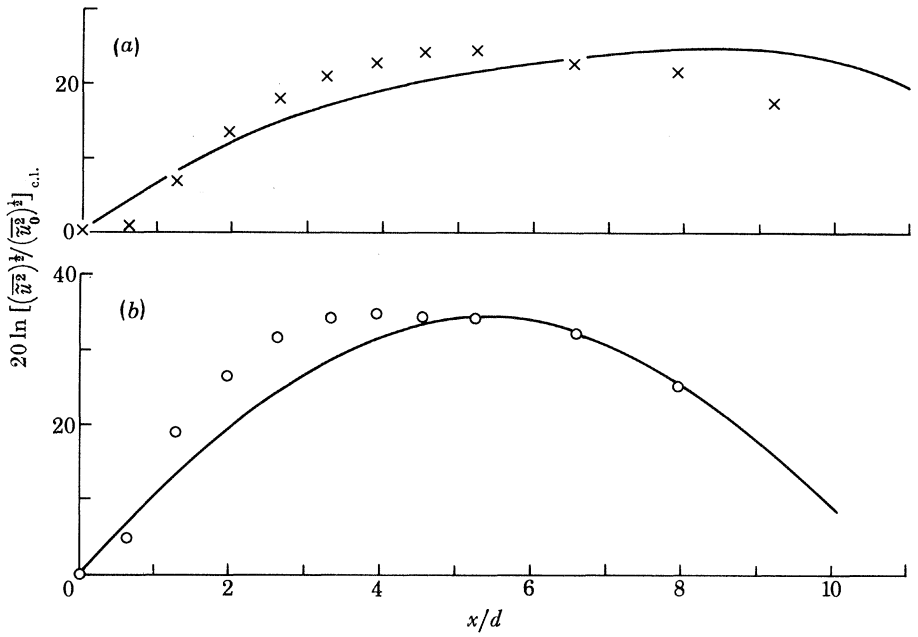

FIGURE 13. Large-scale structure r.m.s. axial velocity component ratio $[(\overline{\tilde{u}^2})^{\frac{1}{2}}/(\overline{\tilde{u}_0^2})^{\frac{1}{2}}]_{\text{c.l.}}$ along the jet; comparison with Moore's (1977) experimental data. (*a*) $St = 0.03$, (*b*) $St = 0.50$.

Binder & Favre-Marinet (1973), Favre-Marinet (1975) and Favre-Marinet & Binder (1979). Filtering produces a signal that contains both the large-scale structure and the fine-grained turbulence components at the filtering frequency. Thus, phase-averaging the axial velocity gives $\tilde{u}_\omega$, while filtering gives $\tilde{u}_\omega + \tilde{u}'_\omega$.

Consequently, there is a difference, between the filtered (Moore 1977) root-mean-square value $(\overline{\tilde{u}_\omega^2 + u'^2_\omega})^{\frac{1}{2}}$ and the present calculated value $(\overline{\tilde{u}_\omega^2})^{\frac{1}{2}}$, which is equivalent to the fine-grained turbulence component $(\overline{u'^2_\omega})^{\frac{1}{2}}$ at the same frequency as the large-scale structure. However, the fine-grained turbulence energy content is spread over the entire spectrum of frequencies, whereas in an idealized situation that of the large-scale structure is concentrated about a monochromatic component. If the coherent signal is sufficiently strong compared to the random signal at the filtering frequency, it is then possible to consider the filtered signal as if it were conditionally averaged. In this respect, however, the quantitative comparisons with Moore's (1977) results are not entirely free from difficulties.

In figures 13 and 14, the calculated values of $(\overline{\tilde{u}^2})^{\frac{1}{2}}$ and $(\overline{\tilde{p}^2})^{\frac{1}{2}}$ are compared with the filtered results of Moore (1977). Since the experiment provides the initial values of $|A|_0^2$, $(\overline{u'^2})^{\frac{1}{2}}$ and U, the initial values for the calculations are obtained and fixed as $|A|_0^2 = 10^{-6.5}$, $E_0 = 0.78 \times 10^{-3}$ and $\theta_0 = 0.034$. The calculated values of $(\overline{\tilde{u}^2})^{\frac{1}{2}}$ and $(\overline{\tilde{p}^2})^{\frac{1}{2}}$ along the jet centreline agree favourably with the observed ones. As in the comparison with Favre-Marinet's (1975) observations, the observed values are lower than the calculated ones in the vicinity of the nozzle exit. Away from the nozzle the observed filtered signals are greater than the calculated ones, since the observed values contain an additional component due to the fine-grained turbulence. In the final stages of the wave's development, just as in Favre-Marinet's (1975) experiment, the observed rate of decay is slightly greater than the calculated one. The observed and calculated maximum amplifications of $(\overline{\tilde{u}^2})^{\frac{1}{2}}$ and $(\overline{\tilde{p}^2})^{\frac{1}{2}}$ are shown in figure 15 as a function of Strouhal number. The calculated peak Strouhal number is about 0.7 but the observed one is about 0.6 for the same initial conditions. The calculated maximum amplifications agree well with those observed at low Strouhal

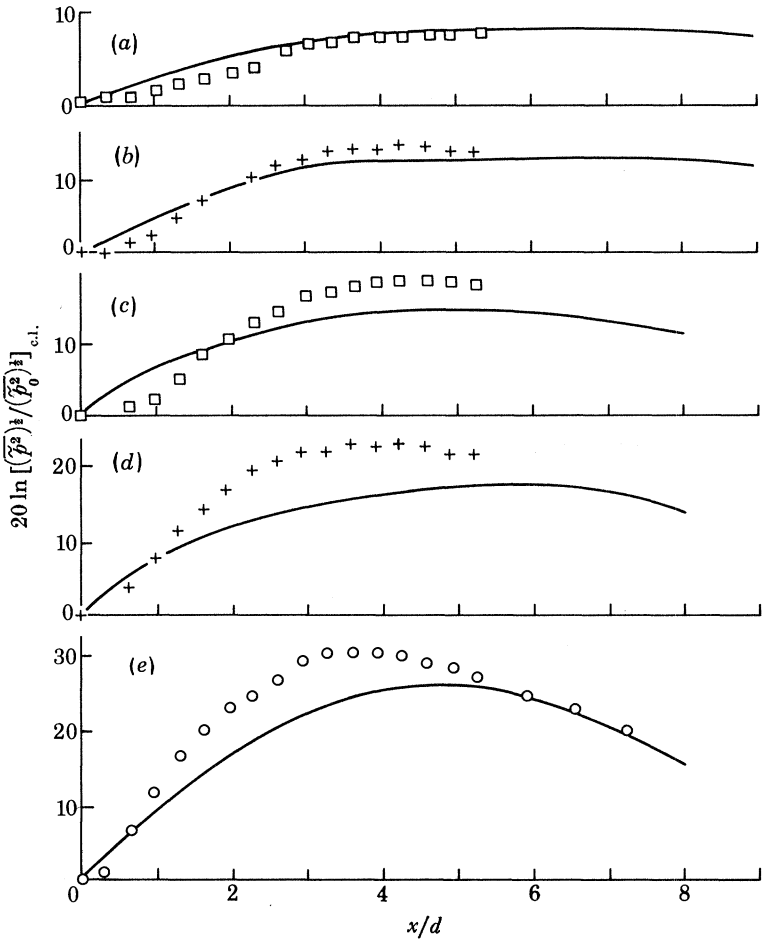

FIGURE 14. Large-scale structure r.m.s. pressure ratio $[(\widetilde{p^2})^{\frac{1}{2}}/(\widetilde{p_0^2})^{\frac{1}{2}}]_{\text{c.l.}}$ along the jet centreline; comparison with Moore's (1977) experimental data. (*a*) $St = 0.18$, (*b*) $St = 0.24$, (*c*) $St = 0.30$, (*d*) $St = 0.35$, (*e*) $St = 0.50$.

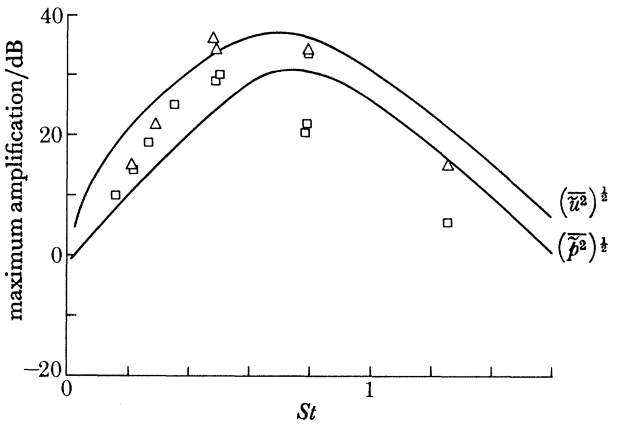

FIGURE 15. Maximum large-scale structure amplification as a function of Strouhal number; comparison with Moore's (1977) experimental data.

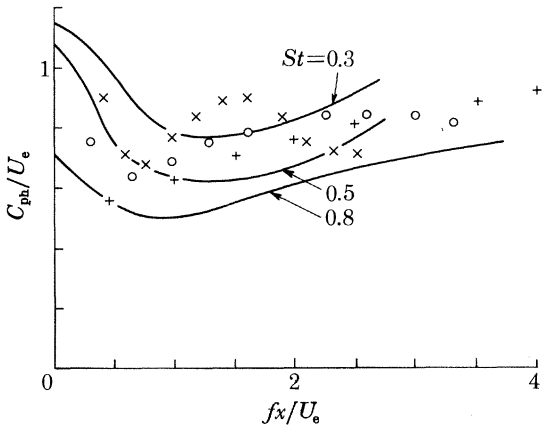

FIGURE 16. Phase speed C_{ph} along the jet for several Strouhal numbers; comparison with Moore's (1977) experimental data: ×, $St = 0.30$; ○, $St = 0.49$; +, $St = 0.78$.

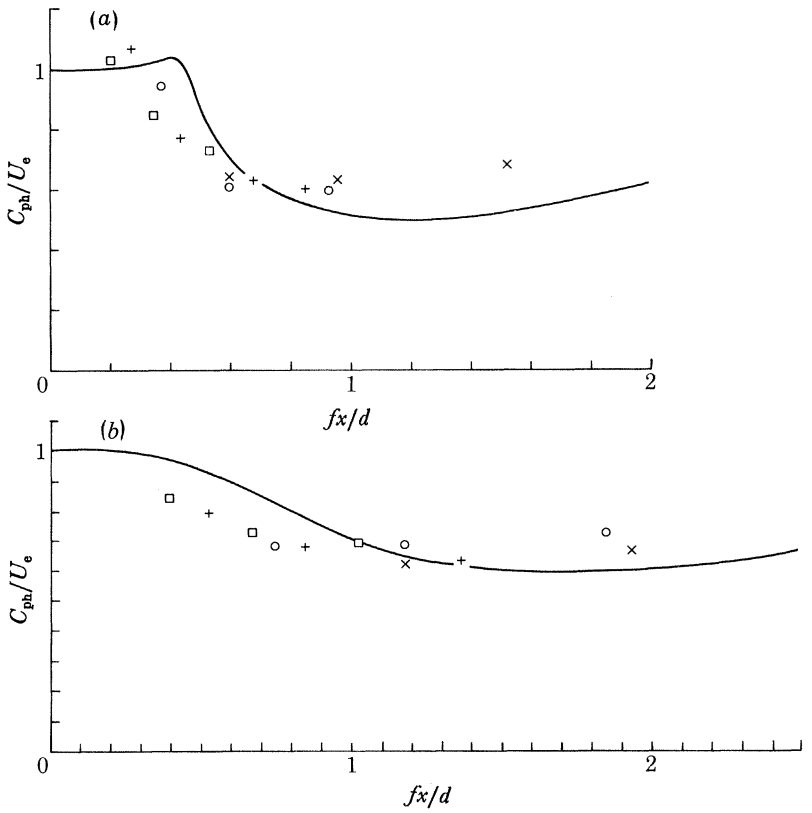

FIGURE 17. Phase speed C_{ph} as a function of the normalized large-scale structure frequency fx/d: comparison with Moore's (1977) experimental data. (*a*) $x/d = 1.19$, (*b*) $x/d = 2.38$. ×, $M = 0.30$; ○, $M = 0.49$; +, $M = 0.66$; □, $M = 0.83$, where M is the jet Mach number.

numbers, but are too great at large Strouhal numbers. Since the streamwise lifespan of the large-scale structure is relatively shorter for large Strouhal numbers, the formation of harmonics, nonlinearity effects and the simultaneous presence of several frequency components may be relatively more pronounced for such a short lifespan, and this may perhaps explain the overestimated amplifications at high Strouhal numbers.

In this framework, the phase velocity of the large-scale structure, C_{ph}, is first obtained from the local linear theory as a function of θ. Once θ along the jet is known from the nonlinear theory, $C_{ph}(x, St, n)$ can be obtained. The distributions of C_{ph} along the jet are compared, in figure 16, with the observed ones, for various Strouhal numbers. The general trend of variation is the same for the calculated and the observed phase velocity: it first decreases to a minimum and then starts to increase slowly along the jet. A clearer comparison for C_{ph} is obtained in figure 17, where a fixed axial location is considered, and some collapse of the data is possible. The frequency of the forced disturbance was changed and the phase-speed measured at the same axial location is plotted against a normalized frequency, fx/d. For a given axial location C_{ph} first decreases to a minimum and then increases with increasing frequency of the forced disturbance. The calculated values of C_{ph} are slightly overestimated at lower frequencies and slightly underestimated at higher frequencies. This deviation probably arises because C_{ph} is basically obtained from the local linear analysis. Again, however, the comparisons are rather encouraging, considering the simplicity of the present formulation.

(*c*) *Further discussion of the comparisons with observations*

In general, the comparisons between theory and observations are reasonably encouraging. The calculations certainly indicate that the agreement is better than it was originally thought to be. Still, there are phenomena affecting the comparisons which are not included in the calculations. Among these is the strong effect of nonlinearity on the shape of the disturbance. The shape assumptions made by using the linear eigenfunctions, in the present analysis for the large-scale structure, were not meant for structural comparisons but only for evaluation of the interaction integrals. Nevertheless, some structural comparisons with the data of Favre-Marinet (1975) were favourable. In a real situation, there may actually be several natural large-scale structure components in addition to the forced fundamental component. A first and second harmonic of the fundamental wave were observed downstream by Crow & Champagne (1971). Thus, energy is drained from the fundamental component to form these harmonics. Since this loss in the energy of the fundamental component is not taken into account here, the calculated rate of decay is also underestimated. Neglecting the rate of viscous dissipation in the large-scale structure energy equation leads to an underestimation of the wave's rate of decay. In addition, neglecting the viscous terms in the linear stability equation, the equation that provides the shape functions for the large-scale structure, would give an overestimated rate of wave production and equivalently an underestimated rate of wave decay. However, the dominant interaction mechanisms are considered in our formulation.

The streamwise lifespan of the large-scale structure is estimated in the present analysis to be about four wavelengths. The experimental observations of Brown & Roshko (1974) and Winant & Browand (1974) at low Reynolds numbers showed that after two or three wavelengths the waves steepen and roll up into concentrations of vorticity. These eddies move downstream and interact with neighbouring eddies by rolling around each other and pairing. The calculations of Damms & Kuchemann (1974) and Moore & Saffman (1975) indicate that eddies can disappear when two strong vortices absorb a weak neighbour. These mechanisms, which are not included here, increase the wave's rate of decay. However, such mechanisms are probably not important for the high levels of forcing in Favre-Marinet's (1975) experiment. In any case, the presence or absence of pairing may now be controlled (Ho & Huang 1978; Bouchard & Reynolds 1978). Observations of Dimotakis & Brown (1976) strongly suggest that for large Reynolds numbers,

PHILOSOPHICAL TRANSACTIONS OF THE ROYAL SOCIETY A MATHEMATICAL, PHYSICAL & ENGINEERING SCIENCES

the interactions between large-scale structure and fine-grained turbulence dominate over those between neighbouring large-scale structures.

The present formulation corresponds to the situation of a well-controlled occurrence of the large-scale structure in a turbulent jet, and the comparisons with observations were most encouraging. It is thus worthwhile to discuss further the physical mechanisms that lead to the observed features. These naturally include the mechanisms for energy transfer. In the sections to follow, results will also be given in terms of the effects of the Strouhal number for azimuthal wave numbers $n = 0$ and $n = 1$. In what follows an almost exhaustive study of the large-scale structure in a round turbulent jet will be given.

7. Nonlinear development of the $n = 0$ mode

With some confidence gained through the discussion in § 6, we now apply the basic formulation discussed in § 3 to a study of downstream evolution of *axisymmetric* modes of the large-scale structure at various frequencies. As pointed out before, the large-scale structure in a round jet consists of several azimuthal components. The doughnut-like axisymmetric component, which is viewed by Crow & Champagne (1971) as puffs and by Binder & Favre-Marinet (1973) as pulses, is considered here by taking $n = 0$ along the jet.

The initial values θ_0 and E_0 are estimated from Moore's (1977) experiments as 0.034 and 10^{-3}, respectively. The value $E_0 = 10^{-3}$ implies that $(\overline{u'^2})^{\frac{1}{2}}$ at the centre of the nozzle exit is approximately 1% of U_e.

Since $|A|_0^2$ varies quite considerably, we first consider, in § 7 (*a*), $|A|_0^2 = 10^{-6.5}$, which corresponds to natural or weakly forced jets. In § 7 (*b*), $|A|_0^2$ is increased to 10^{-5}, 10^{-3}, and 10^{-1} so that we may consider the effect of increasing the initial energy level of the large-scale structure.

(*a*) *Lower levels of excitation*

The development of the axisymmetric modes at $|A|_0^2 = 10^{-6.5}$, $E_0 = 10^{-3}$ and $\theta_0 = 0.034$ is studied here for several Strouhal numbers and the results, shown in figures 18–24, are discussed below.

(i) *The large-scale structure*

The large-scale structure of very low frequency oscillates too slowly to extract any energy from the mean flow. On the other hand, the high-frequency large-scale structure transfers energy to the fine-grained turbulence at a rate that is much greater than the energy production from the mean flow, so that only for the range $0.02 < St < 1.6$ can the large-scale structure first amplify and then decay further downstream along the jet, as shown in figure 18. The wavy large-scale structure grows by extracting energy from the mean flow. As it moves along the jet two mechanisms, one 'turbulent' and one 'inviscid', force the wave to decay. In the turbulent mechanism (the effect of $I_{\text{w.t.}}$) the wave decays as a result of 'turbulent dissipation', where the wave-induced stresses do work against the rates of strain of the large-scale structure and transfer energy to the fine-grained turbulence. In the 'inviscid' mechanism (through the effect of $\tilde{I}_{\text{R.S.}}$) the wave moves along the jet to a region of stable mean velocity profile where its production is reversed and energy is transferred back to the mean flow. The 'inviscid' mechanism is associated with large Strouhal numbers and, as will be shown, is less effective than the turbulent dissipation mechanism.

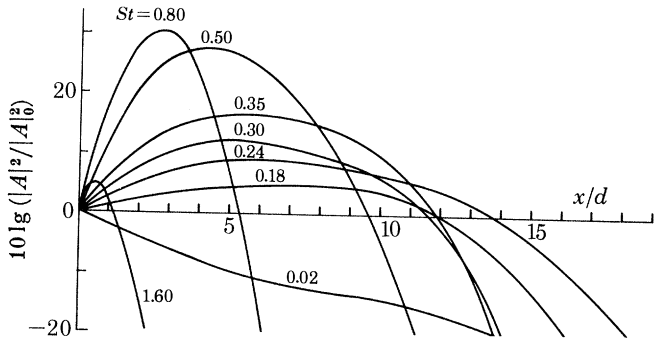

FIGURE 18. Large-scale structure kinetic energy ratio $|A|^2/|A|_0^2$ along the jet for several Strouhal numbers.

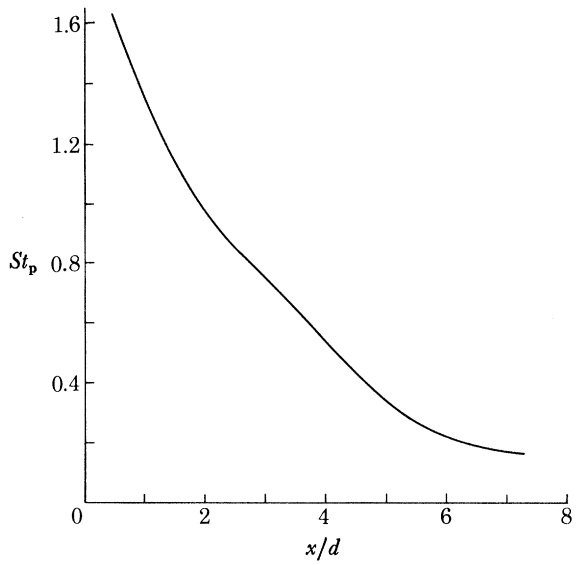

FIGURE 19. Peak Strouhal number, St_p, along the jet.

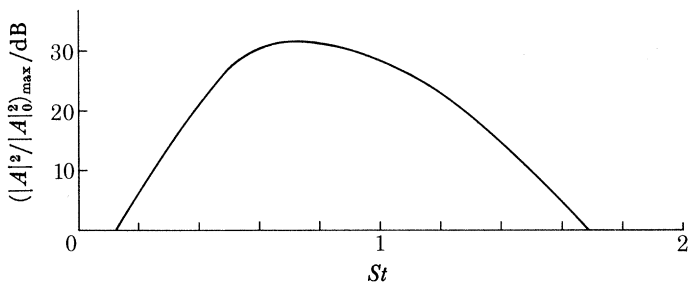

FIGURE 20. Maximum amplification in $|A|^2$ as a function of Strouhal number.

Therefore, turbulent dissipation is the basic mechanism by which the wave decays. Since $\mathrm{d}|A|^2/\mathrm{d}x \propto |A|^2$, once $|A|^2$ reaches zero it remains there.

Figure 18 indicates that the location of peak amplification moves closer to the nozzle as the Strouhal number increases. Thus high-frequency components dominate upstream while low-frequency ones dominate farther downstream, as one would expect (Liu 1974). The peak Strouhal number is a function of the axial location. That is, for each axial location considered

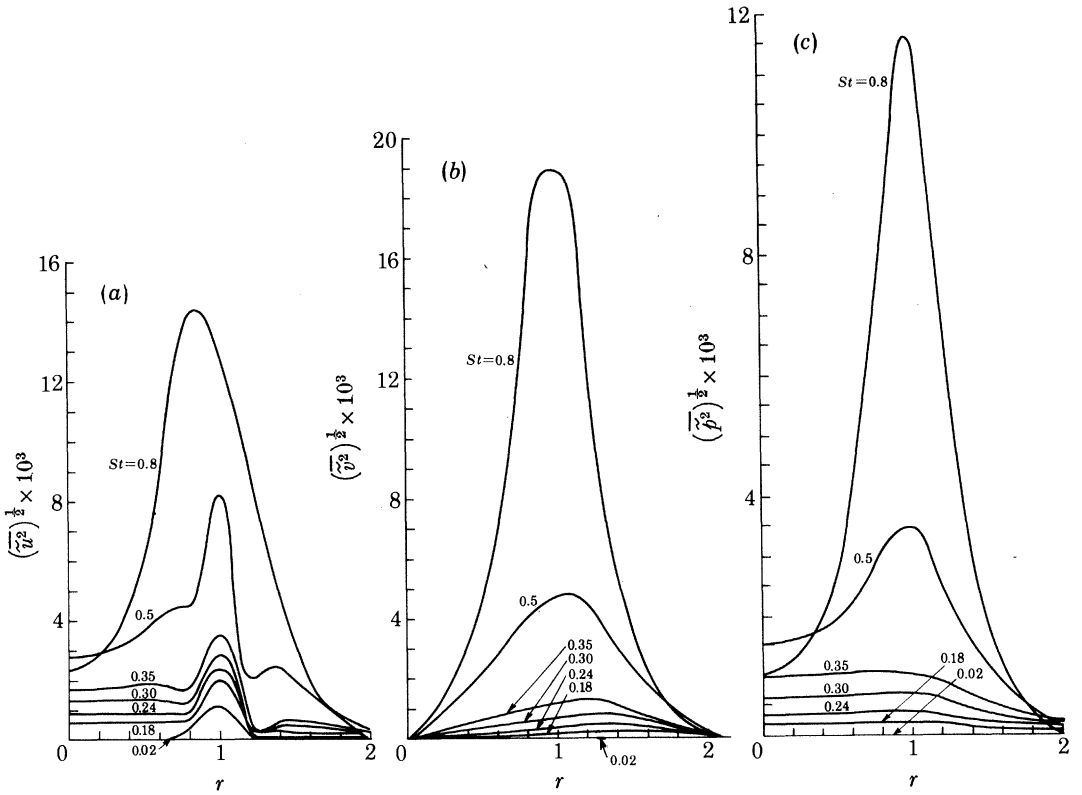

FIGURE 21. Radial distribution of the large-scale structure at $x/d = 1.7$ for several Strouhal numbers. (*a*) r.m.s. streamwise velocity component, $(\overline{\tilde{u}^2})^{\frac{1}{2}}$; (*b*) r.m.s. radial velocity component $(\overline{\tilde{v}^2})^{\frac{1}{2}}$, (*c*) r.m.s. pressure $(\overline{\tilde{p}^2})^{\frac{1}{2}}$.

there is a certain Strouhal number that produces the greatest large-scale structure amplification in this particular section. This peak Strouhal number decreases as the axial location considered moves downstream, as shown in figure 19. Figure 19 also shows that the peak Strouhal number is approximately proportional to x^{-1}, which is in agreement with Chan's (1974*a*) experimental observation that the distributions of the amplitude of the pressure waves along the jet are similar if the data are plotted against a normalized distance ($St\,x$). The maximum amplification in $|A|^2$ attained along the jet is shown, in figure 20, as a function of Strouhal number. With the present initial conditions, $St = 0.7$ produces the greatest amplification in $|A|^2$. Figure 18 also indicates that the streamwise lifespan of the wave is inversely proportional to the Strouhal number. Since the wavelength $2\pi/\alpha_r$ is the primary dimension that describes the wave geometry, it seems as if the wave 'recognizes' physical dimensions relative to its own wavelength. Thus, the rate of wave development at different Strouhal numbers would be the same if it were scaled by the corresponding wavelength. For instance, for all Strouhal numbers considered the wave decays to $|A|^2 = 0.1|A|_0^2$ after a distance that is approximately four times the corresponding wavelength. Thus, irrespective of the Strouhal number, the wave makes almost four cycles along the jet before it disappears.

The radial distributions of $(\overline{\tilde{u}^2})^{\frac{1}{2}}$, $(\overline{\tilde{v}^2})^{\frac{1}{2}}$ and $(\overline{\tilde{p}^2})^{\frac{1}{2}}$ at $x/d = 1.7$, for several Strouhal numbers along the jet, are shown in figure 21. They peak where $(\partial U/\partial r)\,(n^2/r + \alpha^2 r)^{-1}$ has an extremum (Batchelor & Gill 1962; Lees & Gold 1964), and this is very nearly in the vicinity of $r = 1$ where $\partial U/\partial r$ itself has a maximum.

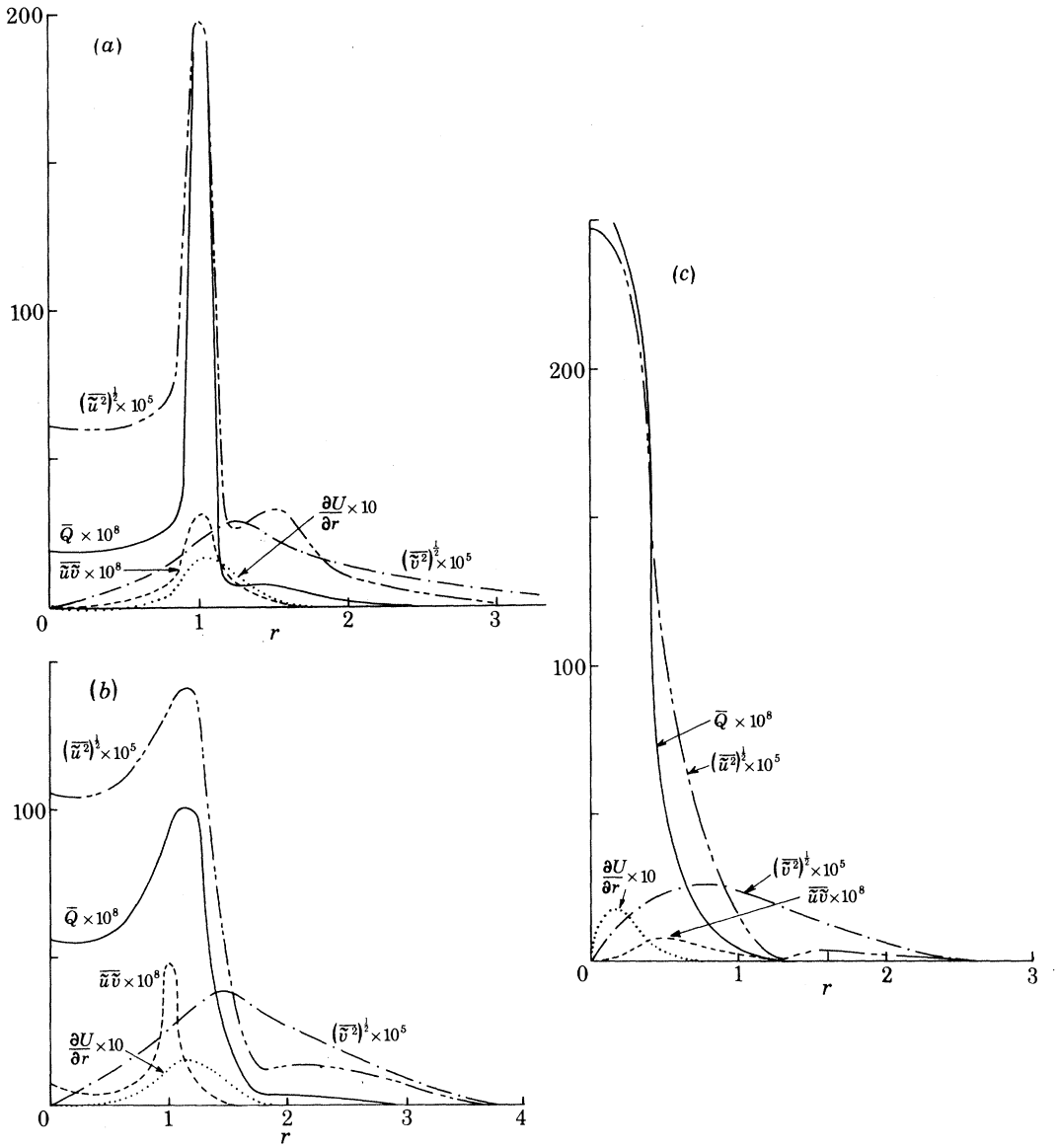

FIGURE 22. Radial distribution of large-scale structure r.m.s. streamwise and radial velocities $(\overline{\tilde{u}^2})^{\frac{1}{2}}$ and $(\overline{\tilde{v}^2})^{\frac{1}{2}}$. Reynolds shear stress $\overline{\tilde{u}\tilde{v}}$, kinetic energy Q and the mean velocity gradient $\partial U/\partial r$; $St = 0.18$. (*a*) $x/d = 1.6$, (*b*) $x/d = 3.6$, (*c*) $x/d = 11.8$.

The radial distributions of $(\overline{\tilde{u}^2})^{\frac{1}{2}}$, $(\overline{\tilde{v}^2})^{\frac{1}{2}}$, $\overline{\tilde{u}\tilde{v}}$, $\partial U/\partial r$, and the large-scale structure local energy $\bar{Q}$, at several stations along the jet, are shown in figure 22. The figure shows that the large-scale structure Reynolds shear stress varies radially in a manner quite similar to that of the variations of $\partial U/\partial r$. Hence, for a given section, the production of the large-scale structure is greatest near the position of maximum $\partial U/\partial r$ and is zero along the jet centreline, as in the mechanism for turbulence production discussed by Townsend (1956).

Similarly, $(\overline{\tilde{u}^2})^{\frac{1}{2}}$, $(\overline{\tilde{v}^2})^{\frac{1}{2}}$ and $\bar{Q}$ peak at nearly the same location at which $\partial U/\partial r$ peaks. For the

initial region of the jet $\partial U/\partial r$ peaks at $r = 1$, but farther downstream the peak of $\partial U/\partial r$ moves towards the jet centreline. Consequently, the concentration of large-scale structure quantities moves from $r = 1$ toward $r = 0$ for downstream locations.

(ii) *The fine-grained turbulence*

For the low initial energy levels of the large-scale structure, the results from the computations of $E(x)$ collapsed onto the $|A|_0^2 = 0$ curve for all Strouhal numbers. Thus figure 23*a* shows that for all the Strouhal numbers considered, $E(x)$ is the same as in the absence of the large-scale structure; recall that the low-level excitation $|A|_0^2 = 10^{-6.5}$ was imposed here. Thus, for very low levels of excitation the large-scale structure has a negligible influence on the fine-grained turbulence.

For the small value $|A|_0^2$ under consideration here the development of fine-grained turbulence is governed by its interaction with the mean flow alone. Because the rate of production is greater in the initial region of the jet, E initially increases rapidly, as shown in figure 23*a*. Farther downstream, the fine-grained turbulence production integral $I'_{\text{R.S.}}$ decreases while the viscous dissipation, which is proportional to $E^{\frac{3}{2}}$, increases. But since the production still exceeds the viscous dissipation, E continues to grow downstream but at a slower rate.

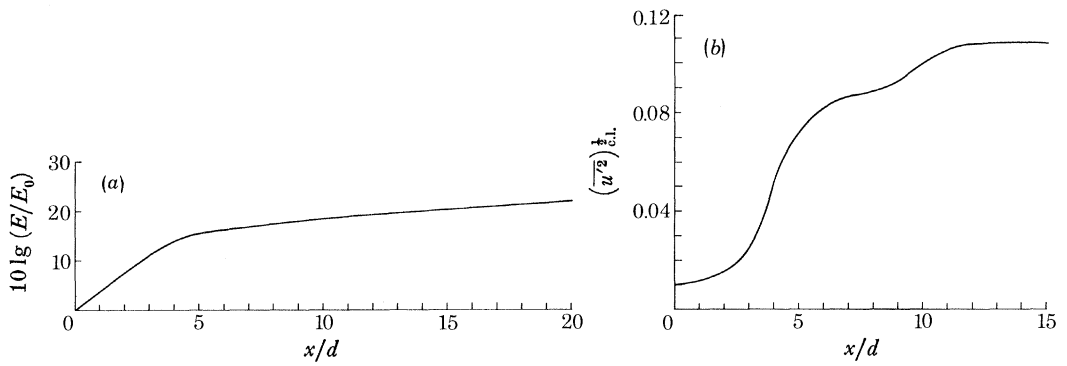

FIGURE 23. Distribution of (*a*) fine-grained turbulence energy ratio E/E_0 and (*b*) centreline r.m.s. streamwise velocity component $(\overline{u'^2})^{\frac{1}{2}}_{\text{c.l.}}$ along the jet; $0.02 \leqslant St \leqslant 1.60$.

The root-mean-square values of the fine-grained turbulence axial velocity $(\overline{u'^2})^{\frac{1}{2}}$ along the jet centreline are also not influenced by the low level of large-scale structure, as shown in figure 23*b*. However, the influence of θ has to be taken into consideration. At the initial region of the jet, the shear layer has not yet approached the jet centreline. Therefore, although E increases, the centreline values of $(\overline{u'^2})^{\frac{1}{2}}$ are small up to $x \approx 3d$. Then the shear layer approaches the centreline and causes the rapid increase shown in figure 23*b*. Away from the initial region, $G(\theta) \sim 1/\theta$ and the turbulent stresses downstream could be written as

$$\overline{u'_i u'_j} \sim E(x)/\theta(x).$$

Since both E and θ are increasing downstream, the growth of $(\overline{u'^2})^{\frac{1}{2}}_{\text{c.l.}}$ is levelled by the growth of θ. Thus $(\overline{u'^2})^{\frac{1}{2}}_{\text{c.l.}}$ attains its maximum at some downstream location.

(iii) *The mean flow*

The development of θ, which characterizes the mean flow shape, is shown in figure 24. Again, the influence of the large-scale structure on the mean flow is negligible for low levels of excitation,

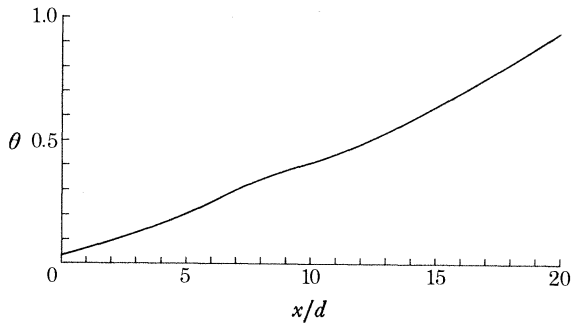

FIGURE 24. Mean flow momentum thickness θ along the jet; $0.02 \leqslant St \leqslant 1.60$.

and the development of the mean flow is governed by its interaction with the fine-grained turbulence alone. Hence, $\mathrm{d}\theta/\mathrm{d}x$ is obtained from (5.1) as

$$\frac{\mathrm{d}\theta}{\mathrm{d}x} \approx -2E(x)\, I'_{\mathrm{R.S.}}(\theta) \Big/ \frac{\mathrm{d}I_1(\theta)}{\mathrm{d}\theta}$$

Since the production rate is initially large, the jet spreads relatively quickly at first. Far downstream, the increase in E is balanced by a corresponding increase in θ in such a way that the jet spreads at a nearly constant rate.

It is seen here that if the large-scale structure is sufficiently weak, the evolution of the mean motion, including the Reynolds stresses, is controlled by the turbulence-mean flow interaction. The large-scale structure can then be obtained subsequent to the mean motion problem, an approximation explored earlier by Liu (1974) and Merkine & Liu (1975).

(*b*) *Higher levels of excitation*

We consider here greater levels of initial excitation, where the influence of the large-scale structure would be pronounced. Three initial levels of the large-scale structure are considered: $|A|_0^2 = 10^{-1}$, 10^{-3} and 10^{-5}. The initial values for E_0 and θ_0 are kept constant at 10^{-3} and 0.034, respectively. The representative Strouhal numbers considered are 0.18, 0.35, 0.50, and 0.80.

(i) *The large-scale structure*

The development of the large-scale structure energy $|A|^2$ is shown in figure 25. Under any level of excitation, the high-frequency waves prevail upstream while the low-frequency ones prevail farther downstream. The large-scale structure is restricted to the upstream region of the jet where $x < 15d$, because of the production and dissipation mechanisms inherent in the local flow structure. Thus beyond this region there is a much smaller probability that any large-scale structure is present. The Strouhal number that produces the peak maximum amplification is a function of the initial values of $|A|_0^2$. For instance, at $|A|_0^2 = 10^{-1}$, 10^{-3}, 10^{-5} and $10^{-6.5}$, the peak Strouhal numbers are 0.35, 0.5, 0.5 and 0.7 respectively. Since these values of $|A|_0^2$ cover almost the whole range of possible initial levels, we conclude that the peak Strouhal number ranges from 0.35 to 0.7 depending on the initial level of excitation. Since $\mathrm{d}|A|^2/\mathrm{d}x \propto |A|^2$, increasing $|A|_0^2$ produces a greater rate of wave development, in addition to enhancing the nonlinear effects. Therefore, as $|A|_0^2$ increases, the location of peak amplification moves upstream and the streamwise lifespan is reduced.

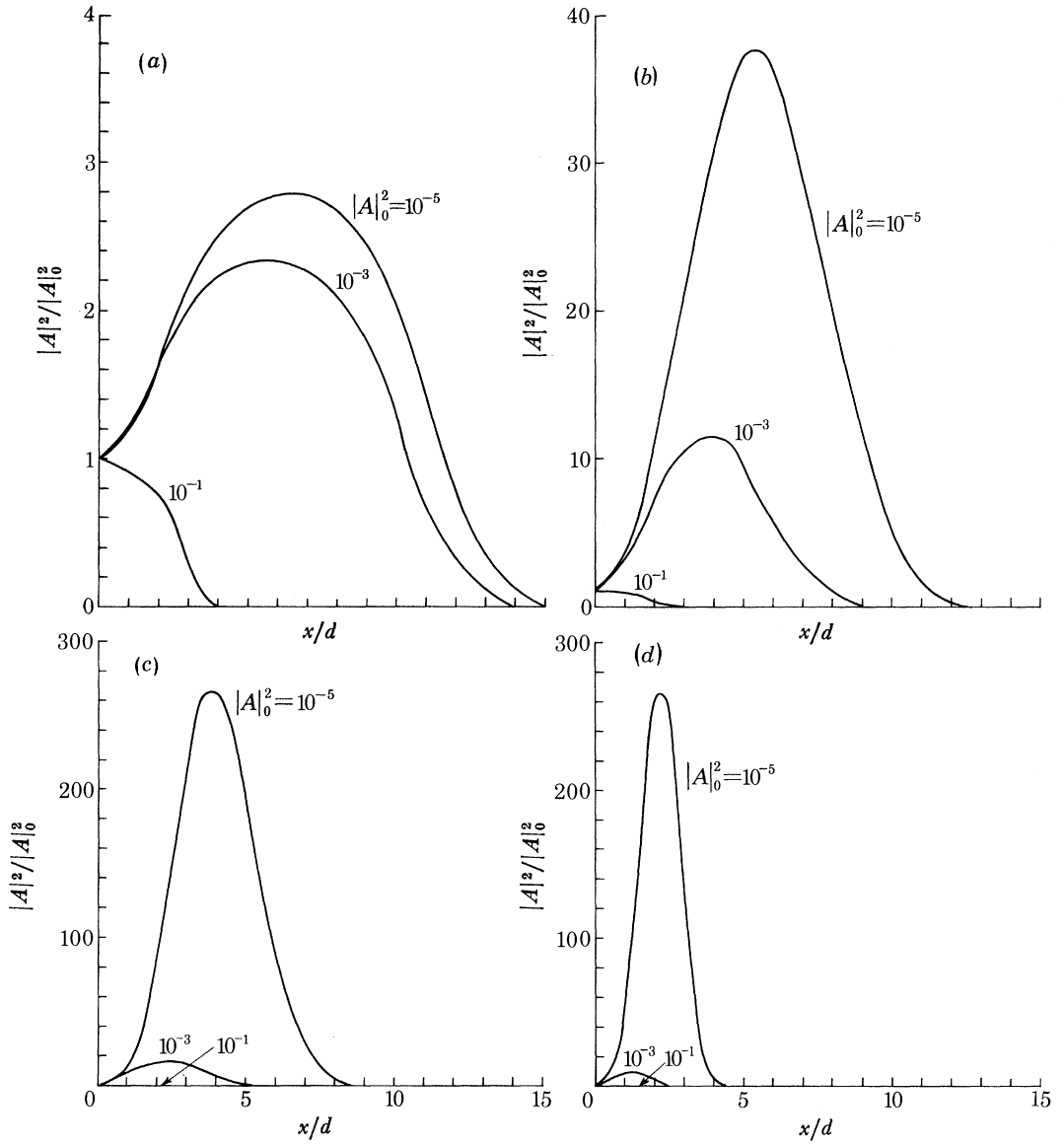

FIGURE 25. Large-scale structure energy ratio $|A|^2/|A|_0^2$ along the jet for several initial large-scale structure energy levels, $|A|_0^2$. (*a*) $St = 0.18$, (*b*) $St = 0.35$, (*c*) $St = 0.50$, (*d*) $St = 0.80$.

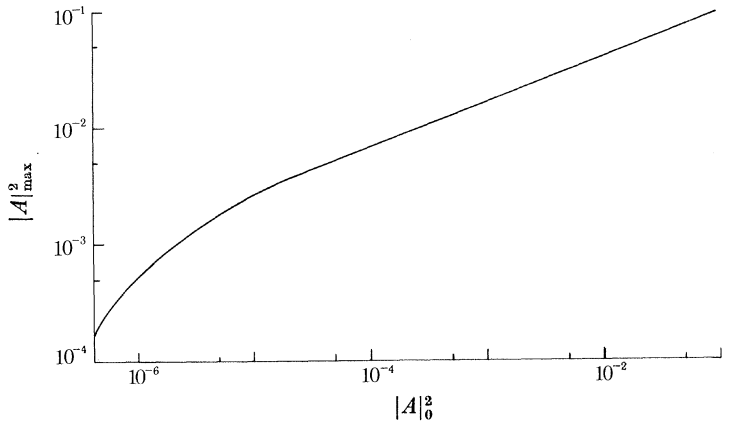

FIGURE 26. Maximum values of the large-scale structure energy $|A|^2$ as a function of the initial energy level $|A|_0^2$.

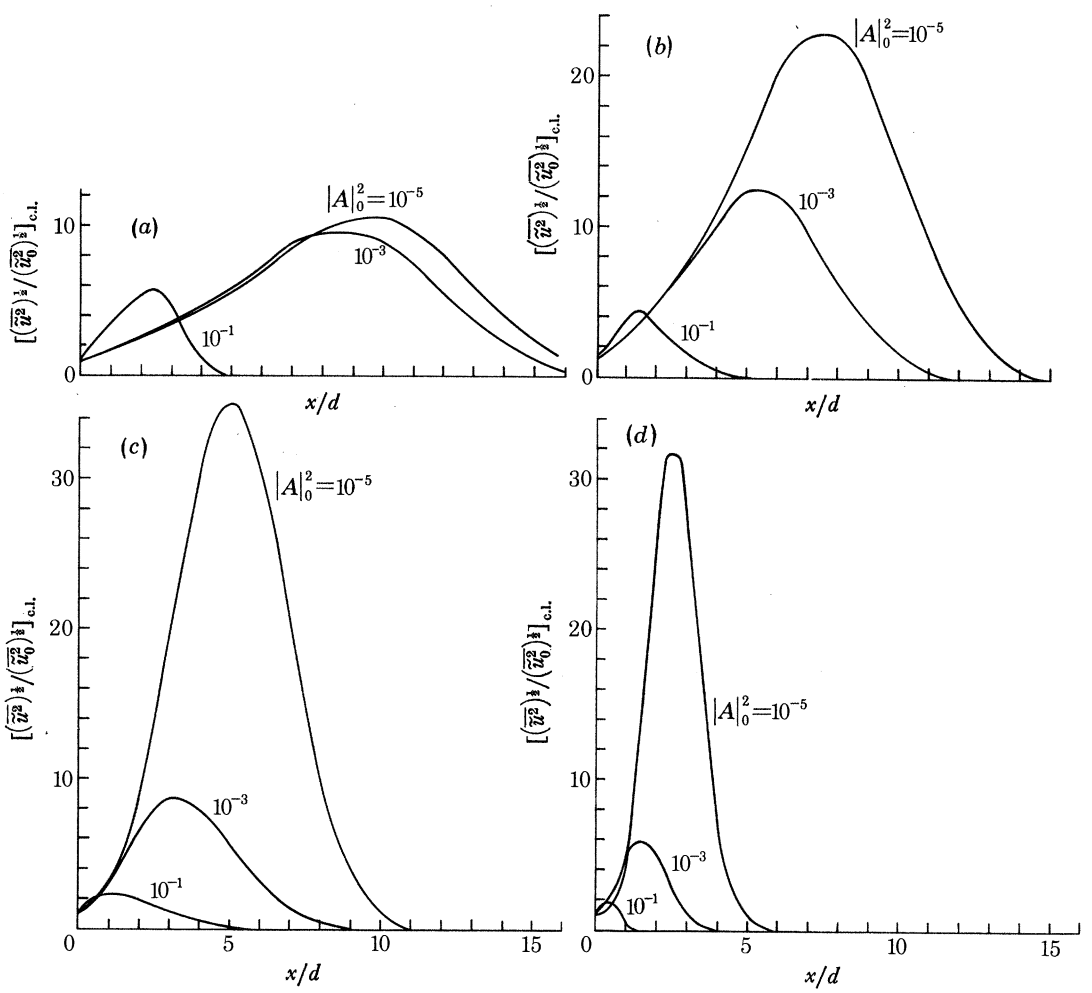

FIGURE 27. Large-scale structure r.m.s. streamwise velocity component ratio $(\overline{\tilde{u}^2})^{\frac{1}{2}}/(\overline{\tilde{u}_0^2})^{\frac{1}{2}}$ along the jet centreline for several initial large-scale structure energy levels $|A|_0^2$. (*a*) $St = 0.18$, (*b*) $St = 0.35$, (*c*) $St = 0.50$, (*d*) $St = 0.80$.

For very low levels of $|A|_0^2$ the influence of the large-scale structure on the fine-grained turbulence is negligible. In such a case, $E(x)$ is independent of $|A|^2$, and (5.2) can be integrated to give

$$|A(x, St, n)|^2 = |A|_0^2 [I_2(x_0, St, n)/I_2(x, St, n)] \exp\left\{\int_0^x [I_{\text{R.S.}}(x', St, n) - E(x')\, I_{\text{w.t.}}(x', St, n)]/I_2(x, St, n)\, \mathrm{d}x\right\},$$

which shows that for low levels of large-scale structure, $|A|^2$ increases linearly with $|A|_0^2$. However, as $|A|_0^2$, increases, the large-scale structure enhances the fine-grained turbulence energy and the above approximation would not be valid. Thus, as observed by Crow & Champagne (1971), $|A|_{\text{max}}^2$ increases nonlinearly with $|A|_0^2$, as shown in figure 26. Figure 26 also shows that a saturation condition is reached for $|A|_0^2 \gtrsim 10^{-1}$, where the wave no longer amplifies.

The large-scale structure axial velocity component at the jet centreline $(\overline{\tilde{u}^2})_{\text{c.l.}}^{\frac{1}{2}}$, shown in figure 27, follows the same trend as that of $|A|$. Increasing $|A|_0^2$ moves the peak upstream and reduces both the lifespan and the maximum amplification. Since increasing $|A|_0^2$ enhances mixing and thus accelerates the spread of the shear layer to the jet centreline, the $|A|_0^2 = 10^{-1}$ case here is slightly amplified (although $|A|^2$ itself was not).

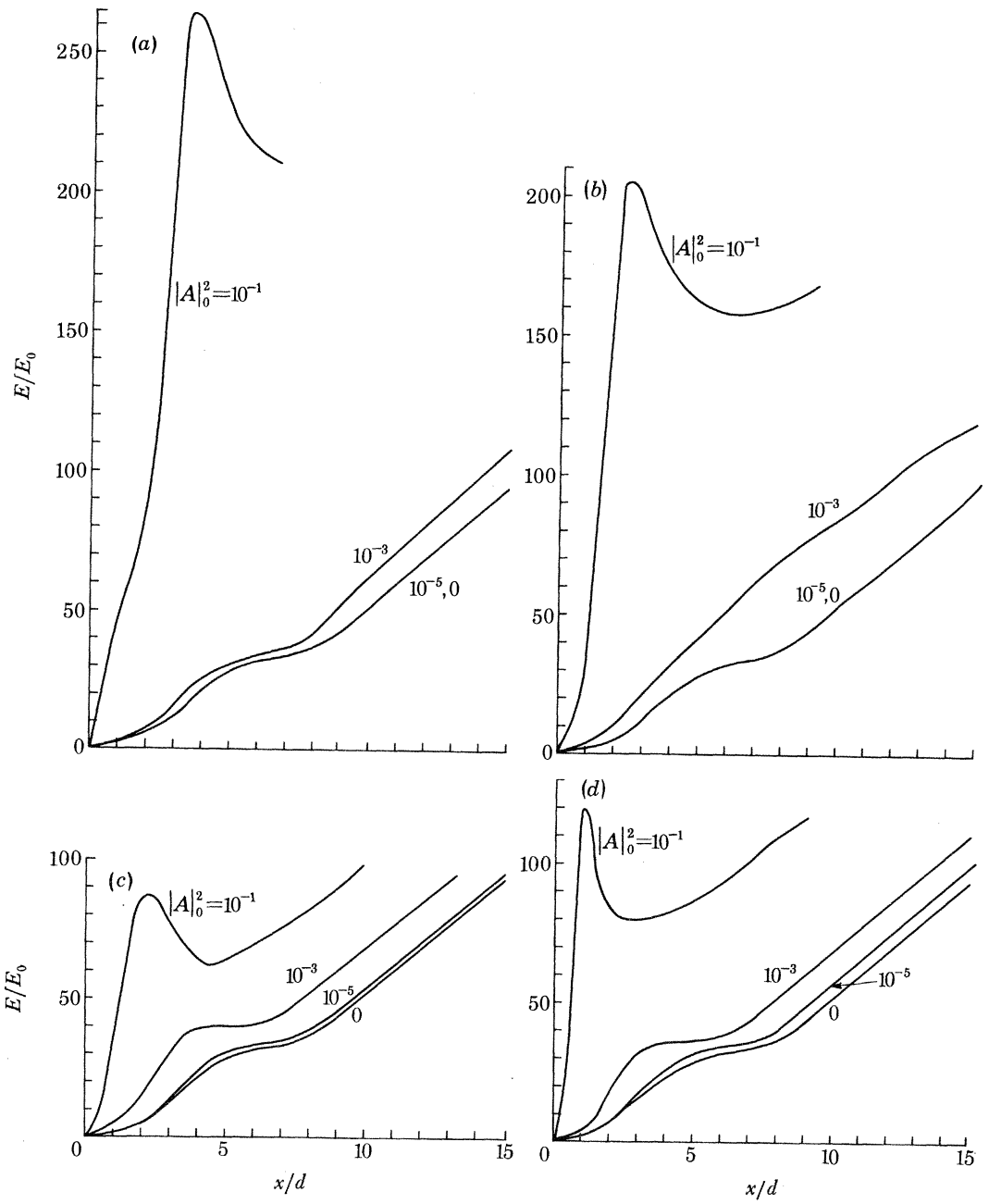

FIGURE 28. Fine-grained turbulence energy ratio E/E_0 along the jet for several initial large-scale structure energy levels $|A|_0^2$. (*a*) $St = 0.18$, (*b*) $St = 0.35$, (*c*) $St = 0.50$, (*d*) $St = 0.80$.

(ii) *The fine-grained turbulence*

It was shown earlier that if $|A|_0^2$ is small the influence of the large-scale structure is negligible. Increasing $|A|_0^2$ increases $|A|^2$ and consequently the energy transfer rate $|A|^2 EI_{\text{w.t.}}$ increases. Thus E increases as $|A|^2$ increases, as indicated in figure 28. Once E is increased, two more mechanisms produce additional increases in E: $|A|^2 EI_{\text{w.t.}}$ increases further, and the fine-grained turbulence production by the mean flow, $EI'_{\text{R.s.}}$, also increases. Therefore, the large-scale structure not only pumps energy from the mean flow to the fine-grained turbulence, but also acts as a catalyst to

enhance the direct transfer of the mean flow energy to the fine-grained turbulence. As a result of these direct and indirect mechanisms, the growth of E along the jet is greatly increased.

An excessive increase in E, such as that produced by $|A|_0^2 = 10^{-1}$, would trigger viscous dissipation, $E^{\frac{3}{2}}I_\epsilon$, which would reduce E until the production exceeded the dissipation again. Once $|A|^2$ reaches zero, its 'turbulent dissipation' vanishes and the growth of E is governed by its interaction with the mean flow alone. Therefore, the rate of growth of E downstream is the same as that at $|A|_0^2 = 0$. However, as a result of the previous actions of the large-scale structure, the downstream values of E itself are greater and depend on $|A|_0^2$.

The effect of the large-scale structure on the fine-grained turbulence is influenced by the

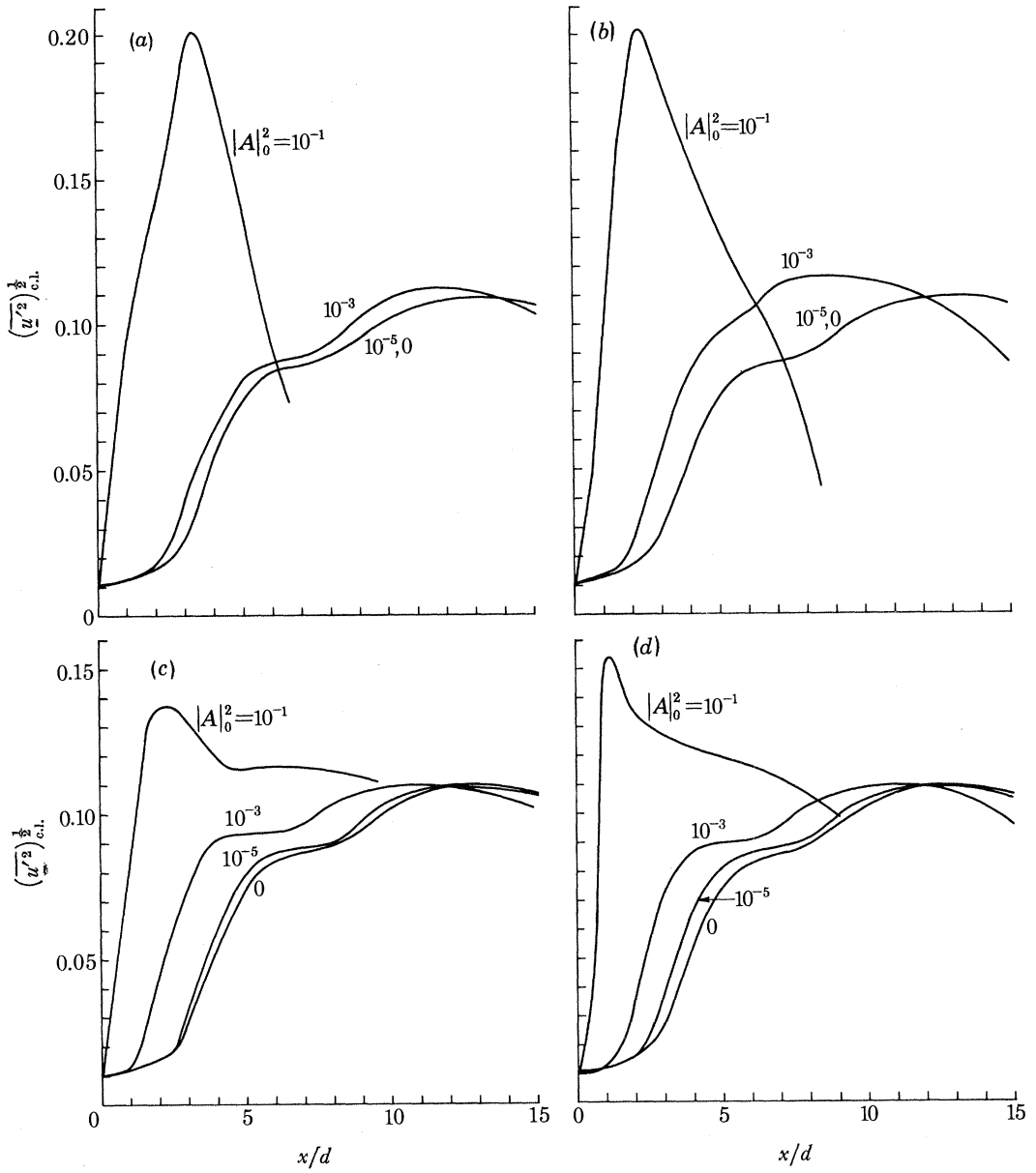

FIGURE 29. Fine-grained turbulence r.m.s. axial velocity component $(\overline{u'^2})^{\frac{1}{2}}$ along the jet centreline for several initial large-scale structure energy levels $|A|_0^2$. (*a*) $St = 0.18$, (*b*) $St = 0.35$, (*c*) $St = 0.50$, (*d*) $St = 0.80$.

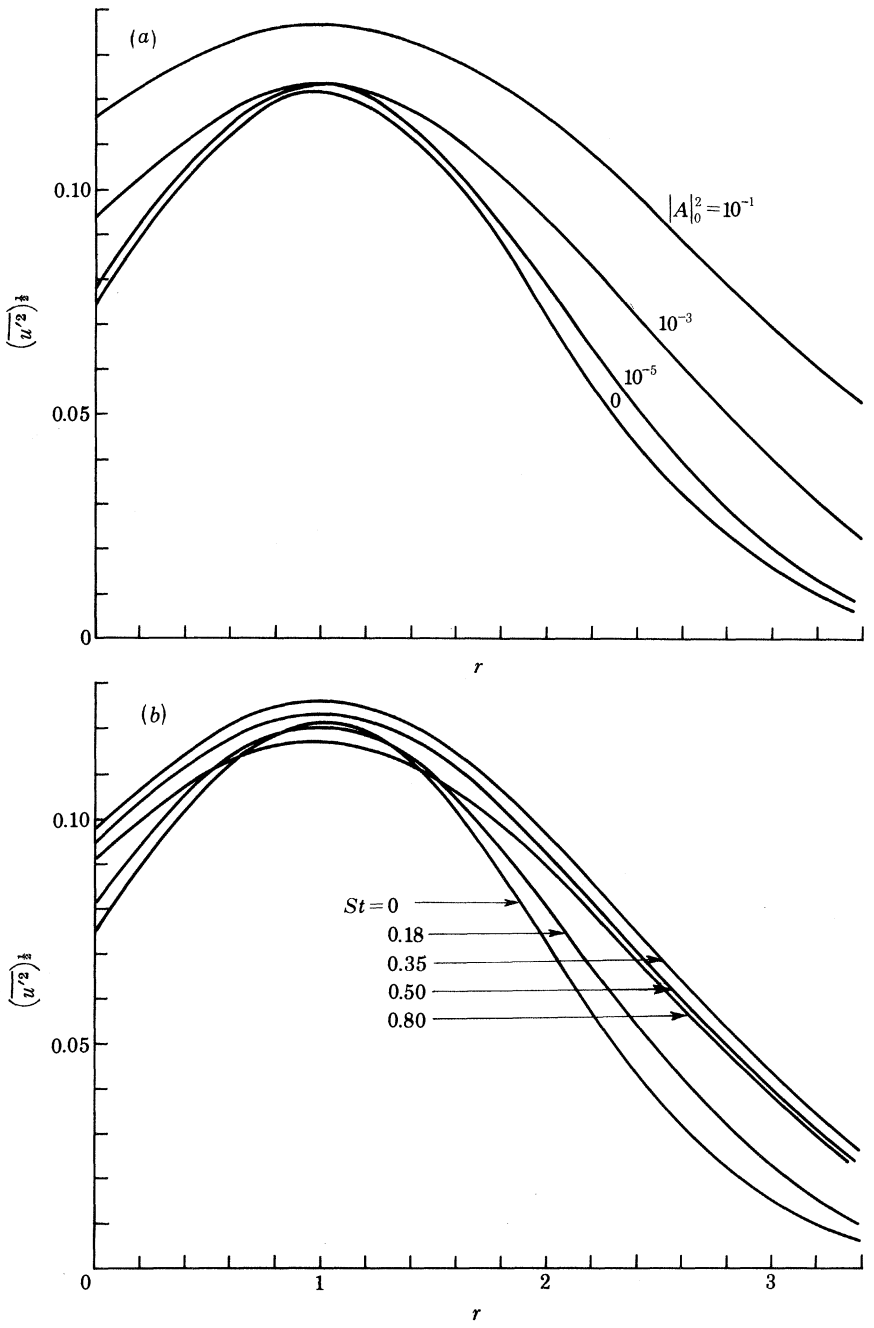

FIGURE 30. Radial distributions of fine-grained turbulence r.m.s. axial velocity component $(\overline{u'^2})^{\frac{1}{2}}$ at $x/d = 5$: (*a*) for various $|A|_0^2$, $St = 0.5$; (*b*) for various St, $|A|_0^2 = 10^{-3}$.

amount of amplification as well as the streamwise lifespan of $|A|^2$. Since both of these two factors vary with $|A|_0^2$ and St, the Strouhal number that produces the maximum influence of the large-scale structure on the fine-grained turbulence differs, depending on $|A|_0^2$. The Strouhal numbers that produce maximum enhancement in E are 0.18, 0.35 and 0.80 for $|A|_0^2 = 10^{-1}$, 10^{-3}, and 10^{-5}, respectively. If it were of interest to raise the fine-grained turbulence level by forcing an

organized structure, the best Strouhal number to do so would range from 0.18 to 0.80 depending on the initial level, $|A|_0^2$ of the large-scale structure.

The response of E to $|A|_0^2$ is naturally reflected in a similar effect of $|A|_0^2$ on the centreline values of $(\overline{u'^2})^{\frac{1}{2}}$, as shown in figure 29. Yet the influence of the extent of the shear layer on the centreline values must also be taken into consideration. The large-scale structure increases not only E, but also θ. Consequently the shear layer approaches the centreline faster with increased $|A|_0^2$. This rapid extension of the shear layer, in addition to the higher values of E, produces a considerable increase in $(\overline{u'^2})^{\frac{1}{2}}$ along the initial part of the jet centreline. But far downstream, where $\overline{u'^2} \sim E/\theta$, the increase in E produced by increasing $|A|_0^2$ cannot balance the corresponding increase of θ. Thus $(\overline{u'^2})^{\frac{1}{2}}$ slightly decreases downstream with increasing $|A|_0^2$. $(\overline{u'^2})^{\frac{1}{2}}$ extends more in the radial direction with increasing $|A|_0^2$, as shown in figure 30*a* for $St = 0.5$ and $x/d = 5$. For $|A|_0^2 = 10^{-3}$, the increases in E and θ are a maximum at $St = 0.35$. The radial extent and the magnitude of $(\overline{u'^2})^{\frac{1}{2}}$ are a maximum for $St = 0.35$ (figure 30*b*).

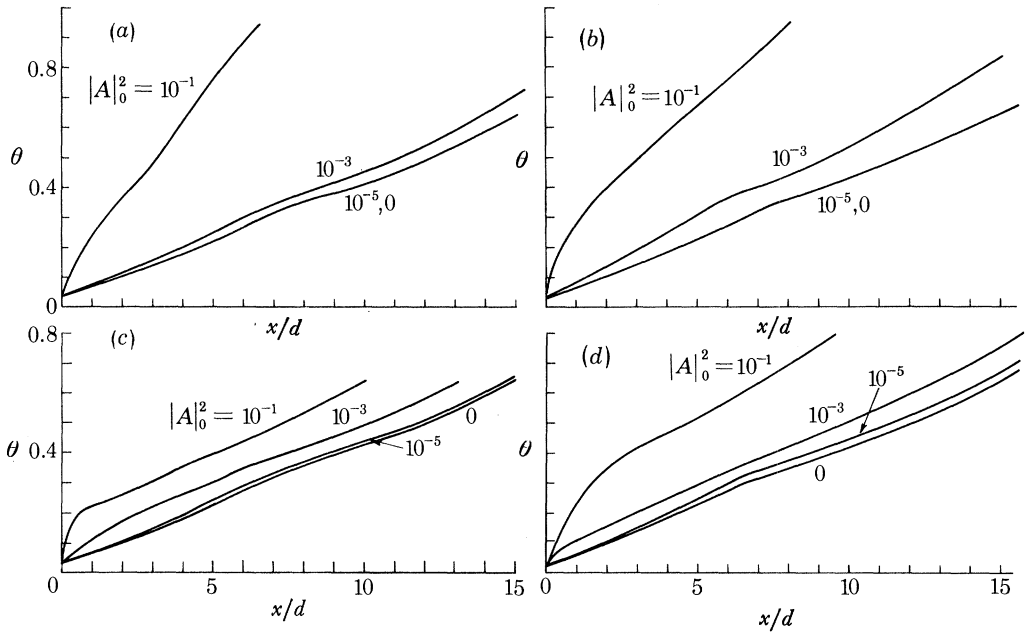

FIGURE 31. Mean flow momentum thickness θ along the jet for several energy levels $|A|_0^2$. (*a*) $St = 0.18$, (*b*) $St = 0.35$, (*c*) $St = 0.50$, (*d*) $St = 0.80$.

(iii) *The mean flow*

Both the large-scale structure and the fine-grained turbulence influence the mean flow shape through θ, as can be seen from the shape assumption (4.1) and the integrated energy equations (5.1)–(5.3). Since both $|A|^2$ and E increase with $|A|_0^2$, the mean flow energy loss consequently increases. As θ is inversely proportional to the energy content of the mean flow, it increases with $|A|_0^2$, as shown in figure 31. Once the large-scale structure has completely decayed, the mean flow growth is governed by its interaction with the fine-grained turbulence alone. Because the large-scale structure alters the values of E and θ downstream, the rate of spreading downstream is slightly greater than the corresponding rate in the complete absence of any large-scale structure.

To display the effect of the large-scale structure in accelerating the mixing process, let us define the end of the potential core as the point where the axial mean velocity U at $r = 0.5$ equals 95 % of its centreline value. Such a definition gives $\theta = 0.25$ for the end of the potential core. By

PHILOSOPHICAL TRANSACTIONS OF THE ROYAL SOCIETY A MATHEMATICAL, PHYSICAL & ENGINEERING SCIENCES

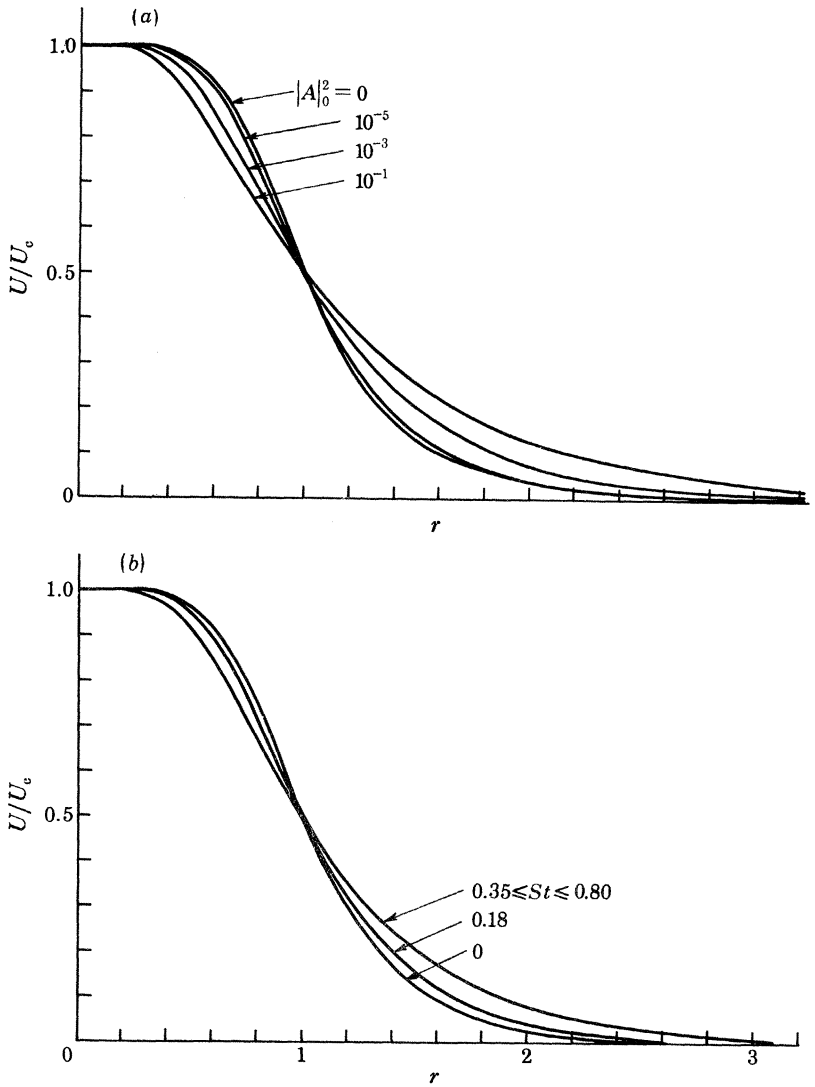

FIGURE 32. Radial distribution of the mean flow velocity ratio U/U_e at $x/d = 5$; (*a*) for various $|A|_0^2$, $St = 0.50$; (*b*) for various St, $|A|_0^2 = 10^{-3}$.

using this definition, figure 31 gives the length of the potential core in the absence of large-scale structure as $5.5d$ and also shows that in the presence of large-scale structure, it could be as short as one diameter length. The end of the potential core indicates that the shear layer has extended to the jet centreline and is consequently an indication of the mixing rate. Thus the large-scale structure can reduce the mixing region considerably.

The effect of the large-scale structure on the mean flow is influenced by both the amplification and the streamwise lifespan of $|A|^2$, and both of these quantities are governed by St and $|A|_0^2$. Consequently, the Strouhal number that produces maximum enhancement in the spreading of the jet depends on the level of excitation. These Strouhal numbers are 0.18, 0.35 and 0.8 for $|A|_0^2 = 10^{-1}$, 10^{-3} and 10^{-5} respectively.

Since θ increases with $|A|_0^2$, the radial extent of the mean flow increases with $|A|_0^2$, as shown in figure 32*a* for $St = 0.5$ and $x/d = 5$. For $|A|_0^2 = 10^{-3}$ and $x/d = 5$, figure 32*b* shows that the radial extension of the mean flow increases with Strouhal number up to $St = 0.35$. Further increase in

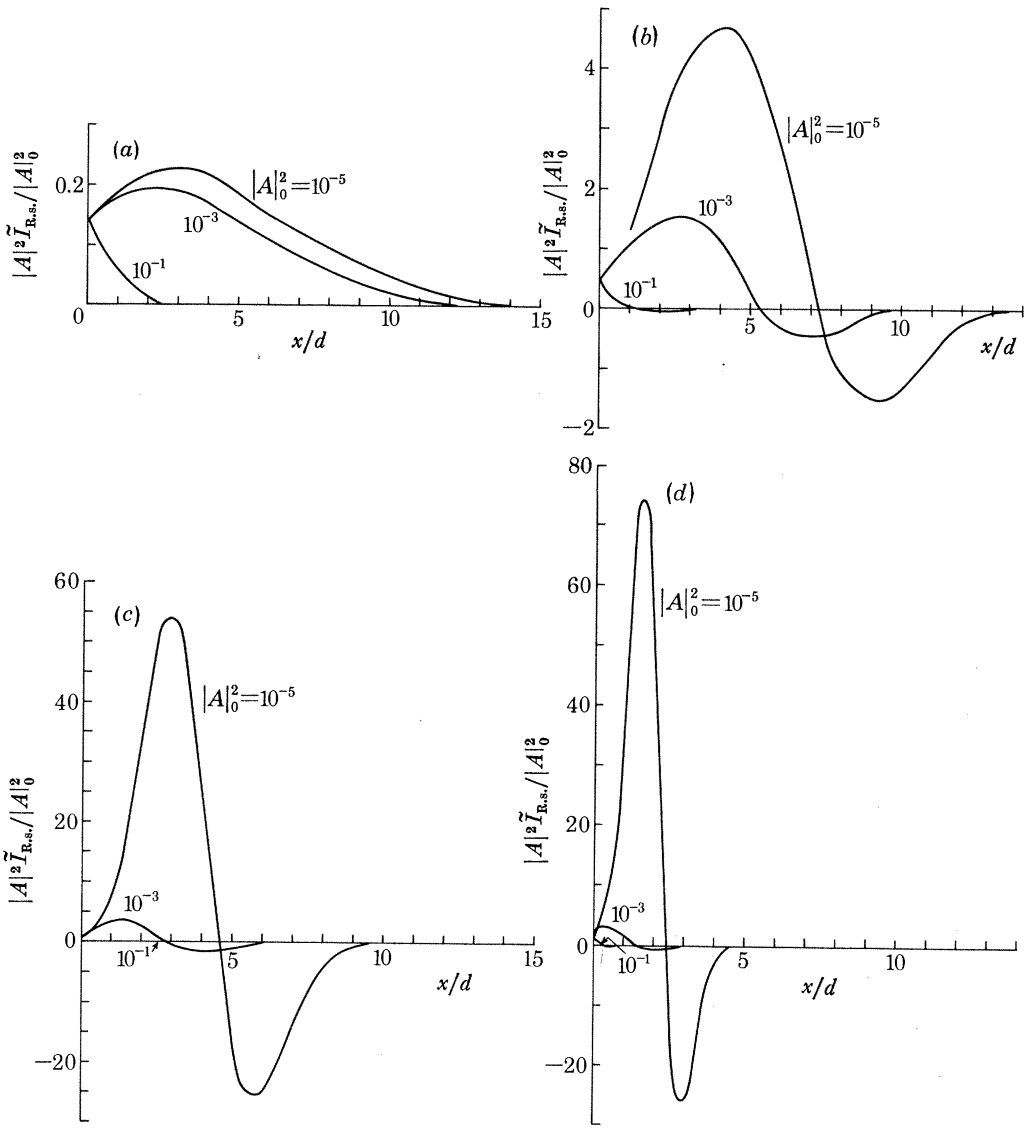

FIGURE 33. Large-scale structure production rate $|A|^2\tilde{I}_{R.s.}/|A|_0^2$ along the jet for various initial energy levels $|A|_0^2$. (*a*) $St = 0.18$, (*b*) $St = 0.35$, (*c*) $St = 0.50$, (*d*) $St = 0.80$.

St, under the same initial conditions, produces the same increase in jet spreading as that for $St = 0.35$. Thus, if it is of interest to accelerate jet spreading by forcing a large-scale structure, it would be appropriate to seek an optimum Strouhal number that produces the greatest increase in the spreading of the jet for a given level of forcing.

(*c*) *The energy transfer mechanisms*

To understand the energy transfer mechanisms, all the energy exchange terms appearing in the nonlinear interaction problem (5.1)–(5.3) are discussed here in detail.

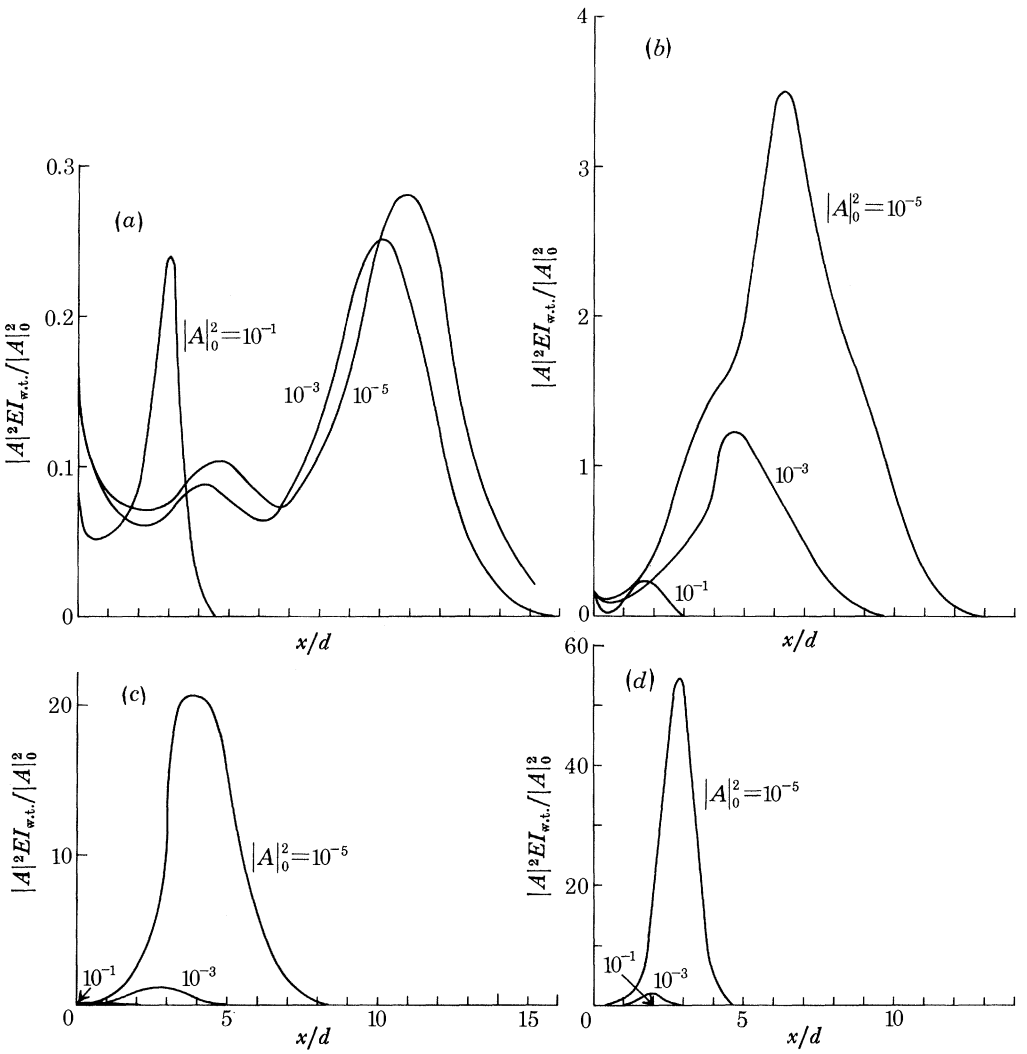

FIGURE 34. Large-scale structure to fine-grained turbulence energy transfer rate $|A|^2EI_{\text{w.t.}}/|A|_0^2$ along the jet for several initial energy levels $|A|_0^2$. (*a*) $St = 0.18$, (*b*) $St = 0.35$, (*c*) $St = 0.50$, (*d*) $St = 0.80$.

(i) *The large-scale structure production*

The large-scale structure production, $|A|^2\tilde{I}_{\text{R.s.}}/|A|_0^2$, as shown in figure 33, first increases to a maximum along the jet as a result of increasing $|A|^2$. Farther downstream, as a result of the weakening mean shear, $\tilde{I}_{\text{R.s.}}$ decreases, as does $|A|^2$, and consequently, the large-scale structure production decreases along the jet. For large St, the production integral $\tilde{I}_{\text{R.s.}}$ becomes negative downstream. Hence the production process is reversed and energy is transferred from the large-scale structure to the mean flow, contributing to the decay of the former. Once $|A|^2 = 0$ the production process ceases.

Since increasing $|A|_0^2$ accelerates the development processes and since $\tilde{I}_{\text{R.s.}}$ goes to zero faster as the Strouhal number increases, the streamwise duration of the production process is approximately proportional to both St^{-1} and $\ln|A|^{-2}$.

(ii) *The interaction between the large-scale structure and the fine-grained turbulence*

Since $I_{\text{w.t.}}$ decreases with θ, the turbulent dissipation $|A|^2 EI_{\text{w.t.}}/|A|_0^2$ first decreases slightly along the jet, as shown in figure 34. But since $|A|^2$ and E are increasing along the jet, the turbulent dissipation increases to a maximum and then decays with $|A|^2$. Once $|A|^2 = 0$, the large-scale structure has no more energy to be lost; the interaction between the large-scale structure and the fine-grained turbulence ceases.

Comparing figures 34 and 33 shows that the turbulent dissipation is much greater than the corresponding negative production. Thus the turbulent dissipation mechanism is the dominant one which gives rise to the decay of the large-scale structure. In the absence of turbulent dissipation, (5.2) gives the wave-growth as

$$|A|^2 = |A|_0^2 [I_2(x_0, St, n)/I_2(x, St, n)] \exp\left\{\int_0^x [\tilde{I}_{\text{R.s.}}(x', St, n)/I_2(x', St, n)]\, dx'\right\},$$

which shows that $|A|^2$ grows exponentially as long as $\tilde{I}_{\text{R.s.}}(x', St, b)$ is positive. Thus, were it not for the turbulent dissipation, the wave would have continued to grow much farther along the jet.

The large-scale structure grows in the initial region of the jet by extracting energy from the mean flow. As the mean shear decreases along the jet, the large-scale structure production cannot balance its turbulence dissipation and consequently decays. Most of the large-scale structure energy has thus been transferred to the fine-grained turbulence, while a smaller portion is returned to the mean flow. It extracts energy from the mean flow only to give it, in addition to its own initial energy, to the fine-grained turbulence.

(iii) *The fine-grained turbulence production by the mean flow*

As E is increased, the large-scale structure acts as a catalyst in increasing the fine-grained turbulence production $EI'_{\text{R.s.}}$ as shown in figure 35. The rate of production is a balance between the level of turbulence E and the jet spreading. Since E increases along the jet while $I'_{\text{R.s.}}(\theta)$ decreases, the production attains its maximum or minimum depending on the rate at which E increases relative to the rate at which $I'_{\text{R.s.}}$ decreases along the jet. Far downstream the growth of E is balanced by a similar growth in θ so that the production $EI'_{\text{R.s.}}$ attains an asymptotic value of approximately 0.005, independent of the initial level of the large-scale structure.

(iv) *The viscous dissipation*

Since I_ϵ decreases with θ, the viscous dissipation $E^{\frac{3}{2}} I_\epsilon$ is also a balance between the level of turbulence E and the radial extension of the jet through θ. Since both E and θ increase along the jet, the viscous dissipation varies accordingly. Since E increases with $|A|_0^2$, the viscous dissipation also increases with $|A|_0^2$, as shown in figure 36. But for the downstream region the growth of E is balanced by a similar growth in θ in such a way as to make the viscous dissipation attain an asymptotic value of approximately 0.004, independent of the initial level of the large-scale structure. Comparing figures 36 and 35 shows that the asymptotic value of the production is greater than the asymptotic value of the viscous dissipation. Consequently, E increases linearly downstream.

The role of the fine-grained turbulence in the interaction process can now be stated. The fine-grained turbulence absorbs energy continuously from the mean flow and the large-scale structure, as long as the latter has any energy, and some of the fine-grained turbulence kinetic energy is converted into internal energy by the viscous dissipation.

PHILOSOPHICAL TRANSACTIONS OF THE ROYAL SOCIETY A MATHEMATICAL, PHYSICAL & ENGINEERING SCIENCES

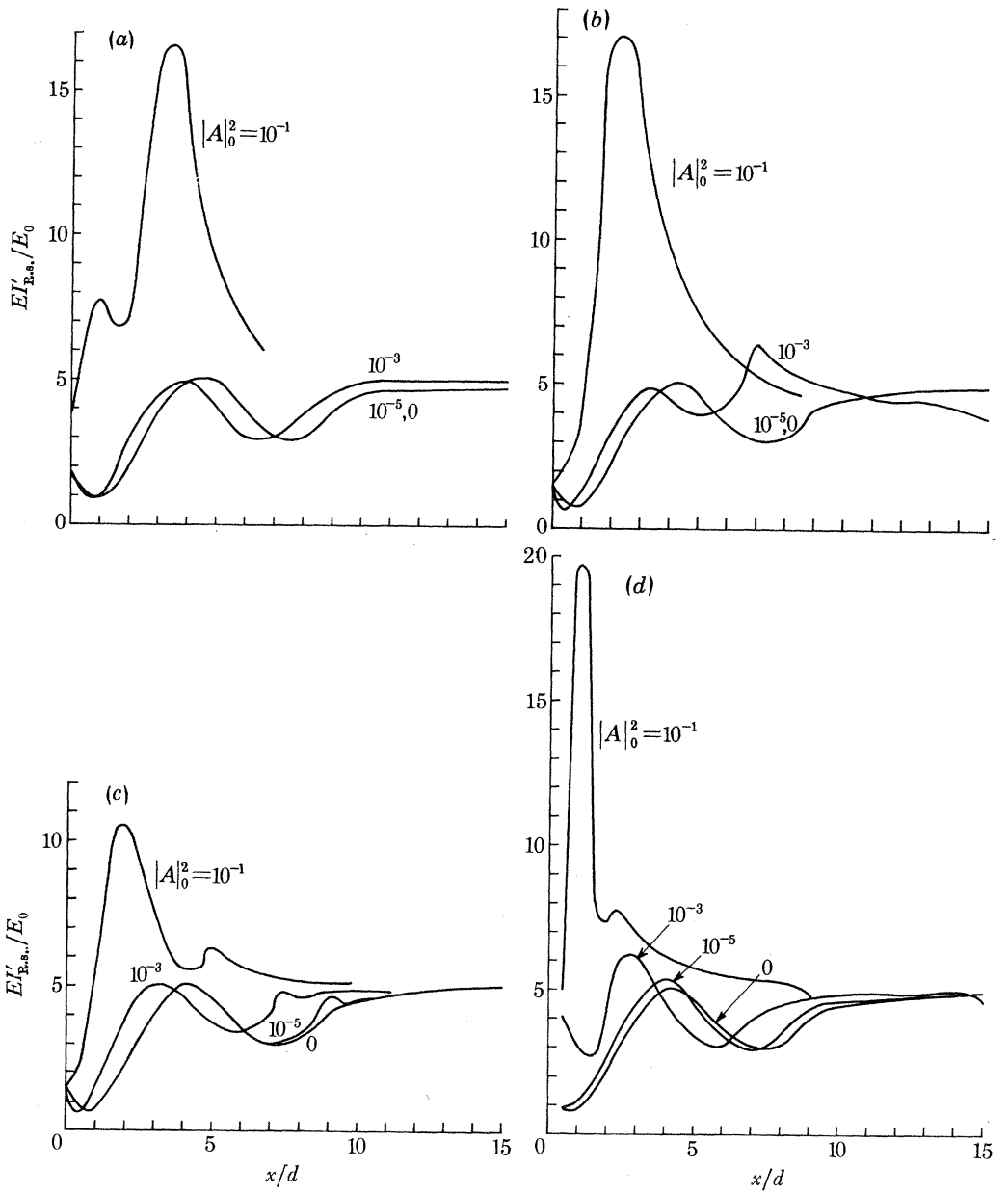

FIGURE 35. Fine-grained turbulence energy production rate $EI'_{\mathrm{R.s.}}/E_0$ along the jet for several initial energy levels $|A|_0^2$. (*a*) $St = 0.18$, (*b*) $St = 0.35$, (*c*) $St = 0.50$, (*d*) $St = 0.80$.

(v) *The mean flow energy loss*

Since both $|A|^2$ and E increase with $|A|_0^2$ the mean flow energy loss $|A|^2\tilde{I}_{\mathrm{R.S.}} + EI'_{\mathrm{R.S.}}$ also increases with $|A|_0^2$, as shown in figure 37. The variation in the mean flow energy loss along the jet follows from the variations of each production term. Far downstream, the loss is governed by the fine-grained turbulence production alone. Since the latter approaches an asymptotic value independent of the large-scale structure, the mean flow energy drain also attains the same asymptotic value independent of the large-scale structure. This asymptotic value indicates that the rate of jet spreading is constant, as we have already seen in figure 31. This is in agreement

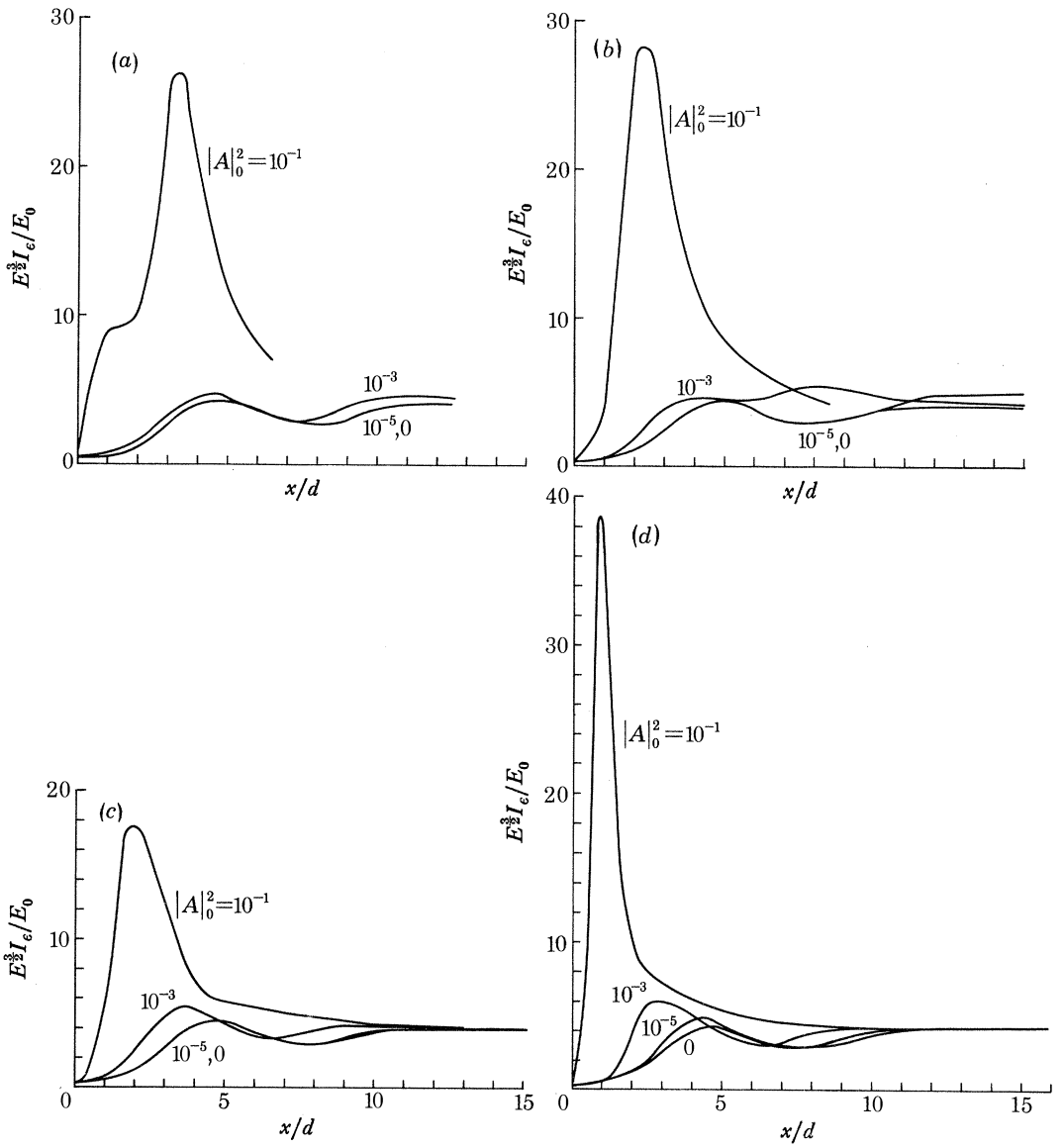

FIGURE 36. Fine-grained turbulence viscous dissipation rate $E^{\frac{3}{2}}I_\epsilon/E_0$ along the jet for several initial energy levels $|A|_0^2$. (*a*) $St = 0.18$, (*b*) $St = 0.35$, (*c*) $St = 0.50$, (*d*) $St = 0.80$.

with experimental observations for the fully developed region of the jet (Corrsin 1943; Corrsin & Uberoi 1950; Albertson *et al.* 1948).

At a given axial location, the difference between the energy loss at a finite $|A|_0^2$ and that at $|A|_0^2 = 0$ represents the increase in the mean flow energy loss as a result of the presence of the large-scale structure. Though the large-scale structure production is negative in some downstream locations, the fine-grained turbulence production exceeds this negative production, so that the net mean flow energy loss is always positive. Therefore, the role of the mean flow in the interaction process is to transfer net energy to the two fluctuating flow components.

The results here indicate that, downstream of the non-equilibrium region brought about by the growing and decaying large-scale coherent structure, the development of the mean flow and

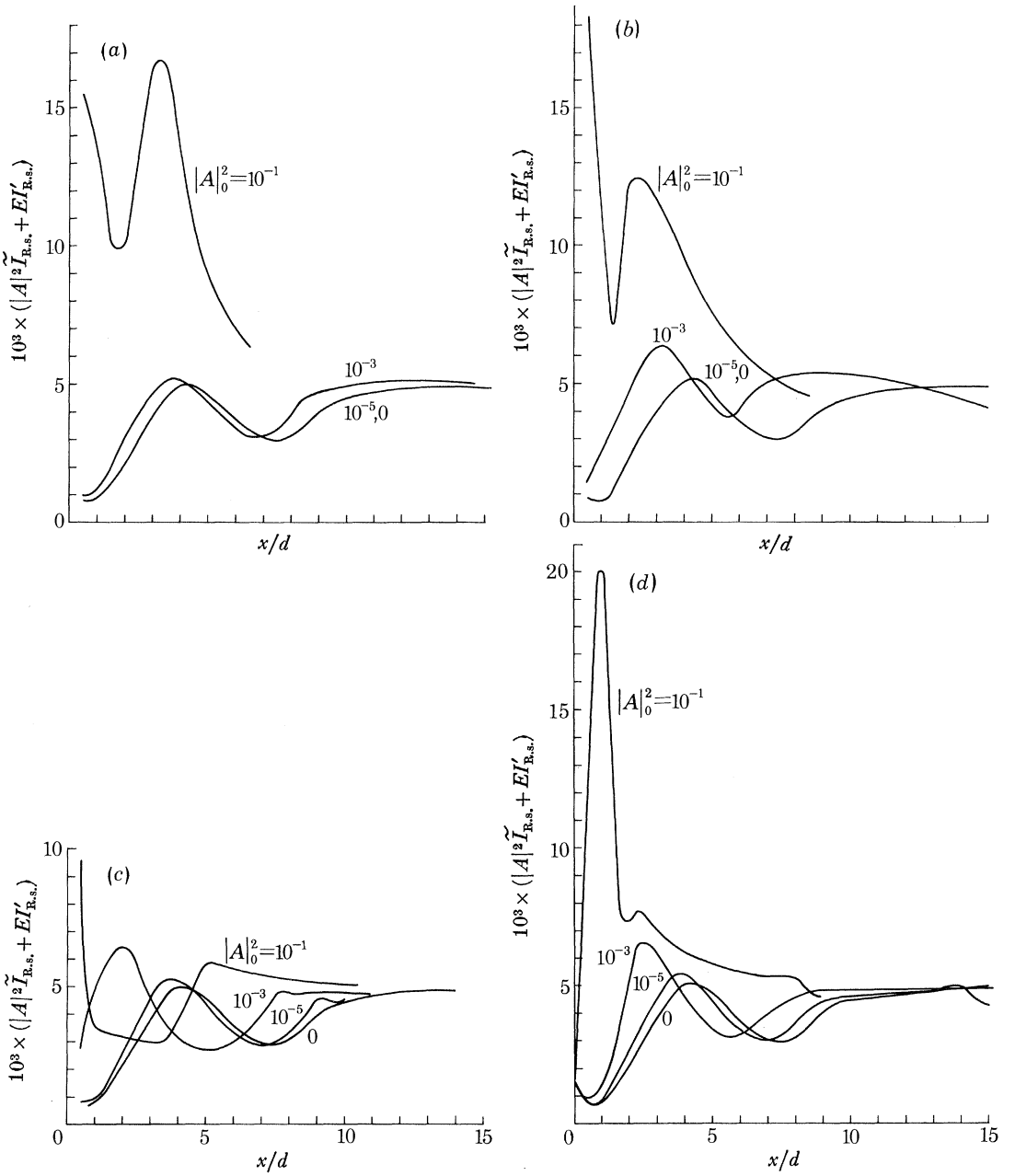

FIGURE 37. Mean flow energy loss rate $|A|^2\tilde{I}_{\mathrm{R.s.}}+EI'_{\mathrm{R.s}}$ along the jet for several initial energy levels $|A|_0^2$. (*a*) $St = 0.18$, (*b*) $St = 0.35$, (*c*) $St = 0.50$, (*d*) $St = 0.80$.

fine-grained turbulence is practically independent of the initial levels of the large-scale structure. This is somewhat reminiscent of the achievement of self-preservation discussed by Townsend (1956).

8. The nonlinear development of the $n = 1$ mode

Since the experimental observations have shown the large-scale structure to consist of several azimuthal components, by taking $n = 1$ we consider here the asymmetric component of the large-scale structure which rotates around the jet centreline like a helix. The results for the $n = 1$

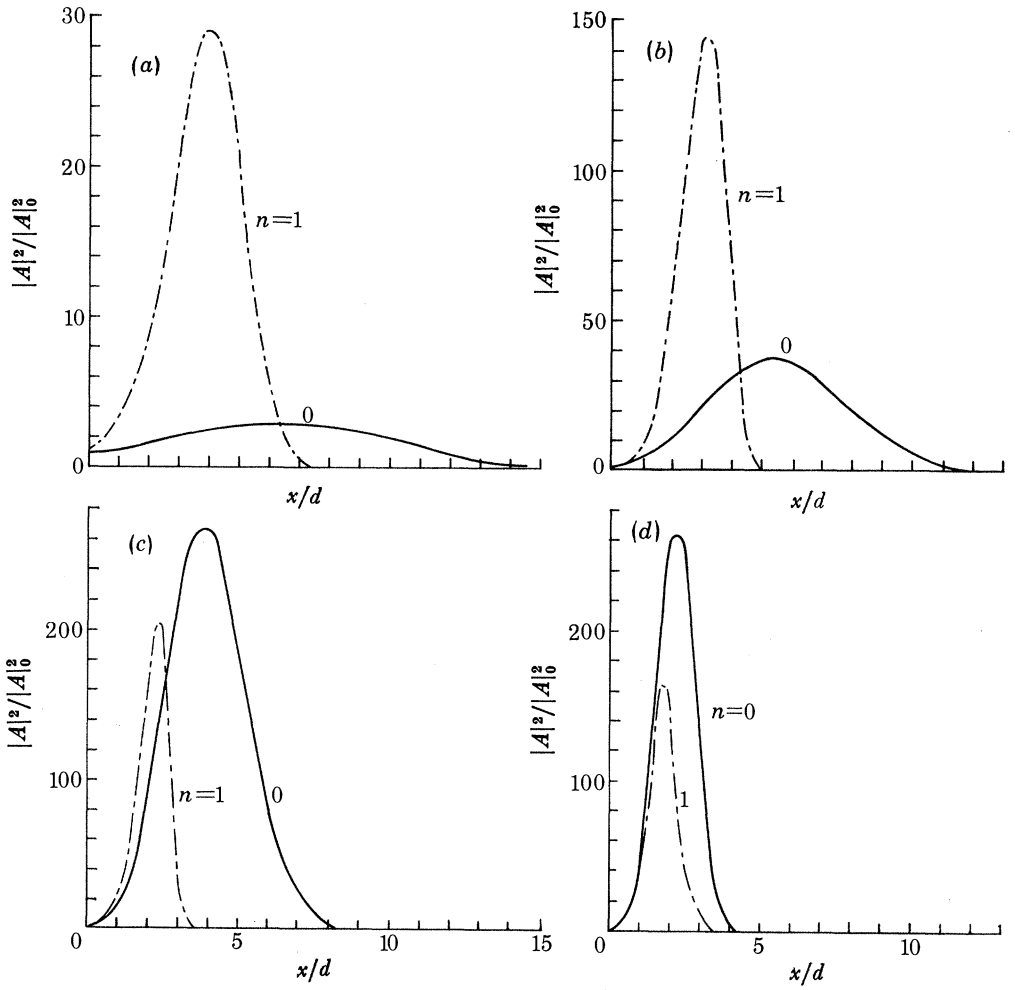

FIGURE 38. Large-scale structure kinetic energy ratio $|A|^2/|A|_0^2$ along the jet: comparisons between the $n = 0$ and $n = 1$ modes. (*a*) $St = 0.18$, (*b*) $St = 0.35$, (*c*) $St = 0.50$, (*d*) $St = 0.80$.

mode are compared with the corresponding results for the $n = 0$ mode under the same initial conditions, $|A|_0^2 = 10^{-5}$, $E_0 = 10^{-3}$ and $\theta = 0.034$. Four Strouhal numbers 0.18, 0.35, 0.50 and 0.80 are considered here, to span the range of Strouhal numbers of interest.

(*a*) *The large-scale structure*

The amplification of $|A|^2$ is shown in figure 38 for both values of n. The production integral $\tilde{I}_{\text{R.s.}}$ for $n = 1$ at small Strouhal numbers is larger than that for the $n = 0$ mode. The results thus show that only at small Strouhal numbers is the $n = 1$ mode amplified more than the $n = 0$ mode.

For all Strouhal numbers considered, the asymmetric wave decays downstream much faster than the axisymmetric wave. The azimuthal action of the wave produces an efficient mechanism for energy transfer between the large-scale structure and the fine-grained turbulence as discussed in §§4 and 5. Thus, the larger values of the interaction integral $I_{\text{w.t.}}$ produce a greater turbulent dissipation, that causes the asymmetric modes to be restricted to a smaller region in the vicinity of the nozzle exit, compared to that of the $n = 0$ mode at the same Strouhal number. For the most part, the jet observations would most likely show the axisymmetric mode to be the dominant one (Michalke & Fuchs 1974).

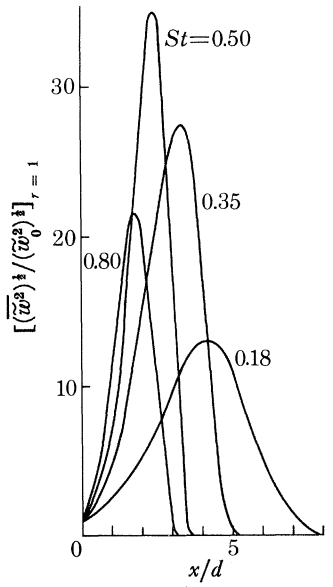

FIGURE 39. Large-scale structure r.m.s. azimuthal velocity component $(\overline{\tilde{w}^2})^{\frac{1}{2}}/(\overline{\tilde{w}_0^2})^{\frac{1}{2}}$ along the centre of the shear layer $r = 1$ for various Strouhal numbers; $n = 1$.

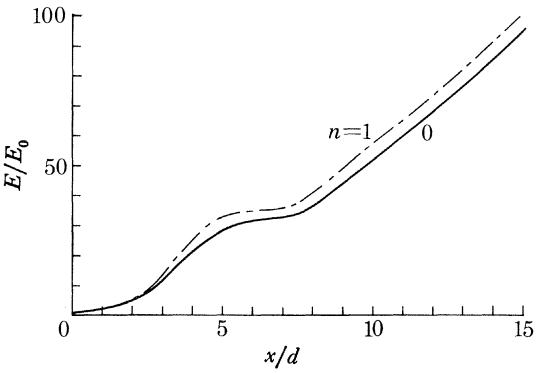

FIGURE 40. Fine-grained turbulence kinetic energy ratio E/E_0 along the jet: comparison between the $n = 0$ and $n = 1$ modes. $St = 0.35$.

The azimuthal velocity $(\overline{\tilde{w}^2})^{\frac{1}{2}}$ is identically zero for $n = 0$. Its distribution along the jet for the $n = 1$ mode is shown in figure 39 for several values of St. As St increases, the peak of $(\overline{\tilde{w}^2})^{\frac{1}{2}}$ moves closer to the nozzle exit; its lifespan is reduced and its peak amplification is achieved about $St = 0.5$, which is also the peak Strouhal number for $|A|^2$ for the initial conditions considered here.

(*b*) *The fine-grained turbulence*

Although the large-scale structure streamwise lifespan is shorter for the $n = 1$ than for the $n = 0$ mode, the turbulent dissipation for $n = 1$ is so effective that the energy loss from the large-scale structure to the fine-grained turbulence is greater than that for $n = 0$. Therefore, E is somewhat larger for $n = 1$, as shown in figure 40 for $St = 0.35$. At smaller St the wave amplification is too weak for the influence of n on E to be pronounced. For $St = 0.35$ the greater amplification of $|A|^2$ at $n = 1$ is added to the efficient turbulent dissipation mechanism to produce the maximum influence of the $n = 1$ mode on E. As the Strouhal number increases further, the wave lifespan is reduced and consequently its effect on E diminishes. Thus the $St = 0.18$, $St = 0.50$ and $St = 0.80$ cases all show negligible influence of n on E, and they are not given here. (The influence on n of E produces a similar effect on the centreline values of $(\overline{u'^2})^{\frac{1}{2}}$, which is not shown here.) Far downstream the effect of n on increasing E is balanced by a corresponding increase in θ in such a way that $(\overline{u'^2})^{\frac{1}{2}}$ becomes independent of n downstream.

(*c*) *The mean flow*

As a result of increasing E, the fine-grained turbulence production is greater for the $n = 1$ than for the $n = 0$ mode. Thus the jet spreading is slightly greater for $n = 1$, as shown in figure 41 for $St = 0.35$. The weak wave amplification at smaller Strouhal numbers and the short wave lifespan at greater Strouhal numbers make the influence of n on the mean flow more pronounced only in the range $0.35 \leqslant St \leqslant 0.50$.

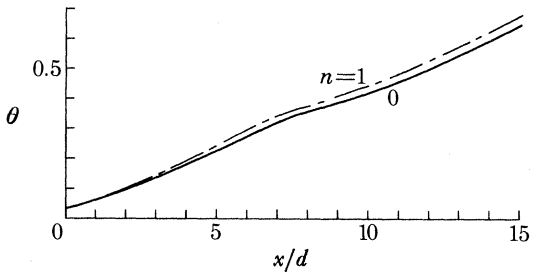

FIGURE 41. Mean flow momentum thickness along the jet: comparison between the $n = 0$ and $n = 1$ modes. $St = 0.35$.

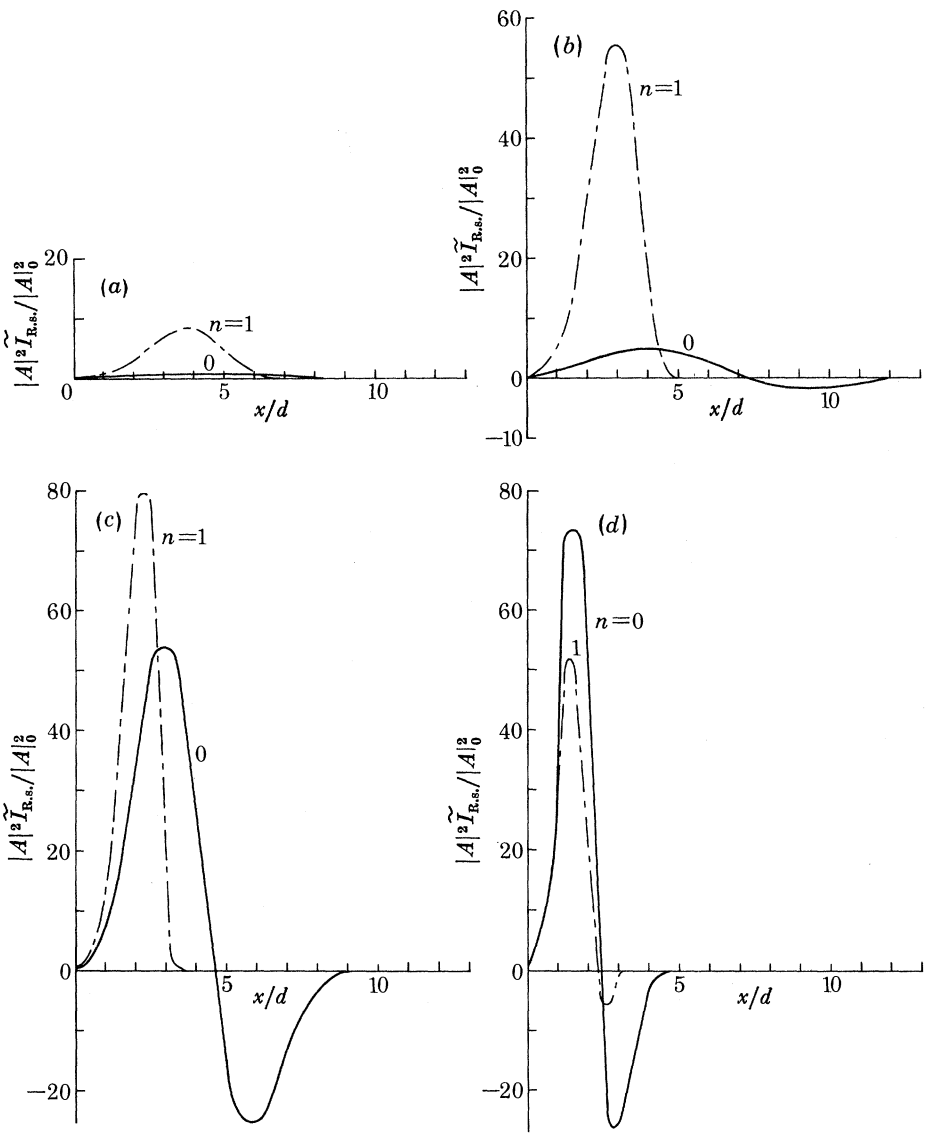

FIGURE 42. Large-scale structure production rate $|A|^2\tilde{I}_{R.s.}/|A|_0^2$ along the jet: comparison between the $n = 0$ and $n = 1$ modes. (*a*) $St = 0.18$, (*b*) $St = 0.35$, (*c*) $St = 0.50$, (*d*) $St = 0.80$.

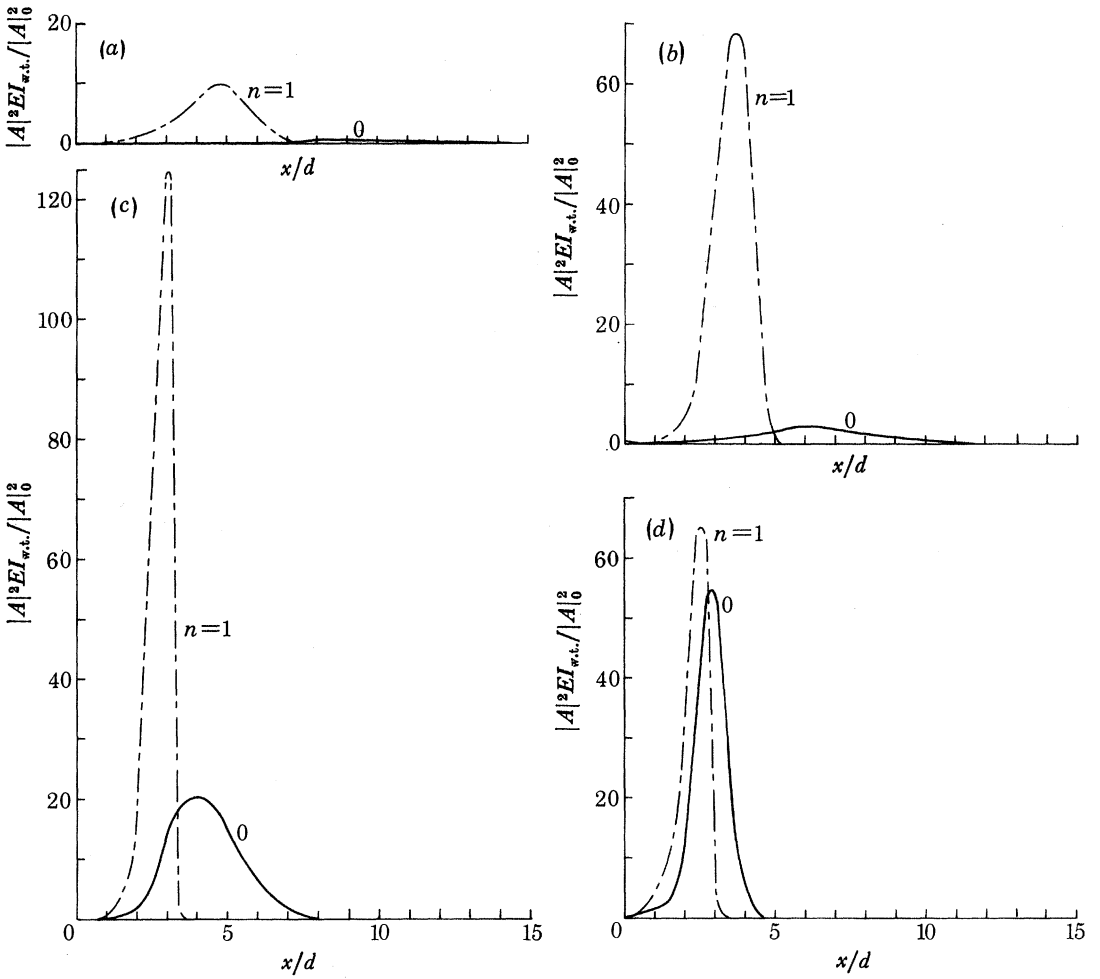

FIGURE 43. Large-scale structure to fine-grained turbulence energy transfer rate $|A|^2EI_{w.t.}/|A|_0^2$ along the jet: comparison between the $n = 0$ and $n = 1$ modes. (*a*) $St = 0.18$, (*b*) $St = 0.35$, (*c*) $St = 0.50$, (*d*) $St = 0.80$.

(*d*) *Energy transfer mechanisms*

To display the difference in the energy exchange mechanisms for the two modes, the energy exchange terms are compared for both values of n.

As a result of the larger production integral $\tilde{I}_{\text{R.s.}}$, $|A|^2\tilde{I}_{\text{R.s.}}/|A|_0^2$ is greater for $n = 1$ than for $n = 0$ at small Strouhal numbers, as shown in figure 42. The rapid decay of the asymmetric mode reduces the duration of wave production and the wave decays before the production becomes negative. The 'inviscid' decaying mechanism is less pronounced for $n = 1$, than for $n = 0$, while turbulent dissipation is again the basic mechanism by which the $n = 1$ mode decays.

As previously discussed, the additional wave-induced stresses and rates of strain for the $n = 1$ mode increases its turbulent dissipation integral $I_{\text{w.t.}}$, as shown in figure 43. This thus explains the rapid decay of the asymmetric wave shown in figure 38.

The larger values of E for the $n = 1$ mode automatically increases the fine-grained turbulence production $EI'_{\text{R.s.}}$, as shown in figure 44. But far downstream the effect of n on E is balanced by a similar effect on θ and the production attains the asymptotic value of 0.005, irrespective of n.

Similarly, the viscous dissipation $E^{\frac{3}{2}}I_\epsilon$ is greater for $n = 1$, because of E, as shown in figure 45.

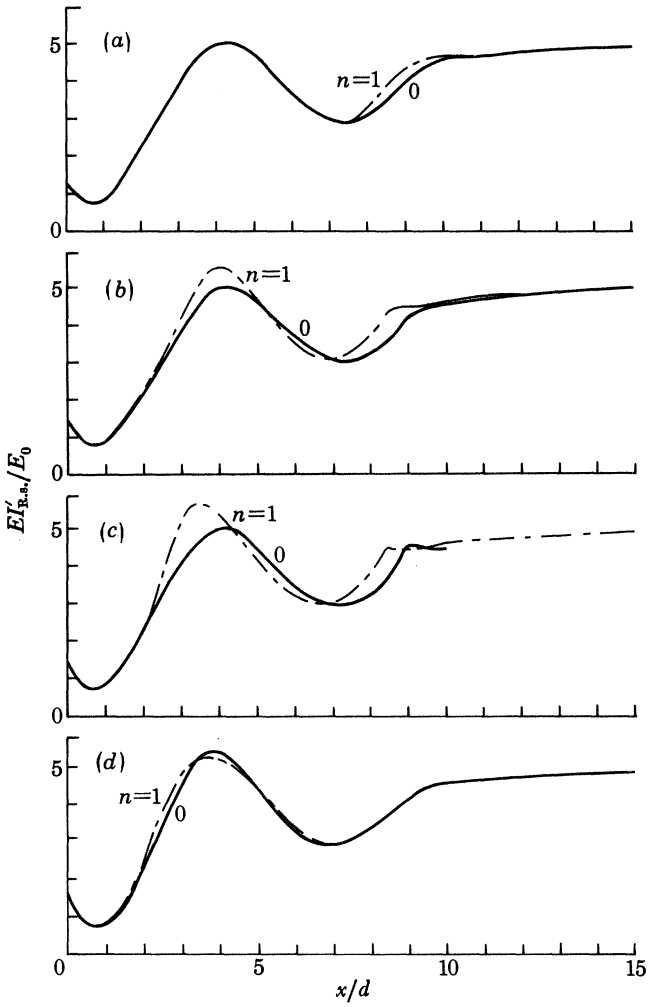

FIGURE 44. Fine-grained turbulence production rate $EI'_{R.s.}/E_0$ along the jet: comparison between the $n = 0$ and $n = 1$ modes. (*a*) $St = 0.18$, (*b*) $St = 0.35$, (*c*) $St = 0.50$, (*d*) $St = 0.80$.

Yet, since the viscous dissipation is proportional to $E^{\frac{3}{2}}$ rather than E, the influence of n on E is balanced by a similar influence on θ and the viscous dissipation attains its asymptotic value of 0.004 downstream, irrespective of n. The present results again show features of the observed self-preservation of the downstream region of the jet.

For this level, $|A|_0^2 = 10^{-5}$, the mean flow energy loss is mainly a result of the fine-grained turbulence. Since the production of the latter is slightly greater for $n = 1$ than for $n = 0$, the mean flow energy loss is also slightly greater for $n = 1$, as shown in figure 46. Therefore, if it is of interest to accelerate the rate of mixing by forcing an organized structure, an asymmetric wave could be more efficient than the axisymmetric one.

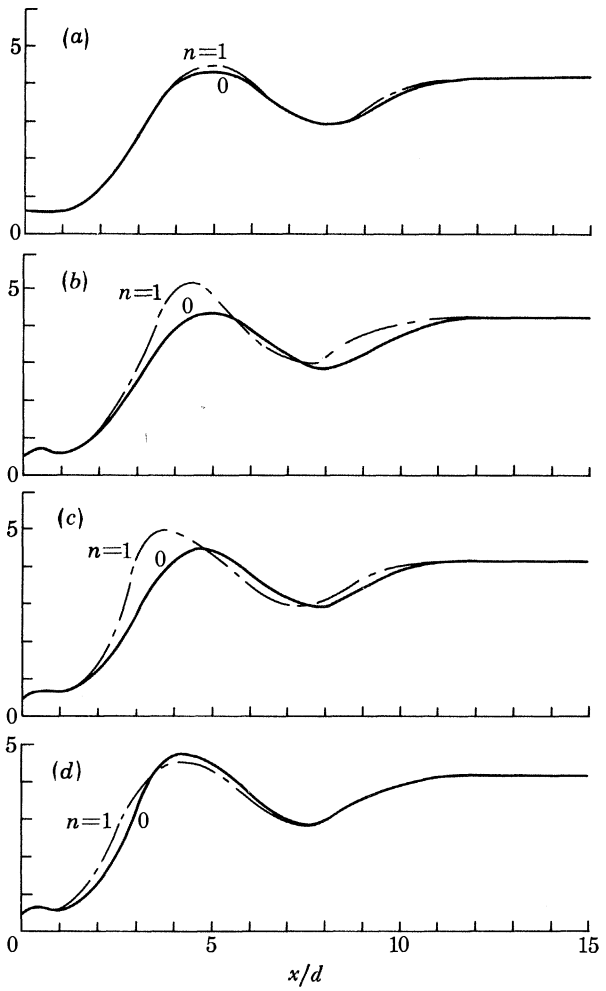

FIGURE 45. Fine-grained turbulence viscous dissipation rate $E^{\frac{3}{2}}I_\epsilon/E_0$ along the jet: comparison between the $n = 0$ and $n = 1$ modes. (*a*) $St = 0.18$, (*b*) $St = 0.35$, (*c*) $St = 0.50$, (*d*) $St = 0.80$.

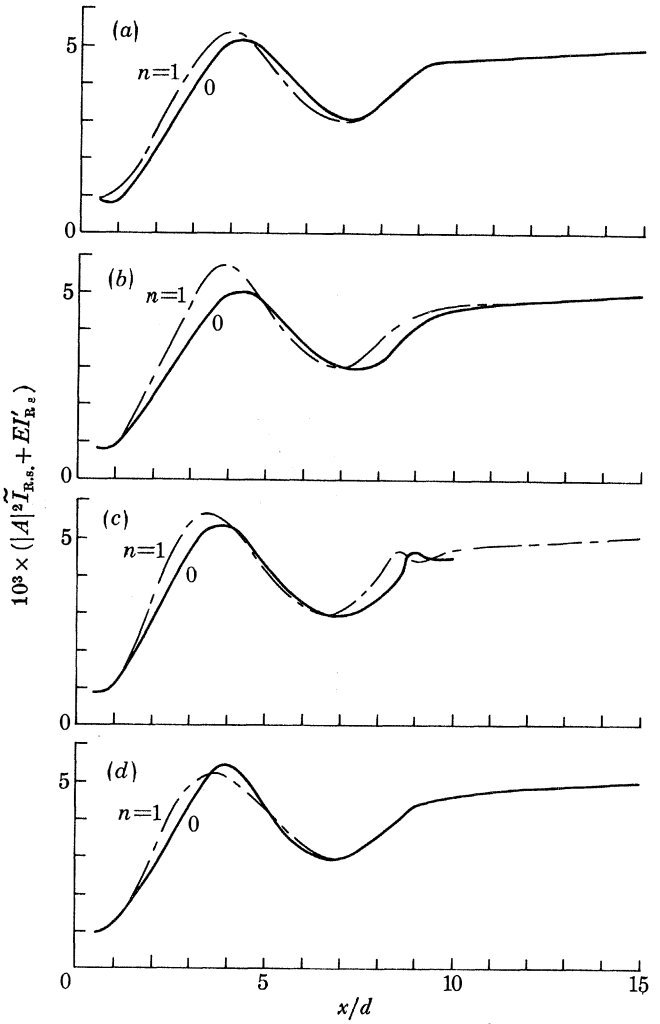

FIGURE 46. Mean flow energy loss rate $|A|^2\tilde{I}_{\mathrm{R.s.}} + EI'_{\mathrm{R.s.}}$ along the jet: comparison between the $n = 0$ and $n = 1$ modes. (*a*) $St = 0.18$, (*b*) $St = 0.35$, (*c*) $St = 0.50$, (*d*) $St = 0.80$.

9. Controlling the development of the large-scale structure

In the two preceding sections, the development of the large-scale structure was shown to depend on the initial level of excitation, the Strouhal number, and the azimuthal wavenumber. We now consider controlling the development of large-scale structure by adjusting the initial fine-grained turbulence level E_0 and the mean flow momentum thickness θ_0. We shall discuss this in terms of the $n = 0$ mode; the effects on the $n = 1$ mode would be qualitatively similar. This initial level of the large-scale structure is taken to be $|A|_0^2 = 10^{-5}$. Two Strouhal numbers, 0.35 and 0.8, are considered to represent the low and high frequencies respectively.

(*a*) *The influence of the initial fine-grained turbulence level*

E_0 could be as small as zero, corresponding to the laminar case, and as large as 0.1 ,which means that values of $(\overline{u'^2})^{\frac{1}{2}}$ at the centre of the nozzle exit correspond to about 30 % of the jet exit velocity. Values of $E_0 = 10^{-1}$, 10^{-3}, and 10^{-5} are considered here, while θ_0 is taken to be 0.034.

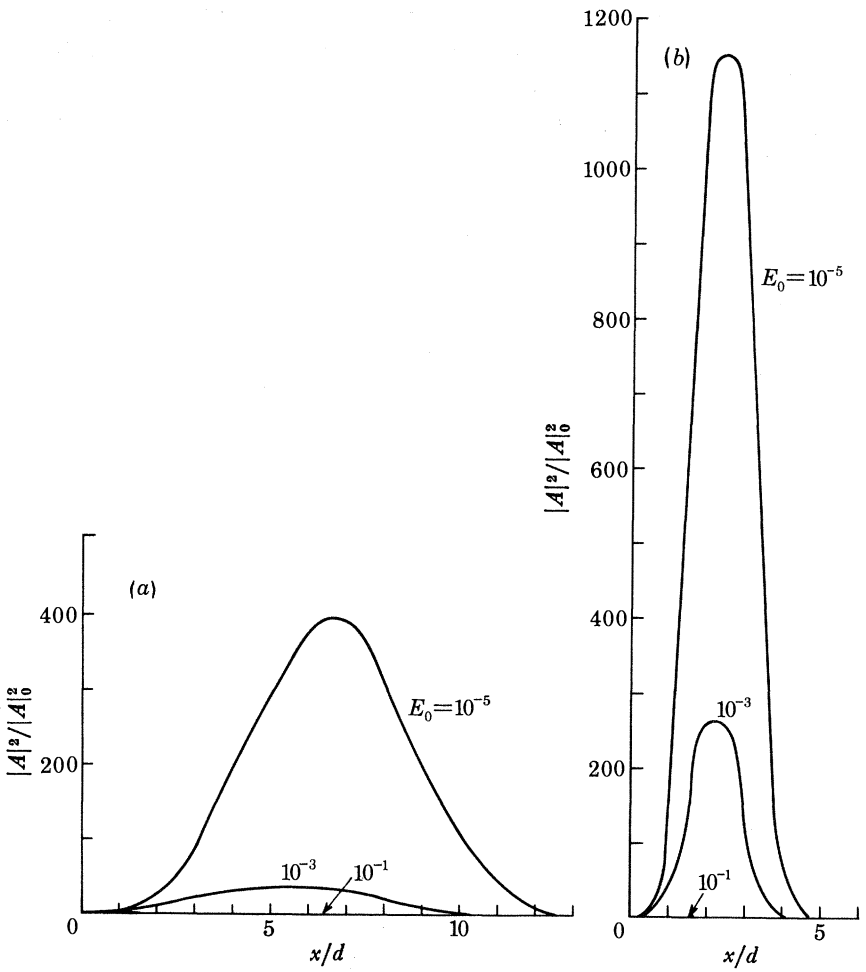

FIGURE 47. Effect of initial fine-grained turbulence energy levels E_0 on the development of large-scale structure energy ratio $|A|^2/|A|_0^2$ along the jet. (*a*) $St = 0.35$, (*b*) $St = 0.80$.

It is easily shown from (5.2) that the fine-grained turbulence has a damping effect on the large-scale structure. Since $\mathrm{d}E/\mathrm{d}x \propto E$, the growth of E increases with E_0. Consequently, the turbulent dissipation $|A|^2 EI_{\mathrm{w.t.}}/|A|_0^2$ increases with E_0, and accelerates the damping of the large-scale structure, as shown in figure 47. If E_0 is identically zero, E remains equal to zero along the jet and the amplification of the large-scale structure is given by

$$\frac{|A(x)|^2}{|A|_0^2} = \frac{I_2(x_0, St, n)}{I_2(x, St, n)} \exp \int_0^x \frac{\tilde{I}_{\mathrm{R.s.}}(x', St, n)}{I_2(x', St, n)}\, \mathrm{d}x',$$

which shows that there is a continuous growth of $|A|^2$ as long as $\tilde{I}_{\mathrm{R.s.}}$ is positive. The saturation and damping of $|A|^2$ would be provided by the character of $\tilde{I}_{\mathrm{R.s.}}$ alone.

When $E_0 \neq 0$, its role is to produce a turbulent dissipation that damps the large-scale structure. The large-scale structure could be reduced, or possibly eliminated, by increasing the initial fine-grained turbulence level. This is entirely in accordance with the observations of Chandrsuda *et al.* (1978). According to the physical picture brought out here, it is thus important to study the

initial levels E_0 and $|A|_0^2$ (and θ_0 as well) in any 'natural' or forced experiments in order to explain the appearance or non-appearance of the large-scale structure.

Since the viscous dissipation is proportional to $E^{\frac{5}{2}}$, while the fine-grained turbulence production is proportional to E, increasing E_0 produces an increase in $E^{\frac{5}{2}}I_\epsilon$ greater than the corresponding increase in $EI'_{\text{R.s.}}$. The rate of growth of E thus decreases with increasing E_0, as shown in figure 48.

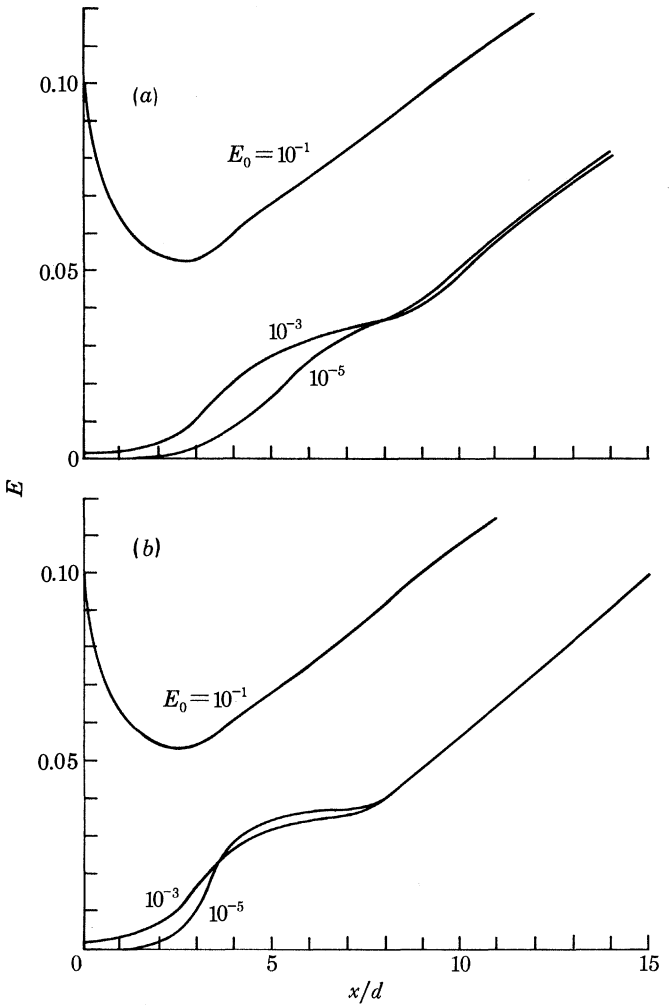

FIGURE 48. Effect of initial fine-grained turbulence energy levels E_0 on the development of fine-grained turbulence energy E along the jet. (*a*) $St = 0.35$, (*b*) $St = 0.80$.

A large increase in E_0 (for example, $E_0 = 0.1$) causes the viscous dissipation to exceed the fine-grained turbulence production; thus E decreases until the production exceeds the dissipation and E increases again. By this competitive mechanism the behaviour of E is self-adjusting so that E increases downstream at a rate that is practically independent of E_0. However, far-downstream the values of E themselves increase with E_0.

Because of the increase in E, the fine-grained turbulence production increases with E_0. Consequently the jet spreading rate also increases with E_0, as shown in figure 49. Thus, the mixing rate could also be increased by increasing E_0. This result has also been confirmed by the experimental observations of Hussain & Zedan (1978*a*).

To understand the relative effectiveness of the large-scale structure and fine-grained turbulence in enhancing the mixing process, we again take $\theta = 0.25$ as an indication of the end of the potential core. At $St = 0.35$, increasing $|A|_0^2$ from 10^{-5} to 10^{-3}, as in figure 31*b*, produces a 28 % reduction in the length of the potential core, while the same increase in E_0 from 10^{-5} to 10^{-3}, as in figure 49, produces only an 18 % reduction in the length of the potential core. The large-scale structure then appears to be a more efficient means, than the fine-grained turbulence, to accelerate the jet spreading and mixing, as is confirmed by the observations of Binder & Favre-Marinet (1973).

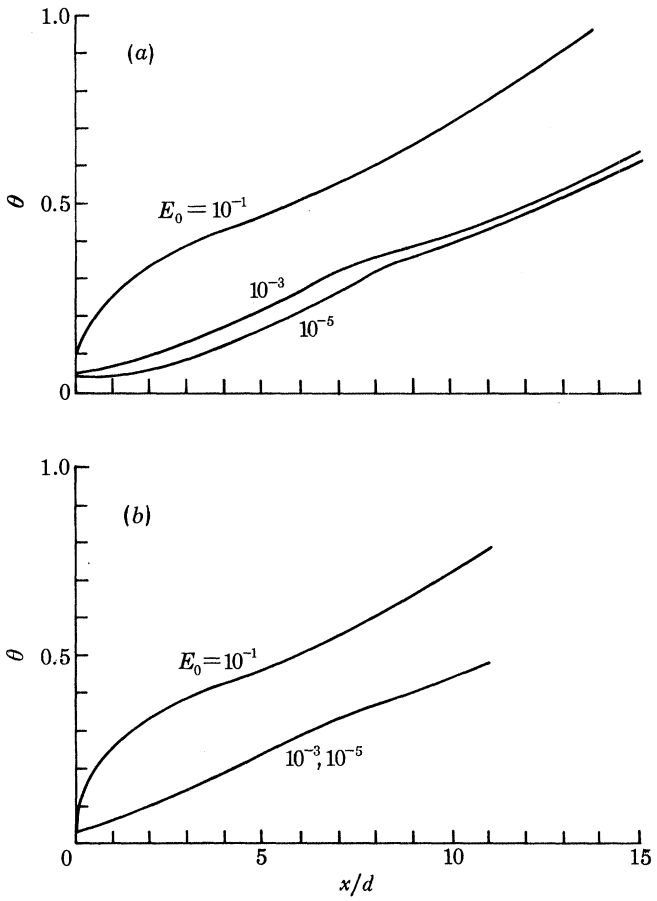

FIGURE 49. Effect of initial fine-grained turbulence energy levels E_0 on the development of mean flow momentum thickness θ. (*a*) $St = 0.35$, (*b*) $St = 0.80$.

(*b*) *The effect of the initial mean velocity profile*

The role of the initial mean velocity profile can be investigated by studying θ_0: $\theta_0 = 0$ produces a top-hat profile, and as θ_0 increases the mean velocity profile becomes smoother. The degree of smoothness of the mean velocity profile varies with the nozzle geometry and the conditions ahead of the nozzle. To study the effect of smoothing the mean velocity profile at the nozzle exit, θ_0 is taken to be 0.034, 0.100 and 0.200 while $|A|_0^2$ and E_0 are taken as 10^{-5} and 10^{-3} respectively.

Since the tendency to instability, as contained in $\tilde{I}_{\text{R.S.}}$, decreases with increasing θ_0, the large-scale structure production and consequently its amplification decreases with increasing θ_0, as shown in figure 50. Therefore, the large-scale structure development could be suppressed by

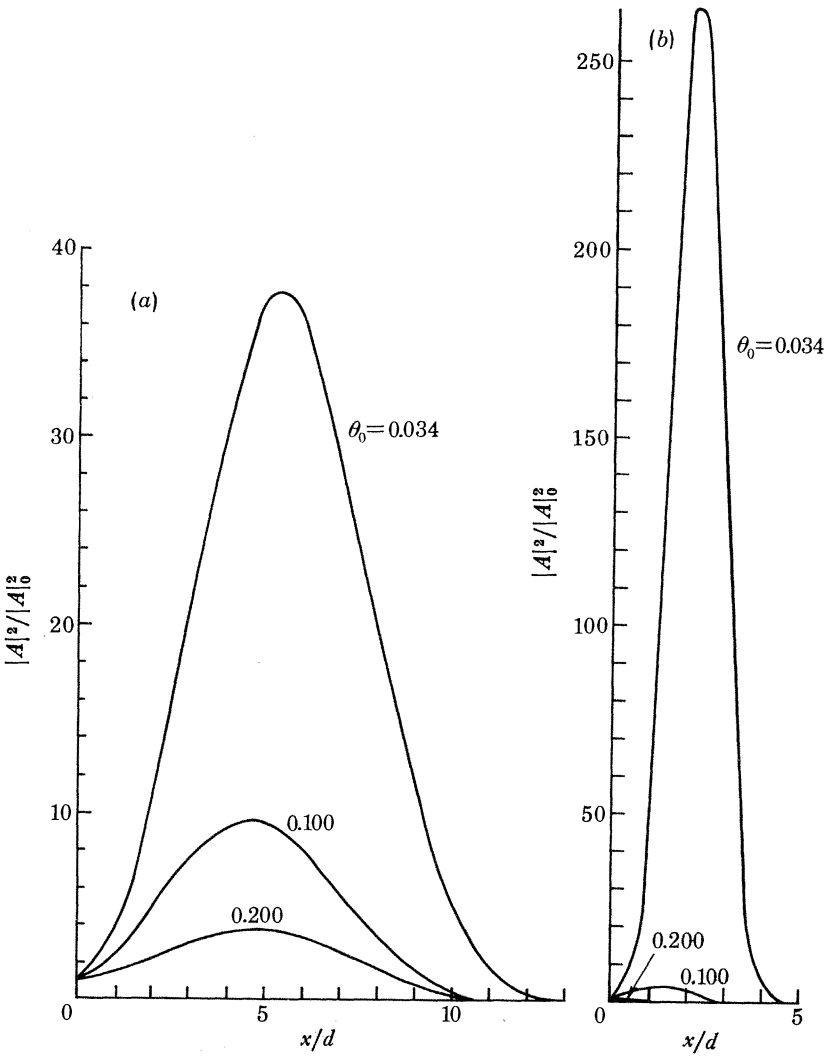

FIGURE 50. Effect of initial momentum thickness θ_0 on the development of large-scale structure energy ratio $|A|^2/|A|_0^2$ along the jet. (*a*) $St = 0.35$, (*b*) $St = 0.80$.

using a smooth mean flow at the nozzle exit. Experimentally this has been found to be practicable by Chan & Templin (1974).

For $|A|_0^2 = 10^{-5}$, the large-scale structure would not, in general have a significant influence on the fine-grained turbulence. Increasing θ_0 reduces both the production integral $I'_{\text{R.S.}}$ and the viscous dissipation integral I_ϵ. Increasing θ_0 from 0.034 to 0.1 reduces the viscous dissipation more than the production. Therefore E increases as θ_0 increases to 0.1, as shown in figure 51. As θ_0 continues to increase, the reduction in production exceeds the reduction in dissipation. Therefore E decreases with increasing θ_0, to 0.2. For the downstream region, the influence of θ_0 on E is balanced by a similar influence on θ and the growth rate of E is again independent of θ_0, which again is consistent with the observed self-preservation of the fully developed jet.

For the same value of $|A|_0^2$, the development of the mean flow is governed primarily by its interaction with the fine-grained turbulence alone. Because the mean shear decreases with increasing θ_0, the production $EI'_{\text{R.S.}}$, and consequently $\mathrm{d}\theta/\mathrm{d}x$, decrease with increasing θ_0. But

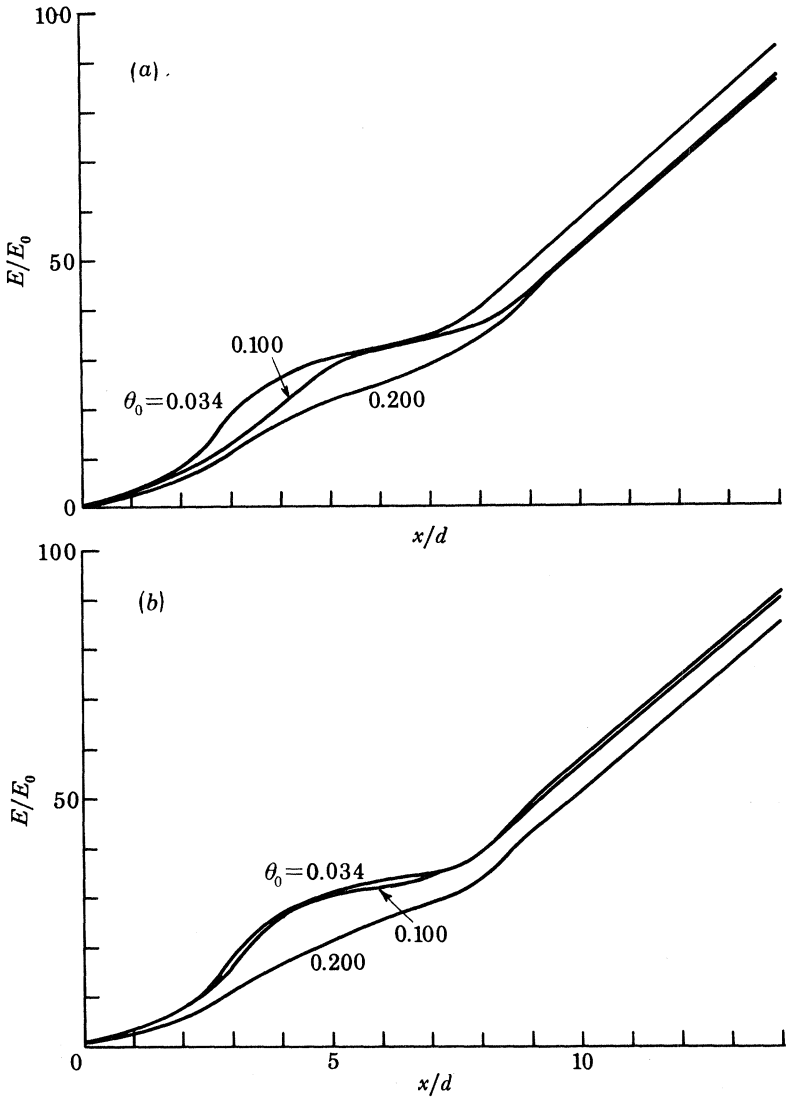

FIGURE 51. Effect of initial momentum thickness θ_0 on the development of fine-grained turbulence energy ratio E/E_0 along the jet. (*a*) $St = 0.35$, (*b*) $St = 0.80$.

far downstream, where the production is independent of θ_0, the rate of spreading of the jet is also independent of θ_0, as shown in figure 52. This is consistent with Hussain & Zedan's (1978*b*) observation that the initial momentum thickness Reynolds number has an insignificant effect on the rate of spreading of the jet. We have seen, however, that θ_0 has a rather spectacular effect on the large-scale structure (figure 50) in the nonequilibrium region and a consequent effect on the fine-grained turbulence energy levels both locally and in the far downstream region (figure 51).

Some aspects of this work were first presented at the Eighth U.S. National Congress of Applied Mechanics (Liu 1978) and at the 1979 Spring Meeting of the American Physical Society,

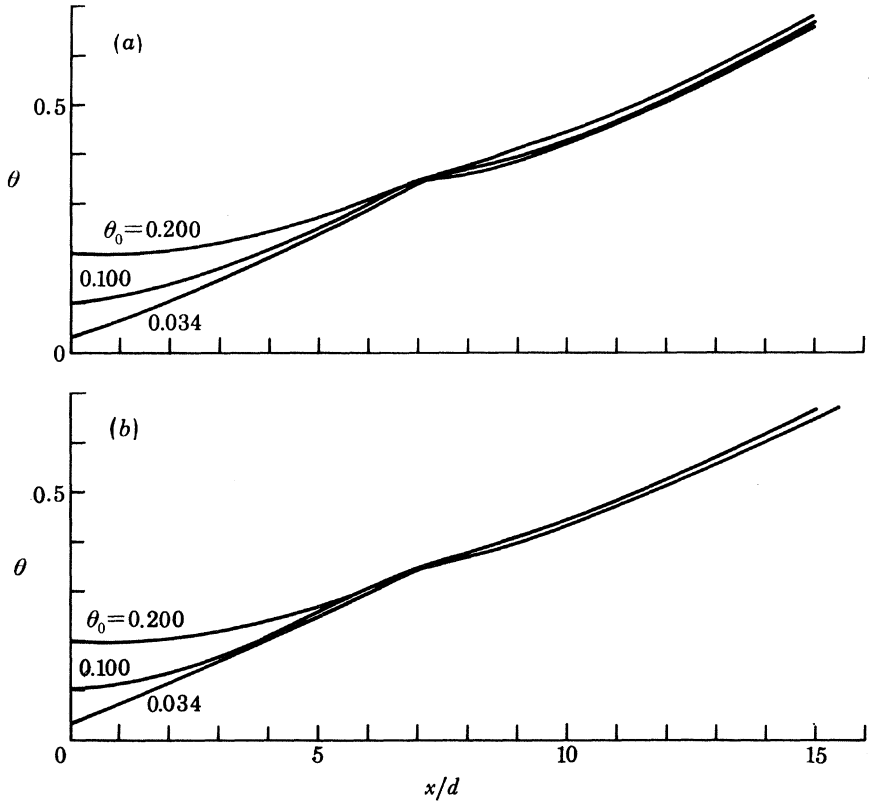

FIGURE 52. Effect of initial momentum thickness θ_0 on the development of mean flow momentum thickness θ. (*a*) $St = 0.35$, (*b*) $St = 0.80$.

Symposium of the Division of Fluid Dynamics (Liu 1979). The numerous beneficial conversations with J. T. Stuart, F.R.S. and the hospitality of the Department of Mathematics, Imperial College to one of us (J.T.C.L.) are gratefully acknowledged. The comments of D. G. Crighton, Sir James Lighthill, F.R.S. and J. T. Stuart, F.R.S. on the draft of the manuscript are greatly appreciated. This work was partially supported by the Fluid Mechanics Program, National Science Foundation through Grants NSF ENG-76-24585 and NSF CME-78-22127; the Fluid Dynamics Program, Office of Naval Research and the National Aeronautics and Space Administration, Langley Research Centre through Grant NSG-1076. Partial support from the United Kingdom Science Research Council to J.T.C.L. through its Senior Visiting Fellowship Programme is also gratefully acknowledged.

REFERENCES

Albertson, M. L., Dai, Y. B., Jensen, R. A. & Rouse, H. 1948 Diffusion of submerged jets. *Proc. Am. Soc. civ. Engrs* **74**, 1571.

Alper, A. & Liu, J. T. C. 1978 On the interactions between large-scale structure and fine-grained turbulence in a free shear flow. II. The development of spatial interactions in the mean. *Proc. R. Soc. Lond.* A **359**, 497.

Batchelor, G. K. 1967 *An introduction to fluid dynamics*. Cambridge University Press.

Batchelor, G. K. & Gill, A. E. 1962 Analysis of the stability of axisymmetric jets. *J. Fluid Mech.* **14**, 529.

Betchov, R. & Criminale, Jr., W. O. 1967 *Stability of parallel flows*. New York: Academic Press.

Bishop, K. A., Ffowcs Williams, J. E. & Smith, W. 1971 On the noise sources of the unsuppressed high speed jet. *J. Fluid Mech.* **50**, 21.

Binder, G. & Favre-Marinet, M. 1973 Mixing improvement in pulsating turbulent jets. In *Fluid mechanics of mixing* (eds Uram, E. M. & Goldschmidt, V. W.), 167–172. New York: Am. Soc. mech. Engrs.

Bouchard, G. E. & Reynolds, W. C. 1978 Control of vortex pairing in a round jet. *Bull. Am. phys. Soc.* **23**, 1013.
Bradshaw, P., Ferriss, D. H. & Atwell, N. P. 1967 Calculation of boundary-layer development using the turbulent energy equation. *J. Fluid Mech.* **28**, 593.
Bradshaw, P., Ferriss, D. H. & Johnson, R. F. 1964 Turbulence in the noise-producing region of a circular jet. *J. Fluid Mech.* **19**, 591.
Browand, F. K. 1966 An experimental investigation of the instability of an incompressible, separated shear layer. *J. Fluid Mech.* **26**, 281.
Brown, G. L. & Roshko, A. 1974 On density effects and large structure in turbulent mixing layers. *J. Fluid Mech.* **64**, 775.
Candel, S., Guedel, A. & Julienne, A. 1975 Refraction and scattering of sound in an open wind tunnel flow. Presented at the Sixième congrès de simulation aérospatiale, 22–24 September 1975, Ottawa.
Chan, Y. Y. 1974*a* Spatial waves in turbulent jets. *Physics Fluids* **17**, 46.
Chan, Y. Y. 1974*b* Spatial waves in turbulent jets. II. *Physics Fluids* **17**, 1667.
Chan, Y. Y. 1975 Nonlinear spatial wave development in an axisymmetric turbulent jet. *Rep. natn. Res. Coun. Can.* no. 14756.
Chan, Y. Y. 1976 Spatial waves of higher modes in an axisymmetric turbulent jet. *Physics Fluids* **19**, 2042.
Chan, Y. Y. & Templin, J. T. T. 1974 Supression of spatial waves by distortion of the jet velocity profile. *Physics Fluids* **17**, 2124.
Chandrsuda, C., Mehta, R. D., Weir, A. D. & Bradshaw, P. 1978 Effect of free-stream turbulence on the large structure in turbulent mixing layers. *J. Fluid Mech.* **85**, 693.
Corrsin, S. 1943 Investigations of flow in an axially symmetric heated jet of air. *Natn. advis. Comm. Aeronaut. Adv. Conf. Rep.* no. 3123 (also W-94).
Corrsin, S. & Uberoi, M. S. 1950 Spectrum and diffusion in a round turbulent jet. *Tech. Notes natn. advis. Comm. Aeronaut., Wash.* no. 2124.
Crow, S. C. & Champagne, F. H. 1971 Orderly structure in jet turbulence. *J. Fluid Mech.* **48**, 547.
Damms, S. M. & Kuchemann, D. 1974 On the vortex-sheet model for mixing between two parallel streams. I. Description of the model and experimental evidence. *Proc. R. Soc. Lond.* A **339**, 451.
Davies, P. O. A. L., Fisher, M. J. & Barratt, M. J. 1963 The characteristics of the turbulence in the mixing region of a round jet. *J. Fluid Mech.* **15**, 337.
Davies, P. O. A. L. & Yule, A. J. 1975 Coherent structures in turbulence. *J. Fluid Mech.* **69**, 517; corrigendum, *J. Fluid Mech.* **74**, 797 (1976).
Dimotakis, P. E. & Brown, G. L. 1976 Large structure dynamics and entrainment in the mixing layer at high Reynolds numbers. *J. Fluid Mech.* **78**, 535.
Favre-Marinet, M. 1975 Structure des jets pulsants. Docteur-Ingénieur thesis, l'Université Scientifique et Médicale de Grenoble.
Favre-Marinet, M. & Binder, G. 1979 Structure des jets pulsants *J. Méc.* **18**, 356.
Freymuth, P. 1966 On transition in a separated laminar boundary layer. *J. Fluid Mech.* **25**, 683.
Gatski, T. B. & Liu, J. T. C. 1980 On the interactions between large-scale structure and fine-grained turbulence in a free shear flow. III. A numerical solution. *Phil. Trans. R. Soc. Lond.* A **293**, 473.
Hinze, J. O. 1959 *Turbulence.* p. 473. New York: McGraw-Hill.
Ho, C. M. & Huang, L. S. 1978 Subharmonics and vortex merging in an unsteady shear layer. *Bull. Am. phys. Soc.* **23**, 1007.
Hussain, A. K. M. F. & Reynolds, W. C. 1970 The mechanics of an organized wave in turbulent shear flow. *J. Fluid Mech.* **41**, 241.
Hussain, A. K. M. F. & Zedan, M. F. 1978*a* Effects of the initial condition on the axisymmetric free shear layer: effect of the initial fluctuation level. *Physics Fluids* **21**, 1475.
Hussain, A. K. M. F. & Zedan, M. F. 1978*b* Effects of the initial condition on the axisymmetric free shear layer: effects of the initial momentum thickness. *Physics Fluids* **21**, 1100.
Kelly, R. E. 1967 On the stability of an inviscid shear layer which is periodic in space and time. *J. Fluid Mech.* **27**, 657.
Kendall, J. M. 1970 The turbulent boundary layer over a wall with progressive surface waves. *J. Fluid Mech.* **41**, 259.
Ko, D. R. S., Kubota, T. & Lees, L. 1970 Finite disturbance effect in the stability of a laminar incompressible wake behind a flat plate. *J. Fluid Mech.* **40**, 315.
Ko, D. R. S. 1971 Integral theory for the instability of laminar compressible wakes behind slender bodies. *A.I.A.A. Jl.* **9**, 1977.
Ko, N. W. M. & Davies, P. O. A. L. 1971 The near field within the potential cone of subsonic cold jets. *J. Fluid Mech.* **50** 49.
Lau, J. C. & Fisher, M. J. 1975 The vortex-street structure of 'turbulent' jets. Part I. *J. Fluid Mech.* **67**, 299.
Laurence, J. C. 1956 Intensity, scale and spectra of turbulence in mixing region of free subsonic jet. *Rep. natn. advis. Comm. Aeronaut., Wash.* no. 1292.
Lees, L. & Gold, H. 1964 Stability of laminar boundary layers and wakes at hypersonic speeds. I. Stability of laminar wakes. In *Fundamental phenomena in hypersonic flow, Proc. Int. Symp.*, p. 310. Cornell University Press.

PHILOSOPHICAL TRANSACTIONS OF THE ROYAL SOCIETY A MATHEMATICAL, PHYSICAL & ENGINEERING SCIENCES

Liepmann, H. W. 1952 Aspects of the turbulence problem. Second part. *Z. Angew. Math. Phys.* **3**, 407.
Liepmann, H. W. & Laufer, J. 1974 Investigation of free turbulent mixing. *Tech. Notes natn. advis. Comm. Aeronaut., Wash.* no. 1257.
Lighthill, M. J. 1963 Introduction. Boundary layer theory. In *Laminar boundary layers* (ed. L. Rosenhead), pp. 46–113. Oxford University Press.
Lin, C. C. 1955 *The theory of hydrodynamic stability*. Cambridge University Press.
Liu, J. T. C. 1971 Nonlinear development of an instability wave in a turbulent wake. *Physics Fluids* **14**, 2251.
Liu, J. T. C. 1974 Developing large-scale wavelike eddies and the near jet noise field. *J. Fluid Mech.* **62**, 437.
Liu, J. T. C. and Alper, A. 1977 On the large-scale structure in turbulent free shear flows. *Proceedings of Symposium on Turbulent Shear Flows*, 18–20 April 1977, pp. 11.1–11.11. Pennsylvania State University.
Liu, J. T. C., Alper, A. & Mankbadi, R. 1977 The large-scale coherent structure in turbulent shear flows and its radiation properties. In *Structure and mechanisms of turbulence* (ed. H. Fiedler), vol. 2. Berlin: Springer–Verlag.
Liu, J. T. C. & Gururaj, P. M. 1974 Finite-amplitude instability of the compressible laminar wake: comparison with experiments. *Physics Fluids* **17**, 532.
Liu, J. T. C. & Lees, L. 1970 Finite-amplitude instability of the compressible laminar wake. Strongly amplified disturbances. *Physics Fluids* **13**, 2932.
Liu J. T. C. & Merkine, L. 1976 On the interactions between large-scale structure and fine-grained turbulence in a free shear flow. I. The development of temporal interactions in the mean. *Proc. R. Soc. Lond.* A **352**, 213.
Liu, J. T. C. 1978 On the modelling of large-scale coherent structures in free turbulent shear flows. *8th U. S. National Congress of Appl. Mech.* 26–30 June 1978, University of California, Los Angeles.
Liu, J. T. C. 1979 Sound generation by large-scale coherent eddies in turbulent jets. *Bull. Am. phys. Soc.* **24**, 557.
Mack, L. M. 1965 Computation of the stability of laminar compressible boundary layer. In *Methods in computational physics*, vol. 4. New York: Academic Press.
Maestrello, L. & McDaid, E. 1971 Acoustic characteristics of a high-subsonic jet. *A.I.A.A. Jl.* **9**, 1058.
Marble, F. E. & Broadwell, J. E. 1977 The coherent flame model for turbulent chemical reactions. *Project SQUID Tech. Rep.* TRW-9-PU.
Mellor, G. L. & Herring, H. J. 1973 A survey of the mean turbulent field closure models. *A.I.A.A. Jl.* **11**, 590.
Merkine, L. & Liu, J. T. C. 1975 On the development of large-scale wavelike eddies in a plane turbulent jet. *J. Fluid Mech.* **70**, 353.
Michalke, A. 1971 Instabilität eines kompressiblen runden Freistrahls unter Berücksichtigung des Einflusses der Strahlgrenzschichtdicke. *Z. Flugwiss.* **19**, 319.
Michalke, A. & Fuchs, H. V. 1974 Description of turbulence and noise of an axisymmetric shear flow. DLR-FB 4-2, Deutsche Forschungs und Versuchsanstalt für Luft- und Raumfahrt E. V., Institut für Turbulenzforschung, Berlin.
Miksad, R. W. 1972 Experiments on the nonlinear stages of free shear-layer transition. *J. Fluid Mech.* **56**, 695.
Miksad, R. W. 1973 Experiments on nonlinear interactions in the transition of a free shear layer. *J. Fluid Mech.* **59**, 1.
Mollo-Christensen, E. 1967 Jet noise and shear flow instability seen from an experimenter's viewpoint. *J. appl. Mech.* **34**, 1.
Moore, C. J. 1977 The role of shear-layer instability waves in jet exhaust noise. *J. Fluid Mech.* **80**, 321.
Moore, D. W. and Saffman, P. G., 1975 The density of organized vortices in a turbulent mixing layer. *J. Fluid Mech.* **69**, 465.
Morris, P. J. 1974 A model for the structure of jet turbulence as a source of noise. *A.I.A.A. Pap. no.* 74–1.
Morris, P. J. 1977 The spatial viscous instability of axisymmetric jet. *J. Fluid Mech.* **77**, 511.
Murthy, S. N. B. (ed.) 1975 *Turbulent mixing in nonreactive and reactive flows*, New York: Plenum Press.
Reynolds, W. C. 1972 Large-scale instabilities of turbulent wakes. *J. Fluid Mech.* **54**, 481.
Reynolds, W. C. & Hussain, A. K. M. F. 1972 The mechanics of an organized wave in turbulent shear flow. 3. Theoretical models and comparisons with experiments. *J. Fluid Mech.* **54**, 263.
Roshko, A. 1976 Structure of turbulent shear flows: a new look. *A.I.A.A. Jl.* **14**, 1349.
Rotta, J. C. 1951 Statistische Theorie nichthomogener Tubulenz. *Z. Phys.* **129**, 547.
Sami, S., Carmody, T., & Rouse, H. 1967 Jet diffusion in the region of flow establishment. *J. Fluid Mech.* **27**, 231.
Smith, C. R. & Abbott, D. E. (eds) 1978 *Coherent structure of turbulent boundary layers*. Bethlehem: Lehigh University.
Stuart, J. T. 1958 On the nonlinear mechanism of hydrodynamic stability. *J. Fluid Mech.* **4**, 1.
Stuart, J. T. 1963 Hydrodynamic stability. In *Laminar boundary layers* (ed. L. Rosenhead), pp. 492–579. Oxford University Press.
Stuart, J. T. 1965 Hydrodynamic stability. *Appl. Mech. Rev.* **18**, 523.
Townsend, A. A. 1956 *The structure of turbulent shear flow*. Cambridge University Press.
Winant, C. D. & Browand, K. K. 1974 Vortex pairing: the mechanism of turbulent mixing-layer growth at moderate Reynolds number. *J. Fluid Mech.* **63**, 237.
Yamamoto, K. & Arndt, R. E. A. 1978 On the acoustic field generated by subsonic jets at low Reynolds numbers. Project Rep. no. 170. St. Anthony Falls Hydraulic Laboratory, University of Minnesota.

PHILOSOPHICAL TRANSACTIONS OF THE ROYAL SOCIETY A MATHEMATICAL, PHYSICAL & ENGINEERING SCIENCES